1998

Temperature dependent linear and non-linear optical spectroscopy for condensed phase systems

Mohamad Toutounji
Iowa State University

INFORMATION TO USERS

This manuscript has been reproduced from the microfilm master. UMI films the text directly from the original or copy submitted. Thus, some thesis and dissertation copies are in typewriter face, while others may be from any type of computer printer.

The quality of this reproduction is dependent upon the quality of the copy submitted. Broken or indistinct print, colored or poor quality illustrations and photographs, print bleedthrough, substandard margins, and improper alignment can adversely affect reproduction.

In the unlikely event that the author did not send UMI a complete manuscript and there are missing pages, these will be noted. Also, if unauthorized copyright material had to be removed, a note will indicate the deletion.

Oversize materials (e.g., maps, drawings, charts) are reproduced by sectioning the original, beginning at the upper left-hand corner and continuing from left to right in equal sections with small overlaps. Each original is also photographed in one exposure and is included in reduced form at the back of the book.

Photographs included in the original manuscript have been reproduced xerographically in this copy. Higher quality 6" x 9" black and white photographic prints are available for any photographs or illustrations appearing in this copy for an additional charge. Contact UMI directly to order.

UMI

A Bell & Howell Information Company
300 North Zeeb Road, Ann Arbor MI 48106-1346 USA
313/761-4700 800/521-0600

Temperature dependent linear and non-linear optical spectroscopy for condensed phase systems

by

Mohamad Toutounji

A dissertation submitted to the graduate faculty

in partial fulfillment of the requirements for the degrree of

DOCTOR OF PHILOSOPHY

Major: Physical Chemistry

Major Professor: Gerald J. Small

Iowa State University

Ames, Iowa

1998

Graduate College
Iowa State University

This is to certify that the Doctoral dissertation of

Mohamad Toutounji

has met dissertation requirements of Iowa State University

Signature was redacted for privacy.

Major Professor

Signature was redacted for privacy.

For the Major Program

Signature was redacted for privacy.

For the Graduate College

TABLE OF CONTENTS

CHAPTER 1. LINEAR OPTICAL RESPONSE THEORY (LINEAR SPECTROSCOPY) FOR CONDENSED PHASE SYSTEMS

1.1 Introduction

A substantial part of the history of quantum mechanics is associated with efforts directed toward an understanding of the interaction between light and matter at the atomic and molecular levels. The interaction of electromagnetic radiation with matter is one of the richest probes into the structure and dynamical processes of matter. It is difficult to understand the microscopic structure of matter without spectroscopic techniques.

One response of the medium to the electric field **E** of the radiation field takes the form of a dielectric polarization density **P**. The interaction of radiation with the medium generates a polarization which serves as a source of the new radiation field according to Maxwell's equation

$$\nabla^2\mathbf{E}(\mathbf{r},t)+\frac{1}{c^2}\frac{\partial^2}{\partial t^2}\mathbf{E}(\mathbf{r},t)=-\frac{4\pi}{c^2}\frac{\partial^2}{\partial t^2}\mathbf{P}(\mathbf{r},t), \tag{1.1}$$

where c is the speed of light. Since the optical polarization is the only material quantity that appears in Maxwell's equation (the right hand side of Maxwell's equation in a vacuum is zero), it carries all microscopic information about the system. Electronic and vibrational relaxations and other dynamical processes will show up in the measurements through their effect on the optical polarization. Therefore, calculating the optical polarization is essential for obtaining spectroscopic information. Eq. (1.1) can be solved self-consistently [1, 2, 3].

Spectroscopic measurements can be classified according to the order of the response of the system under study with respect to the applied fields. The polarization to nth order in the **E** field is denoted $\mathbf{P}^{(n)}$,

$$\mathbf{P}=\mathbf{P}^{(1)}+\mathbf{P}_{NL}, \tag{1.2}$$

where

$$\mathbf{P}_{NL} = \mathbf{P}^{(2)} + \mathbf{P}^{(3)} + \text{-------}. \tag{1.3}$$

$\mathbf{P}^{(1)}$ is the linear polarization that controls all linear optical measurements, such as linear absorption and fluorescence, whereas $\mathbf{P}_{NL}$ is the nonlinear polarization that governs multi-wave mixing experiments. The polarization may be classified according to the power law of the field. For example, $\mathbf{P}^{(1)}$ corresponds to linear interactions, that is, interactions in which the polarization is proportional to the applied field and has the same frequency. $\mathbf{P}^{(2)}$ is proportional to product of two fields, or to the square of a single field, and may contain frequencies not found in the incident field(s), and the nth order polarization $\mathbf{P}^{(n)}$ is proportional to n fields (or a combination of fields corresponding to an nth order product) and may contain numerous frequency combinations, although in most current experiments $n \leq 3$. $\mathbf{P}^{(2)}$ is the lowest order nonlinear polarization for anisotropic media such as interfaces. quantum wells, ad monolayers, while $\mathbf{P}^{(3)}$ is the lowest order nonlinear polarization in an isotropic medium representing nonlinear processes (4-wave mixing experiments) such as photon echo, hole-burning, and pump-probe spectroscopies.

Evidently, the optical polarization of the medium plays a major role in the calculations and interpretations of optical measurements. In the following sections we will see that $\mathbf{P}$ is calculated in terms of the optical *response function* which, in turn, is calculated from the dipole moment *correlation function*. Therefore, we shall present a brief definition and description of classical time correlation functions in Section 1.1.1 in order to facilitate discussion of the dipole moment time correlation function formalism of spectroscopy in Section 1.1.2. This will help us understand the underlying physics of any time-domain or frequency domain spectroscopic measurements of condensed phase systems involving linear and quadratic electron-phonon coupling in the following sections.

1.1.1 Classical Time Correlation Functions

Correlation functionts occur quite frequently in statistical physics. The time correlation function approach was initially developed by Green and Kubo [4, 5-8] in certain areas of non-equilibrium statistical mechanics. Time correlation functions are as important in non-equilibrium statistical mechanics as the partition function is in equilibrium statistical mechanics.

The description of a classical time correlation function is presented below. Let p(t) and q(t) denote all the momenta and the spatial coordinates needed to describe the system of interest, and let p(0) = p and q(0) = q denote the phase space coordinates at some initial time, t = 0. The p(t) and q(t) are related to p and q through the equations of motion of the system as follows

$$p(t)=p(p, q; t)$$
$$q(t)=q(p, q; t). \tag{1.4}$$

Let A{p(t), q(t)} be some function of the phase space coordinates of the system. Using Eq. (1.4), one can write

$$A\{p(t), q(t)\} = A\{p, q; t\} = A(t). \tag{1.5}$$

A classical time correlation function of A(t) is defined as

$$C(t) = \langle A(0)\, A(t)\rangle = \int \ldots\ldots \int dp\, dq\, A(p, q; 0)\, A(p, q; t)\, f(p,q) \tag{1.6}$$

where $f(p,q)$ is the equilibrium phase space distribution function. If A(t) is a vectorial function, then C(t) is written as

$$C(t) = \langle \mathbf{A}(0) \cdot \mathbf{A}(t) \rangle. \tag{1.7}$$

For instance, consider the velocity correlation function $C(t) = \langle \mathbf{V}(0) \cdot \mathbf{V}(t) \rangle$ for a gas. When $t = 0$, $C(0) = \langle \mathbf{V}(0) \cdot \mathbf{V}(0) \rangle = \langle \upsilon^2 \rangle$, which is simply the equilibrium average of υ^2, which equals $3kT/m$ for a gas by equipartition theorem. Here, k is Boltzmann constant, T is the temperature, and m is the mass of the particle. As time evolves, a particle will suffer collisions which will cause its velocity and direction to change and, as a result, its velocity at time t will be less and less correlated with its initial value $\mathbf{V}(0)$. After a sufficient number of collisions $\mathbf{V}(t)$ will be completely uncorrelated with its initial value, $\mathbf{V}(0)$, and C(t) will be equal to zero.

Therefore, we expect the velocity correlation to start at its initial value $C(0) = 3kT/m$, which is the correlation maximum value, and to eventually decay to zero. Assuming that C(t) decays exponentially with a damping constant γ, i.e., $C(t) = (3kT/m) \exp(-\gamma t)$, it is clearly seen that C(t) is maximmum at $t = 0$, and then starts to decay as time evolves till it becomes zero. We can see from the above example that a possible definition of time correlation function is that it describes the average decay of a property of a system from its initial value. Another possible definition is that time correlation function describes how long some given property of a system persists until it is averaged out by the microscopic motion of the molecules of the system. Afterall, C(t) of a quantity A is an average over an ensemble of systems according to Eq. (1.6).

An important property of time correlation functions is that they satisfy stationary average over time [4-9]:

$$\langle A(0)\, B(t) \rangle = \langle A(s)\, B(t+s) \rangle, \tag{1.8}$$

or with $s = -t$,

$$\langle A(0)\, B(t) \rangle = \langle A(-t)\, B(0) \rangle. \tag{1.9}$$

The property in Eq. (1.9) is called stationarity. Hence, this average depends on the time difference "s" rather than on absolute times ($t_1 = 0$ or $t_2 = t$) separately . Classical correlation functions are even functions of time[3-7, 10-13]. A demonstration that a classical correlation function is even goes as follows:

with

$$C(-t) = \langle A(0)\, A(-t) \rangle, \tag{1.10}$$

and using the fact that the correlation functions are invariant under time translation (stationarity) and that classical dynamical variables commute, one obtains

$$\begin{aligned} C(-t) &= \langle A(-t)\, A(0) \rangle \\ &= \langle A(0)\, A(t) \rangle \\ &= C(t). \end{aligned} \tag{1.11}$$

Clearly, $C(0) = \langle A(0)\, A(0) \rangle = \langle A^2 \rangle$.

1.1.2 Quantum Correlation Functions in Spectroscopy

Consider a system of interacting molecules in a quantum state described by the initial state $|i\rangle$. If this system interacts with an electric field of frequency ω, transitions to other quantum states $|f\rangle$ of the molecules may be induced provided the field frequency closely matches one of the Bohr frequencies

$$\omega_{fi} = (E_f - E_i)/\hbar. \tag{1.11}$$

Using the standard formulas of quantum mechanical time-dependent perturbation theory in the Schrödinger representation, we can write an equation for the absorption lineshape $\sigma(\omega)$, which represents the quantum mechanical transitions of the absorbing molecules from $|i\rangle$ to $|f\rangle$, as

$$\sigma(\omega) = \sum_i \sum_f \rho_i |\langle f|\mathbf{v}|i\rangle|^2 \, \delta(\omega_{fi} - \omega), \tag{1.12}$$

where ρ_i (the density operator, *vide infra*) is the probability of finding the system in the initial state $|i\rangle$ and $\mathbf{v}$ is the dipole moment operator. This formula represents the Fermi Golden Rule [14-17] in the Schrödinger picture of spectroscopy as transitions between Bohr stationary states since Eq. (1.12) is derived from first-order time-dependent perturbation theory in which the operators are independent of time and the wave functions are time dependent.

The Heisenberg picture [3, 5, 11-16, 18-21] of quantum mechanics gives an equivalent expression in which the time evolution of the of the system is placed in the operators, and the quantum states are time-independent. The Heisenberg picture leads naturally to a time correlation function; in this case, the dipole moment correlation function. In the Heisenberg picture, the dipole moment operator $\mathbf{v}$ is written as

$$\mathbf{v}(t) = \exp(iHt/\hbar)\mathbf{v}\exp(-iHt/\hbar), \tag{1.13}$$

where H is the Hamiltonian of the system. By using the Fourier expansion of the Dirac delta function, Eq. (1.13), and the closure relation [3-17, 20]

$$\sum_f |f\rangle\langle f| = 1, \tag{1.14}$$

Eq. (1.12) can be written in the Heisenberg picture as [5, 6, 11, 16, 18, 21]

$$\sigma(\omega) = \frac{1}{2\pi}\int_{-\infty}^{\infty} dt \langle \mathbf{v}(0).\mathbf{v}(t)\rangle \exp(i\omega t). \tag{1.15}$$

Equation (1.15) is the Fermi Golden Rule in the Heisenberg picture. Thus the lineshape function in the Heisenberg picture is the Fourier transform of the time-correlation function of the dipole moment operator of the absorbing molecules. Taking the inverse Fourier transform of Eq. (1.15) yields the dipole moment time-correlation functions follows

$$< \mathbf{v}(0).\mathbf{v}(t) >= \int_{-\infty}^{\infty} d\omega\ \sigma(\omega)\exp(-i\omega t). \tag{1.16}$$

For the sake of clarity, from this point on, we will not use a vector notation , and will not specify the components of vector quantities such as E, P or v, unless this is essential.

Let us consider a more general quantum mechanical time-correlation function taken at different times

$$C(t_1,t_2) = \langle A(t_1)\, B(t_2)\rangle \tag{1.17}$$

$C(t_1,t_2)$ is an expectation value of products of physical quantities A and B taken at different times. $C(t_1,t_2)$ characterizes the correlation which exists on average between interactions occurring at times t_1 and t_2. As pointed out earlier, the correlation function $C(t_1,t_2)$ depends on the time difference $t_1 - t_2 = \tau$ and therefore it is maximum when $t_1 = t_2$ (because $C(\tau)$ always peaks at $\tau = 0$) and decreases with increasing $t_1 - t_2 = \tau$, ultimately vanishes as $\tau \to \infty$. The correlation time τ is a measure of the time during which, on average, some memory of the interaction is retained. In terms of the density operator ρ (which is assumed to be known

to the reader, see Refs.[3, 5, 6, 8, 11, 14-16, 18-21]), the expectation value of a physical quantity A in state $|m\rangle$ is

$$\langle A\rangle = Tr\{\rho A\} = \sum_n \langle n|\rho A|n\rangle. \tag{1.18a}$$

Using the invariance of the trace to a cyclic permutation of operators, Tr{ABC} = Tr{BCA} = Tr{CAB}, Eq. (1.18a) can be written as

$$\langle A\rangle = Tr\{A\rho\} = \sum_n \langle n|A\rho|n\rangle, \tag{1.18b}$$

where $\{|n\rangle\}$ is some arbitrary complete orthonormal basis set. Using the relation $\rho = \sum_m P_m |m\rangle\langle m|$ in Eq. (1.18) one obtains

$$\langle A\rangle = \sum_n \sum_m p_m \langle n|m\rangle\langle m|A|n\rangle = \sum_m p_m \langle m|A|m\rangle. \tag{1.19}$$

Since the quantum mechanical time-correlation function $C(t_1,t_2)$ is an ensemble average, one can apply Eq. (1.18b) as

$$\begin{aligned} C(t_1,t_2) &= Tr\{\rho A(t_1)B(t_2)\} \\ &= \sum_n \langle n|\rho A(t_1)B(t_2)|n\rangle. \end{aligned} \tag{1.20}$$

Using the Heisenberg representation, $C(t_1,t_2)$ becomes

$$\begin{aligned} C(t_1,t_2) = Tr\{&\rho \exp(iHt_1/\hbar)A(0)\exp(-iHt_1/\hbar)\exp(iHt_2/\hbar) \\ &\times B(0)\exp(-iHt_2/\hbar)\}. \end{aligned} \tag{1.21}$$

Furthermore, according to the stationary condition (correlation function $C(t_1,t_2)$ depends on the time difference $t_1 - t_2 = \tau$) $C(t_1,t_2)$ can be written as

$$C(t_1,t_2) = \langle A(t_1)\, B(t_2)\rangle = \langle A(t_1 - t_2)\, B(t_2 - t_2)\rangle = \langle A(\tau)\, B(0)\rangle. \tag{1.22}$$

Using the Heisenberg representation, $C(t_1,t_2)$ becomes

$$C(t_1,t_2) = \langle A(\tau)\, B(0)\rangle = Tr\{\rho \exp(iH\tau/\hbar)\, A(0) \exp(-iH\tau/\hbar) B(0)\}. \tag{1.23}$$

In fact, Eq. (1.23) can be derived directly from Eq. (1.21) by using the cyclic property of the trace and the fact that ρ commutes with H.

In the classical limit Eq. (1.20) can be written as, given that the trace corresponds to an integral over phase space in the classical limit)

$$C(t_1,t_2) = \int\cdots\int dp\, dq\, f(p,q)\, A(t_1)\, B(t_2), \tag{1.23}$$

where $f(p,q)$ is the equilibrium distribution function in phase space [6, 22] whose quantum mechanical analog is the density operator ρ as follows

$$\rho = \frac{\exp(-\beta H)}{Tr(\exp(-\beta H))} \leftrightarrow f(p,q) = \frac{\exp(-\beta H_c(p,q)}{\int\cdots\int dp\, dq \exp(-\beta H_c(p,q))}. \tag{1.24}$$

where $H_c(p,q)$ denotes the classical Hamiltonian.

In view of time-correlation functions central importance in understanding the response of physical systems to external perturbation, some of their properties are now examined. Several important properties of a one-sided correlation function (time dependence

occurs only on the right-hand side v(t) of $\langle v(0)v(t)\rangle$) follow from the fact that $\sigma(\omega)$ is a real quantity. Assuming that C(t) is a one-sided correlation function we have

$$\begin{aligned}\sigma(\omega) &= \sigma^*(\omega) \\ &= \frac{1}{2\pi}\int_{-\infty}^{\infty} dt\, C^*(t)\exp(-i\omega t),\end{aligned} \tag{1.25}$$

(where the asterisk (*) denotes the complex conjugate). Upon changing the integration variable to -t, Eq. (1.25) becomes

$$\begin{aligned}\sigma(\omega) &= -\frac{1}{2\pi}\int_{\infty}^{-\infty} dt\, C^*(-t)\ \exp(i\omega t) \\ &= \frac{1}{2\pi}\int_{-\infty}^{\infty} dt\, C^*(-t)\ \exp(i\omega t)\end{aligned} \tag{1.26}$$

Comparing Eqs. (1.15) and (1.26), we have

$$C(t) = C^*(-t). \tag{1.27}$$

Since C(t) is a complex function (by Eq. (1.27)), it can be broken into real and imaginary parts

$$C(t) = C'(t) + iC''(t) \tag{1.28}$$

it follows from Eq. (1.27) that

$$C'(t) = C'(-t) \tag{1.29a}$$

and

$$C''(t) = -C''(-t). \tag{1.29b}$$

Thus the real part of the correlation function is an even function of time while the imaginary part is an odd function of time.

Quantum mechanical correlation functions are generally complex quantities and have both even and odd parts as a function of time [3-6, 10-13, 18]. If the correlation function is obtained by a cononical Boltzmann ensemble, then the real (even) and imaginary (odd) parts are related to each other. Using the following relationship (which comes from Eq. (6.9b) in Ref. [3])

$$\chi''(\omega) = \frac{\rho_i}{\hbar}[1 - \exp(-\beta\hbar\omega)]\sigma(\omega), \tag{1.30}$$

where $\chi''(\omega)$ is imaginary part of the susceptibility $\chi(\omega)$ and $\beta = (kT)^{-1}$, one can see that

$$\sigma(\omega) = \sigma(-\omega)\exp(-\beta\hbar\omega) \tag{1.31}$$

given that $\chi''(\omega)$ is an odd function. Utilizing Eq. (1.31), one can show that the imaginary part of the quantum mechanical correlation function, C"(t), can be determined by differentiating the real part, C'(t), [23-25]

$$C''(t) = -Tan[(\beta\hbar/2)\frac{\partial}{\partial t}]C'(t). \tag{1.32}$$

In the high temperature limit, $\beta\hbar/2 << 1$, Eq. (1.32) can expanded to give

$$C''(t) = -(\beta\hbar/2)\frac{\partial}{\partial t}C'(t). \tag{1.33}$$

Thus at high temperatures the imaginary part of the correlation function has insignificant contribution, which goes to zero in the classical limit ($\hbar \to 0$). Therefore, the imaginary part, C"(t), is purely quantum mechanical.

Using the symmetry properties in Eq. (1.29), one can eliminate the negative times from the integration in Eq. (1.15). For example

$$\begin{aligned}
\sigma(\omega) &= \frac{1}{2\pi}\int_{-\infty}^{\infty} dt\, C(t)\exp(i\omega t) \\
&= \frac{1}{2\pi}\int_{0}^{\infty} dt\, C(-t)\exp(-i\omega t) + \frac{1}{2\pi}\int_{0}^{\infty} dt\, C(t)\exp(i\omega t) \\
&= \frac{1}{2\pi}\int_{0}^{\infty} dt\, C^{*}(t)\exp(-i\omega t) + \frac{1}{2\pi}\int_{0}^{\infty} dt\, C(t)\exp(i\omega t) \\
&= \frac{1}{2\pi}\int_{0}^{\infty} dt[C^{*}(t)\,\exp(-i\omega t) + C(t)\,\exp(i\omega t)] \\
&= \mathrm{Re}\frac{1}{\pi}\int_{0}^{\infty} dt\, C(t)\,\exp(i\omega t).
\end{aligned} \tag{1.34}$$

Eq. (1.34) is convenient for numerical calculations because it limits the integration to only positive times.

Although the calculation of correlation functions for all times is a difficult dynamical calculation, one could do a Taylor series expansion of the correlation functions about the initial time; see Refs.[6, 10, 12, 13, 22] for details. For further discussions of time-correlation functions in spectroscopy, the reader is referred to refs.[4, 12, 13, 15, 18, 21, 23-31].

1.1.3 Linear Optical Response Function

Practically all physical experiments involve the application of an external perturbation or force $f(t')$ on a system initially in equilibrium in order to elicit a response, $y(t)$. Such is the case, for example, when an electric field induces an electric dipole moment in atoms or molecules. If the perturbation is sufficiently weak , the relation between $y(t)$ and $f(t')$ is linear. As the perturbation grows in magnitude, the assumption of linear dependence becomes less tenable and ultimately must be replaced by a non-linear dependence. The response then no longer depends on the first power of $f(t')$ but rather on higher powers or, if several perturbations are acting sequentially, on their product. Specifically, it is assumed that $f(t')$ is the electric field $E(\mathbf{r},t')$, and $y(t)$ is the polarization $P(\mathbf{r},t)$ (response of the system) a rising from a redistribution of charges within the system exposed to the electric field.

We begin with the linear case to introduce the general formalism of a system responding to an external perturbation. A non-local spatial dependence of the response at a point $\mathbf{r}$ depends not only on $E(\mathbf{r},t')$ but also on $E(\mathbf{r}',t')$ where $E(\mathbf{r}',t')$ is the perturbation at other points $\mathbf{r}'$. Here we will not consider the spatial dependence of the response function under the local spatial dependence assumption, i.e., the response at a point depends only on the force (the electric field) acting on the same point and no other [3]. The general relation between $E(\mathbf{r},t')$ and the response $P(\mathbf{r},t)$, to first order, may then be written as

$$P^{(1)}(\mathbf{r},t) = \int_{-\infty}^{t} S^{(1)}(t,t')\, E(\mathbf{r},t')\, dt', \tag{1.35}$$

where t is the time the field is applied and $S^{(1)}(t,t')$ is the first order *response function* (also called the after effect or Green's function; it is an intrinsic property of the physical system and is independent of the applied field. (Equation. (1.35) is known as Kubos' formula [4, 8, 12]). In general, there may be a delay between the applied field and the polarization induced

by the field. The response function represents a time lag of the system. If the system can respond instantaneously to $E(\mathbf{r},t')$, then $S^{(1)}(t,t')$ is a delta function. Ordinarily, however, the system lags behind $E(\mathbf{r},t')$, and $S^{(1)}(t,t')$ is monotonically decaying function of time. The lower limit in the integral has been set equal to $-\infty$ to allow $E(\mathbf{r},t')$ to build up gradually from the distant past. The response function $S^{(1)}(t,t')$ depends on the difference $t-t'$ rather than on t and t' separately. Equation. (1.35) then assumes the form

$$\begin{aligned} P^{(1)}(\mathbf{r},t) &= \int_{-\infty}^{t} S^{(1)}(t-t')\, E(\mathbf{r},t')\, dt' \\ &= \int_{-\infty}^{0} S^{(1)}(\tau)\, E(\mathbf{r},t+\tau)\, d\tau. \end{aligned} \tag{1.36}$$

Next the linear optical polarization will be calculated in terms of the linear response function, which was first developed by Kubo [4, 8, 12]. Although Mukamel has done extensive work on calculating the response functions[3], his formalism will not be adopted in this chapter because it involves Liouville space notation. Therefore, the linear optical polarization will be calculated in Hilbert space, and the resulting response function will be compared to Mukamel's result [3].

One can start calculating the optical polarization by assuming that the system is in thermal equilibrium at $t=t_0$ (later taken to be $-\infty$) with respect to its Hamiltonian H_0, and its state is

$$\rho(t_0)=\rho(-\infty)=\frac{\exp(-\beta H_0)}{Tr\{\exp(-\beta H_0)\}}. \tag{1.37}$$

When the perturbation $H'(t)$ is applied to the system at $t=t_0$, the system becomes in non-equilibrium state for $t>t_0$ that can be described by the quantum Liouville equation in the

Schrödinger picture [3-21]

$$\frac{\partial}{\partial t}\rho(t) = -\frac{i}{\hbar}[H_0,\rho(t)] - \frac{i}{\hbar}[H'(t),\rho(t)] \tag{1.38}$$

where the total Hamiltonian of the system at $t > t_0$ is

$$H = H_0 + H'(t) \tag{1.39a}$$

where

$$H'(t) = -\mathrm{v}\ E(\mathbf{r},t) \tag{1.39b}$$

It turns out to be more convenient to transform Eq. (1.38) to the interaction picture[3-21] as

$$\frac{\partial}{\partial t}\tilde{\rho}(t) = -\frac{i}{\hbar}[\tilde{H}'(t),\tilde{\rho}(t)] \tag{1.40}$$

where $\tilde{\rho}(t)$ and $\tilde{H}'(t)$ are the density and the interaction Hamiltonian operators in the interaction picture. For example, the density operator in the interaction picture is

$$\tilde{\rho}(t) = \exp(iH_0(t-t_0)/\hbar)\ \rho(t)\ \exp(-iH_0(t-t_0)/\hbar) \tag{1.41}$$

Eq. (1.40) is quantum Liouville equation in the interaction picture. Of particular importance here is the appearance in the commutator of the perturbation Hamiltonian rather than the total Hamiltonian in Eq. (1.41).

Equation (1.40) is a homogeneous first order ordinary differential equation that can be converted to an integral equation starting with the initial condition $\tilde{\rho}(t) = \rho(t_0)$ as follows:

$$\tilde{\rho}(t) = \rho(t_0) - \frac{i}{\hbar}\int_{t_0}^{t} [\tilde{H}(t'), \tilde{\rho}(t')]\, dt'. \tag{1.42}$$

Successive substitutions of Eq. (1.42) in Eq. (1.40) generates the pertubative expansion of $\rho(t)$ [3, 11, 18, 21, 30-33]

$$\tilde{\rho}(t) = \tilde{\rho}^{(0)}(t) + \tilde{\rho}^{(1)}(t) + \tilde{\rho}^{(2)}(t) + \cdots \tilde{\rho}^{(n)}(t) + \cdots\cdots \tag{1.43}$$

where

$$\tilde{\rho}^{(0)}(t) = \tilde{\rho}(t_0) = \rho(t_0) \tag{1.44a}$$

$$\tilde{\rho}^{(1)}(t) = -\frac{i}{\hbar}\int_{t_0}^{t} dt_1 [\tilde{H}(t_1), \rho(t_0)], \tag{1.44b}$$

$$\begin{aligned} \tilde{\rho}^{(2)}(t) &= -\frac{i}{\hbar}\int_{t_0}^{t} dt_1 [\tilde{H}(t_1), \tilde{\rho}^{(1)}(t_1)] \\ &= \left(-\frac{i}{\hbar}\right)^2 \int_{t_0}^{t} dt_1 \int_{t_0}^{t_1} dt_2 [\tilde{H}(t_1), [\tilde{H}(t_2), \rho(t_0)]], \end{aligned} \tag{1.44c}$$

$$\begin{aligned} \tilde{\rho}^{(n)}(t) = \left(-\frac{i}{\hbar}\right)^n \int_{t_0}^{t} dt_1 \int_{t_0}^{t_1} dt_2 \cdots\cdots \int_{t_0}^{t_{n-1}} dt_n \\ \times [\tilde{H}(t_1), [\tilde{H}(t_2), \cdots\cdots [\tilde{H}(t_n), \rho(t_0) \cdots], \end{aligned} \tag{1.44d}$$

with

$$t > t_1 > t_2 > \cdots > t_0 \tag{1.45}$$

These equations enable us to make successive approximations to $\tilde{\rho}(t)$ when $\tilde{\rho}(t_0) = \rho(t_0)$ is known. They have a wide range applicability in time-dependent perturbation theory and play a fundamental role in the description of linear and nonlinear spectroscopy. For the sake of convenience we shall assume that the operators are in the interaction picture without using

"~" on top of the operators, unless this is essential. In terms of the density operator, the optical polarization $P(\mathbf{r},t)$ can be written as the expectation value of the dipole moment operator as

$$P(r,t) = Tr\{\mathrm{v}\,\rho(t)\}, \tag{1.46}$$

substituting Eq. (1.43) in Eq. (1.46), one obtains

$$\begin{aligned} P(\mathbf{r},t) &= Tr\{\mathrm{v}\,[\rho^{(0)}(t)+\rho^{(1)}(t)+\rho^{(2)}(t)+\cdots+\rho^{(n)}(t)+\cdots]\} \\ &= Tr\{\mathrm{v}\,\rho^{(0)}(t)\}+Tr\{\mathrm{v}\,\rho^{(1)}(t)\}+Tr\{\mathrm{v}\,\rho^{(2)}(t)\}\cdots+ \\ &\quad Tr\{\mathrm{v}\,\rho^{(n)}(t)\}+\cdots \\ &= P^{(0)}(\mathbf{r},t)+P^{(1)}(\mathbf{r},t)+P^{(2)}(\mathbf{r},t)+\cdots+P^{(n)}(\mathbf{r},t)+\cdots \end{aligned} \tag{1.47}$$

It is assumed that $P^{(0)}(\mathbf{r},t)$ vanishes at thermal equilibrium. Clearly, from Eq. (1.47),

$$P^{(n)}(\mathbf{r},t) = Tr\{\mathrm{v}\,\rho^{(n)}(t)\}. \tag{1.48}$$

Therefore with Eq. (1.44b), one obtains

$$P^{(1)}(\mathbf{r},t) = Tr\left\{\mathrm{v}\left(-\frac{i}{\hbar}\int_{t_0}^{t} dt_1\,[\mathrm{H}'(t_1),\rho(t_0)]\right)\right\}. \tag{1.49}$$

One can set $t_0 = -\infty$ and rewrite Eq. (1.49) using Eq. (1.39b) as

$$\begin{aligned} P^{(1)}(\mathbf{r},t) &= Tr\left\{\left(-\frac{i}{\hbar}\int_{-\infty}^{t} dt_1\;\mathrm{v}\;[\mathrm{H}'(t_1),\rho(-\infty)]\right)\right\} \\ &= -\frac{i}{\hbar}\int_{-\infty}^{t} dt_1\;\mathrm{Tr}\{\mathrm{v}\;[\mathrm{v}(t_1),\rho(-\infty)]\}\;E(\mathbf{r},t_1) \end{aligned} \tag{1.50}$$

upon invoking the cyclic property of the trace and the fact that $\rho(-\infty)$ commutes with H_0, Eq. (1.50) becomes

$$\begin{aligned} P^{(1)}(\mathbf{r},t) &= -\frac{i}{\hbar}\int_{-\infty}^{t} dt_1\ \mathrm{Tr}\{[\mathrm{v}(t_1),\rho(-\infty)]\,\mathrm{v}\}\ E(\mathbf{r},t_1) \\ &= -\frac{i}{\hbar}\int_{-\infty}^{t} dt_1\ \mathrm{Tr}\{[\mathrm{v},\mathrm{v}(t_1)]\,\rho(-\infty)\}\ E(\mathbf{r},t_1) \\ &= -\frac{i}{\hbar}\int_{-\infty}^{t} dt_1\ \langle[\mathrm{v},\mathrm{v}(t_1)]\,\rho(-\infty)\rangle\, E(\mathbf{r},t_1) \end{aligned} \tag{1.51}$$

Comparing this expression with Eq. (1.35) or Eq. (1.36), it is seen that the linear response function is of the following form

$$\begin{aligned} S^{(1)}(t) &= -\frac{i}{\hbar}\langle[\mathrm{v},\ \mathrm{v}(t)]\rho(-\infty)\rangle \\ &= \frac{i}{\hbar}\langle[\mathrm{v}(\mathrm{t}),\ \mathrm{v}]\rho(-\infty)\rangle \\ &= \frac{i}{\hbar}(J(t)-J^{*}(t)) \\ &= -\frac{2}{\hbar}\mathrm{Im}\,J(t), \end{aligned} \tag{1.52}$$

where

$$J(t) = \langle \mathrm{v}(\mathrm{t})\ \mathrm{v}\ \rho(-\infty)\rangle \tag{1.53a}$$

and

$$J^{*}(t) = \langle \mathrm{v}\ \mathrm{v}(\mathrm{t})\ \rho(-\infty)\rangle. \tag{1.53b}$$

J(t) is the dipole moment two-point time-correlation function. The response function defined in Eq. (1.52) is identical to Mukamel's result, see Eqs. (5.18)-(5.20) of Ref. [3]. Note that

$P^{(1)}(\mathbf{r},t)$ in Eqs. (1.48)-(1.52) contains two dipole moment operators; Eq. (1.48) indicates that $P^{(n)}(\mathbf{r},t)$ will have $n+1$ dipole moment operators.

This concludes the presentation of the basic description and derivation of the linear optical response function. Non-linear response functions will be discussed in Chapter 2. In the next section the harmonic interactions that can take place when nuclear (vibrational) motions (e.g., phonons in crystals) couple to the electronic transition of a chromophore in a condensed phase will be examined.

1.2 Electron-Phonon Coupling

Normally optical lineshapes for condensed phase systems are determined by the nature of electron-vibration coupling. In the harmonic approximation, phonons (in a solid environment) can couple to the electronic transition of the chromophore linearly, by linearly displacing the upper potential energy curve of the excited electronic state $|e\rangle$ relative to the equilibrium nuclear position of the ground electronic state $|g\rangle$, and quadratically ,by changing the curvature of the upper potential energy curve. This, in turn, changes the force constant, on account of the electronic charge redistribution, which leads to changing the frequency of the vibrational mode upon electronic excitation. Figure 1.1 shows a schematic representation of the potential energy curves of the two electronic states based on the harmonic approximation. The diagonal force constant in the excited state gives rise to diagonal quadratic coupling, while the off-diagonal force constant rotates the normal coordinates of the excited electronic state relative to those of the ground state. This off-diagonal quadratic coupling is the Duschinsky effect [34-36] and is important when Herzberg-Teller coupling (strong dependence on the nuclear coordinates) [34] cannot be neglected [35]. Thus the Duschinsky effect can be neglected for a chromophore that possesses strongly allowed electronic transitions in the Condon approximation (weak dependence on the nuclear coordinates) since Herzberg-Teller coupling seeme to be the most

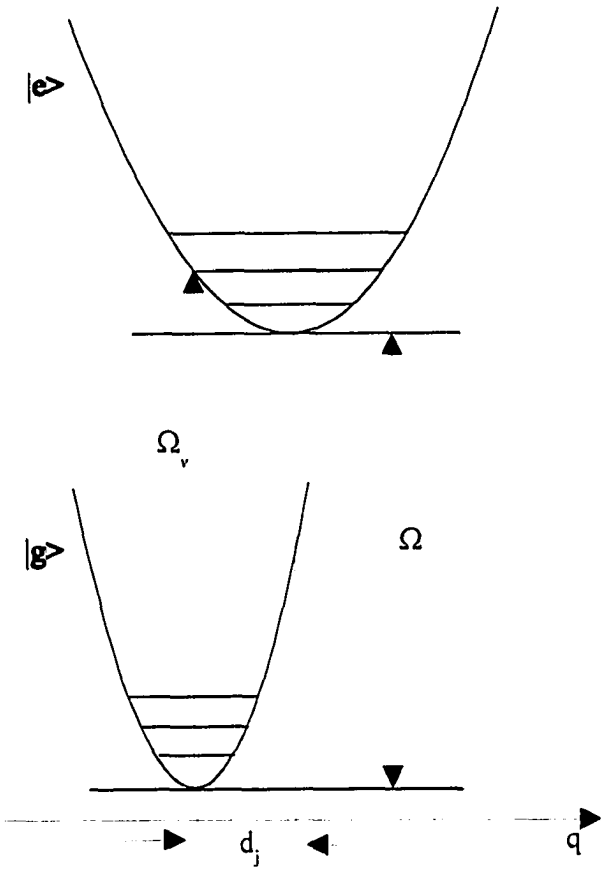

Figure 1.1 Schematic representation of changes of the upper adiabatic potential energy curve relative to the lower one due to both linear and quadratic electron-phonon coupling upon electronic excitation. Ω_v is the vertical (Franck-Condon principle) transition frequency and Ω the adiabatic electronic energy gap. which is defined as the distance between the minima of the potential energy curves. It indicates that the upper potential well has changed in two ways with respect to the lower one upon electronic excitation; it is displaced to the right and it has a different curvature (different force constant) which changes the frequency for the vibrations (phonons) in the excited electronic state.

important requirement for the Duschinsky effect [36]. Note that the Duschinsky effect can only be applied when two or more modes are present. Here we shall consider only the linear (linear displacement) and diagonal quadratic electron-phonon coupling (frequency change).

Consider absorption from the ground electronic state (g) to an excited electronic state (e) and let ω'' and ω' be, respectively, the ground and excited state frequencies of a vibrational mode. Let q be the dimensionless normal coordinate of this mode for the ground electronic state. It is related to the mass-weighted coordinate, Q, by $q = (\omega''/\hbar)^{1/2}Q$. Similarly, we define d as the dimensionless translational displacement between the potential energy minima of the two electronic states. For linear and diagonal quadratic electron-phonon coupling the excited state vibrational Hamiltonian is given exactly by

$$H_e = H_g + \frac{\hbar\omega''}{2}[(r^2-1)q^2 + 2r^2 qd + r^2 d^2] + \hbar\Omega, \tag{1.54}$$

where $r = (\omega'/\omega'')$. $\hbar\Omega$ is the adiabatic electronic energy gap. The r^2d^2 term multiplied by $\hbar\omega''/2$ is the optical reorganization energy. Thus,

$$\Omega_v = \Omega + \omega'' r^2 d^2/2, \tag{1.55}$$

where Ω_v is the vertical (Condon) frequency gap. In Eq. (1.54), H_g is the vibrational Hamiltonian for the ground state:

$$H_g = \hbar\omega''(a^+a + 1/2), \tag{1.56}$$

with a^+ and a the raising and lowering operators for the ground state, i.e. $q = 2^{-1/2}(a^+ + a)$. For a multi-mode system one need only sum Eq. (1.54) over all modes.

The excited state vibrational Hamiltonian can be approximated for r ≥ 0.7 as follows (see Chapter 3 for details)

$$H_e \approx \hbar\omega'\left[\left(a^+a+\frac{1}{2}\right)+(2-r^{-1})d(a^++a)/\sqrt{2}+(2-r^{-1})d^2/2\right]+\hbar\Omega \tag{1.57}$$

It is the elimination of a^{+2} and a^2 that simplifies tremendously evaluation of the linear and non-linear response functions. An approximate electronic dipole moment correlation function for both linear and diagonal quadratic electron-phonon coupling for ≤ 30% frequency change, the linear absorption lineshape function, and the resulting Franck-Condon (FC) factors will be derived using the excited state Hamiltonian in Eq. (1.57) and discussed in Chapter 3.

So as to be able to rest on solid grounds we shall proceed from the simplest electron-phonon coupling cases to successively more involved ones. Let us consider first the linear coupling case and the relevant features such as the reorganizational energy, linear displacement, absorption lineshape function, and FC factors.

1.2.1 Linear Coupling

Linear coupling is considered starting with the well-known expression for the electronic dipole moment correlation function $J(t;T)$, without a damping constant, (which we will obtain in Chapter 3) to illustrate the spectroscopic features that accompany linear electron-phonon coupling. $J(t;T)$, for a multi-mode system reads

$$J(t;T), = \exp[-g(t;T)-i\Omega_v t], \tag{1.58}$$

where the lineshape function

$$g(t;T) = \sum_j g_j(t;T), \tag{1.59a}$$

with

$$g_j(t;T) = S_j[\coth(\beta\hbar\omega_j)(1-\cos(\omega_j t) + iSin(\omega_j t) - i\omega_j t] \tag{1.59b}$$

and the vertical transition frequency, obtained by setting $\omega' = \omega'' = \omega_j$ in Eq. (1.55), (see Figure 1.2)

$$\Omega_v = \Omega + S_j\omega_j. \tag{1.59c}$$

The first term, Ω, in Eq. (1.59c) is the adiabatic electronic energy gap, which is defined as the distance between the minima of the potential energy curves of the two electronic states (see Figure 1.2). The second term in Eq. (1.59c) represents the optical reorganizational energy $\lambda_j \equiv S_j\omega_j$, with $S_j = d_j^2/2$ being Huang-Rhys factor and ω_j is the frequency of mode j. Figure 1.2 illustrates the Franck-Condon principle at the top for different cases of linear displacement and the corresponding absorption spectra. It also shows that the only change in the upper potential energy curve is its nuclear separation (no curvature change) due to only linear coupling. Huang-Rhys factor, S_j, is a dimensionless coupling strength parameter that measures the linear displacement of upper potential energy curve, which is a consequence of the linear interaction between a chromophore (electronic transition) and the surrounding environment (phonons). For example, in Figure 1.2 (a), for $S_j = 0$, the chromophore is not linearly interacting with the phonons and the absorption spectrum is purely electronic. (However, there might be higher-order interactions, e.g., quadratic or anharmonic, taking place, as will be discussed later.) When the phonons couple to the electronic transition S_j is greater than zero. Therefore, the more the phonons coupling to the electronic (0,0) transition (ZPL), the larger S_j (more interaction between the chromophore and its environment) becomes as shown in Figure 1.2 (b) and (c) . For strong electron-phonon coupling ($S_j >> 1$),

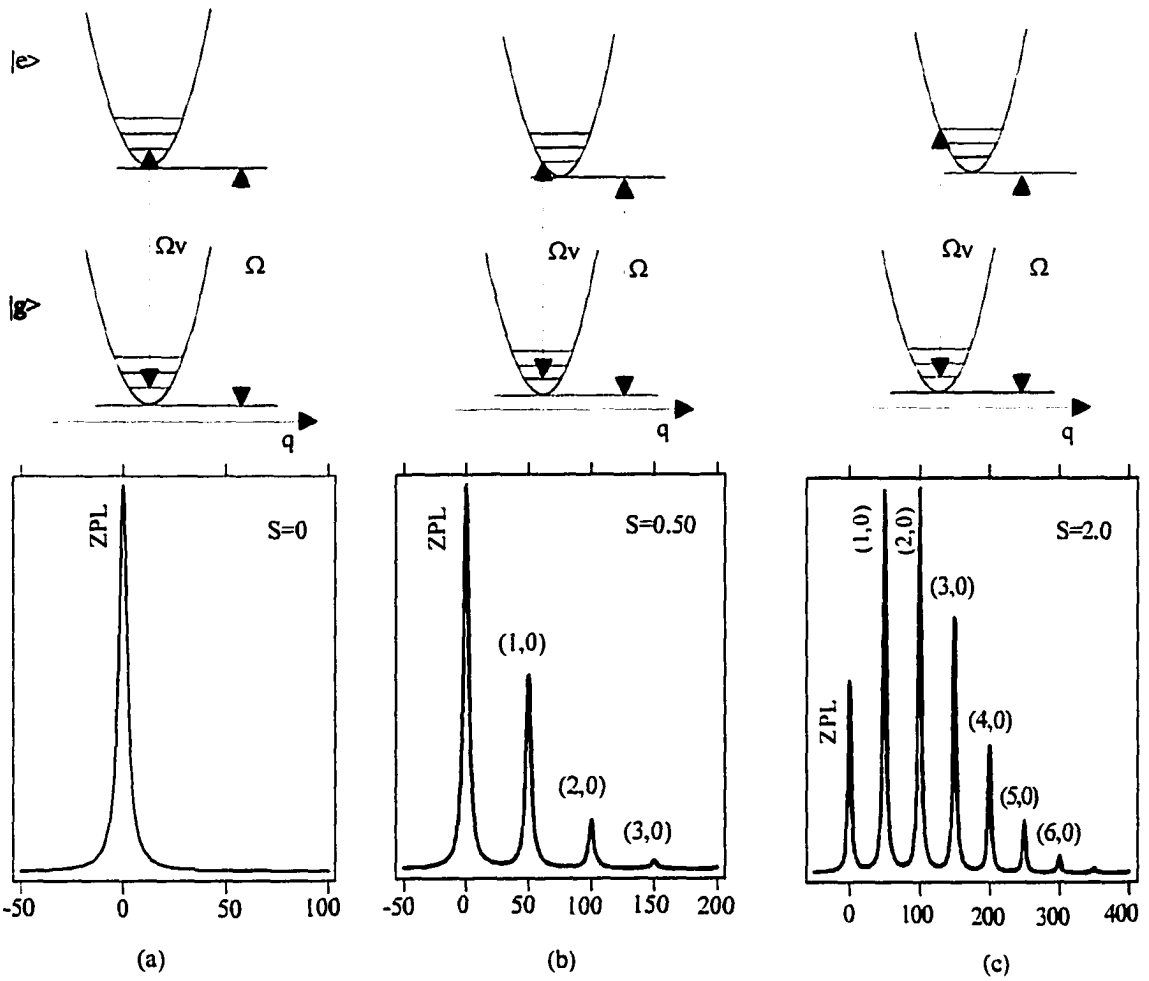

Figure 1.2 Potential energy curves illustrating the basis for Franck-Condon principle and their corresponding absorption spectra calculated using Eq. (1.60) with ω_j= 50 cm^{-1}, $\gamma_j = 5 cm^{-1}$ and T = 0 K. The upper potential energy curve lies directly above the lower one (d = 0), the spectrum is purely electronic ($e^{-S} = 1$) in (a) , is slightly shifted to the right due to S = 0.50 (weak coupling) where the ZPL is still the most intense band ($e^{-S} = 0.60$ $(1 - e^{-S} = 0.40)$) in (b), and with greater linear displacement due to S = 2 (strong coupling) where (2,0) transition is the most intense one and the ZPL is getting weaker ($e^{-S} = 0.13$ $(1 - e^{-S} = 0.87)$) in (c).

the (0,0) transition (zero-phonon line (ZPL)) intensity becomes too weak to be observed and the multi-phonon transitions (phonon sideband (PSB)) will dominate the absorption profile, as in Figure 1.3. Next, we will demonstrate the above discussion by taking the Fourier transform (FT) of Eq. (1.58) to obtain the linear absorption lineshape function in the frequency-domain from which we can deduce FC factors.

FT of Eq. (1.58) for mode j is ($\Omega = 0$) (Appendix B of Chapter 3)

$$\sigma_j(\omega;T) = \exp\left[-S_j \coth\left(\frac{\beta\hbar\omega_j}{2}\right)\right] \sum_{m=-\infty}^{\infty} \exp(m\beta\hbar\omega_j/2)\, I_m(z_o)\, \delta(\omega - m\omega_j), \tag{1.60}$$

where $z_0 = S_j \operatorname{csch}(\beta\hbar\omega_j/2)$ and $I_m(z_0)$ are modified Bessel functions and the integer m signifies the net change in the number of phonons (creations and annihilations) associated with the phononic transitions, but is not a quantum number. Equation (1.60) is not very spectroscopically insightful due to the presence of Bessel functions and the temperature dependence. However, we can work at a simpler level in the limit where $T \rightarrow 0$ K, then $\sigma(\omega)$ becomes

$$\sigma(\omega) = \exp(-S_j) \sum_{m=0}^{\infty} \frac{S_j^{\,m}}{m!}\, \delta(\omega - m\omega_j), \tag{1.61a}$$

and one can write Eq. (1.61a) as

$$\sigma(\omega) = \exp(-S_j)\, \delta(\omega - 0.\omega_j) + \exp(-S_j) \sum_{m=1}^{\infty} \frac{S_j^{\,m}}{m!}\, \delta(\omega - m\omega_j). \tag{1.61b}$$

This form will simplify the discussion of FC factors for the cold transitions below. Since we are in the low temperature limit, the quantum number of the initial state for the absorption

transition is zero. m is the final state quantum number. The presence of a delta function in Eqs. (1.60) and (1.61) implies that the (0, 0) transition (no change in the number of phonons) occurs at ω = 0 and the multi-phonon transitions occur at $\omega = m\omega_j$. For instance, Figure 1.2 (b) is an absorption spectrum with ω_j= 50 cm^{-1}, it shows that the (0,0), (1,0), (2,0), (3,0) transitions appear at ω = 0, 50, 100, 150 cm^{-1}, respectively. The first term in Eq. (1.61b) describes an optical electronic transition without creation of phonons and, therefore, it represents the zero-phonon line (ZPL). The second term in Eq. (1.61b) describes the phonon sideband (PSB). The mth term represents a phononic (vibrational) transition which involves a creation of m phonons. Note that since T = 0 K, annihilation process of phonons does not occur.

The first term in Eq. (1.61b) dictates that the FC factor for the ZPL is

$$|\langle 0|0\rangle|^2 = \exp(-S_j), \tag{1.62}$$

which indicates that when S_j is large, the integrated intensity of the ZPL is relatively small. The second term in Eq. (1.61b) shows that the FC factors for the 0 → m (m ≥ 1) transitions are

$$|\langle m|0\rangle|^2 = \exp(-S_j)\, S_j^m / m!. \tag{1.63}$$

Using Stirling's approximation [37], Eq. (1.63) can be approximated as [38]

$$|\langle m|0\rangle|^2 \approx \exp(-S_j)\exp[-m(\ln(2m/d_j^2) - 1)], \tag{1.64}$$

Eq. (1.64) has a maximum at m = S_j. For example, when S_j = 1, then the 0 → 1 transition will be the most intense band in the spectrum, as evident from Figures 1.2 (c) and 1.3. But if

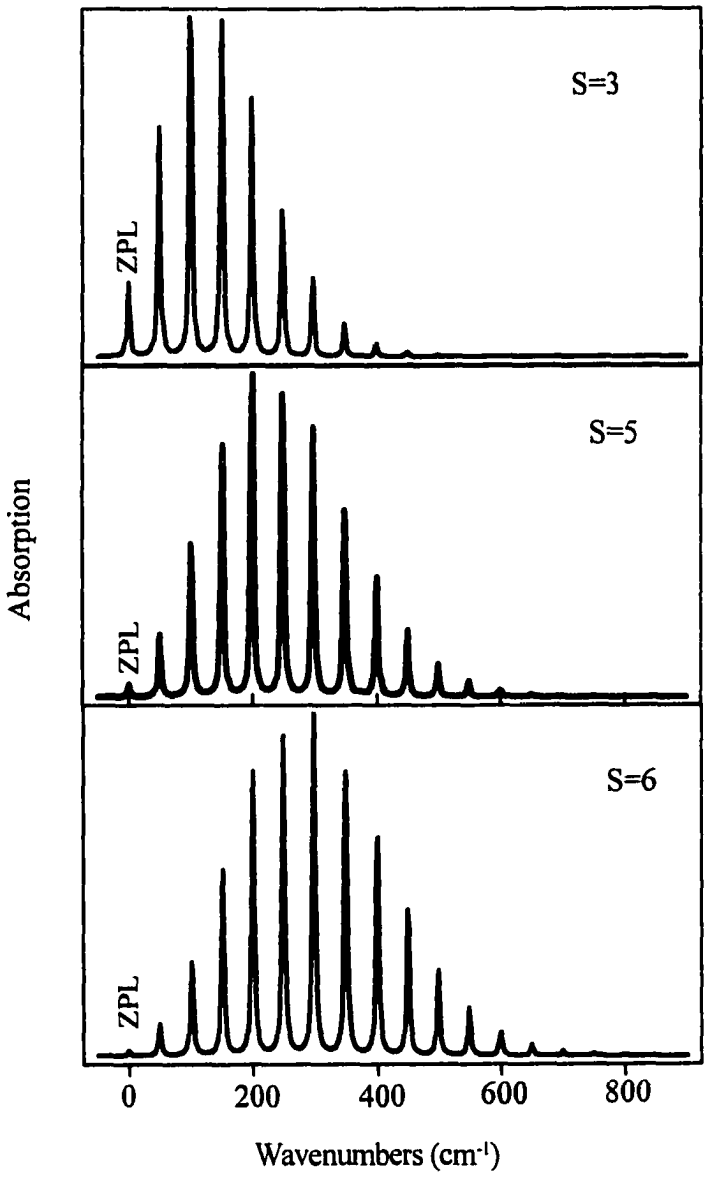

Figure 1.3 Examples of strong linear electron-phonon coupling where the multi-phonon transitions dominate the absorption profile. Parameters are the same as in Figure 1.2 but using different values of S. As S increases the ZPL intensity gets weaker where the most intense transition is the one that creates number of phonons equal S (e.g., for S = 3, 5, 6, (3,0), (5,0), (6,0) transitions are the strongest ones, respectively). Note the ZPL intensity is diminishing for S =5 ($e^{-S} = 0.007$) and 6 ($e^{-S} = 0.002$) and the spectrum is approaching a Gaussian distribution in accordance with Eq. (1.57) .

$S_j < 1$, then the ZPL will be the most intense band in the spectrum, as in Figure 1.2 (b). It is interesting to point out that Eq. (1.63) is the Poisson probability distribution, $P(m)$, and therefore

$$\sum_{m=0}^{\infty} \exp(-S_j) \frac{S_j^m}{m!} = 1. \tag{1.65}$$

An important property of the Poisson distribution is that as S_j gets very large, it becomes a Gaussian distribution (see Figure 1.3) [39] as

$$P(m) = \frac{1}{\sqrt{2\pi S_j}} \exp[-(m - S_j)^2 / 2S_j^2] \tag{1.66}$$

Equation (1.66) clearly shows that the maximum of the absorption profile is at $m = S_j$ as can clearly be seen from Figure 1.3. The other extreme is when $S_j \rightarrow 0$ (the adiabatic potentials are identical), then the absorption spectrum is a $\delta(\omega)$. In this case, the phonons are completely decoupled from the electronic transition, and do not show up in the spectrum (see Figure 1.2 (a)).

Let us compare our FC factor results with those that were first calculated by Huang and Rhys [40] (1950) and Pekar [41] (1950) using the overlap integrals of the simple harmonic oscillator wave functions. FC factors for linear coupling are [38]

$$|\langle m|n\rangle|^2 = \exp(-S_j) \frac{n!}{m!} S_j^{(m-n)} [L_n^{(m-n)}(S_j)]^2, \quad n > m \tag{1.67}$$

where m and n denote the quantum numbers for the final and initial vibrational states, and $L_n^{(m-n)}$ are the associated Laguerre polynomials. Using Eq. (1.67), the FC factors for the $0 \rightarrow$ m transitions are

$$|\langle m|0\rangle|^2 = \exp(-S_j)\frac{1}{m!}S_j^{(m)}[L_0^{(m)}(S_j)]^2, \quad m \geq 0 \tag{1.68}$$

but when $L_0^{(m)}(S_j) = 1$, then Eq. (1.68) is identical to Eq. (1.63). The FC factors in Eq. (1.67) are temperature independent, for temperature dependent FC factors see Eq. (13) of Ref. [42].

In summary, it has been shown, via the absorption lineshape and FC factors, that when S < 1 the ZPL dominates the absorption profile, and when S >> 1 the PSB is the dominant. Therefore, one can conclude that S_j is the most important quantity in the linear coupling approximation, and it gives rise to the PSB and its associated ZPL.

1.2.1.1 Lorentzian Lineshapes

To generate single-site absorption spectra, the delta functions in Eq. (1.61a) need to be replaced with normalized lorentzians such that all bands in the spectrum have a fwhm of γ_j. This results in

$$\sigma(\omega) = \exp(-S_j)\sum_{m=0}^{\infty}\frac{S_j^m}{m!}\frac{\gamma_j/2\pi}{(\omega - m\omega_j)^2 + (\gamma_j/2)^2}, \tag{1.69}$$

and will enable us to see the structure of the absorption profile, i.e., Franck-Condon progressions, see Figures 1.2 and 1.3. Equation (1.60) is unphysical because it implies that the lifetimes of the excited electronic state and the vibrational states are the same. This problem will be resolved in Chapter 3. However, using Eq. (29) of Chapter 3, physical single-site absorption spectra can be generated where the ZPL carries a width of γ_{el} (fwhm) and the progression members carry widths given by

$$(fwhm)_m = \gamma_{el} + m\gamma_j, \quad m \geq 1 \tag{1.70}$$

as shown in Figure 1.4. Of course, at T = 0 K pure electronic dephasing (T_2^*) processes do not take place and, therefore, the above $1/\gamma_{el}$ simply represents the excited electronic state lifetime (T_1).

If the sample temperature T ≠ 0, processes of creation and annihilation of phonons take place; more phonons will be thermally populated and, as a result, more multi-phonon transitions occur. Equation (1.60) shows that the ZPL FC factor is $\exp[-S_j \coth(\beta\hbar\omega_j/2)]$ and that of the PSB is $(1-\exp[-S_j \coth(\beta\hbar\omega_j/2)])$. This thermal population leads to electron-phonon scattering (elastic scattering, i.e., no energy change) and, in turn, causes a phase shift [5, 14, 16, 17] of the excited electronic state wave-function which manifests itself in the absorption spectrum as a spectral broadening of the ZPL. This spectral broadening is called *pure dephasing* and depends on temperature such that it increases as temperature increases For example, as the temperature increases, more phonons are thermally populated, which leads to more scattering of the phonons at the impurity center and results in a greater phase shift (*pure dephasing*). Thus, it is reasonable to assume that the total homogeneous line width of the ZPL is determined by total dephasing time T_2 of the optical transition:

$$\frac{1}{T_2} = \frac{1}{2T_1} + \frac{1}{T_2^*} \tag{1.71}$$

where T_1 is the excited electronic state lifetime and T_2^* is the pure dephasing time.

In order to produce temperature dependent single-site absorption spectra, the delta functions in Eq. (1.60) need to be replaced with normalized lorentzians such that all the bands in the spectrum (including the ZPL) carry γ_j (fwhm) width. Again, this is unphysical, *vide infra*, but it allows us to clearly see how the structure of a single-site absorption profile changes as one raises the temperature. For example, if the sample is heated the integrated

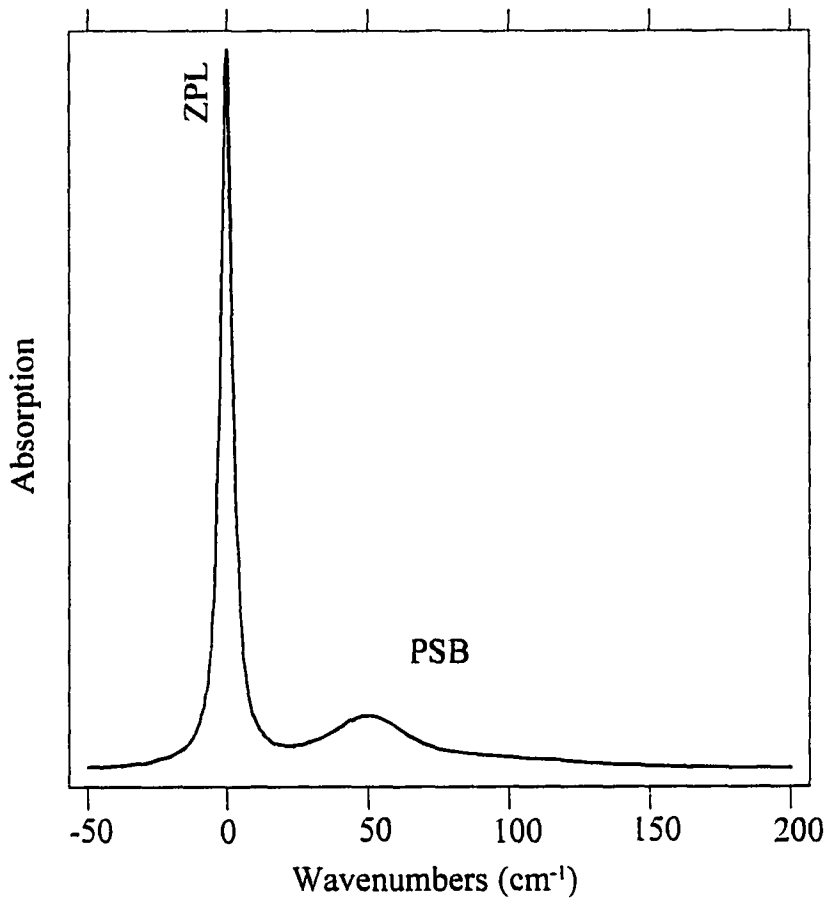

Figure 1.4 Single-site absorption profile calculated with Eq. (29) of Chapter 3 with S = 0.50, $\omega_j = 50\,cm^{-1}$, $\gamma_j = 30\,cm^{-1}$, and $\gamma_{el} = 5\,cm^{-1}$ at T = 0 K. PSB shown as a broad band with its associated sharp peak, the ZPL due to linear electron phonon coupling.

intensity of the ZPL decreases and the intensity of the PSB increases. This is illustrated in Figure 1.5 for the parameters used for Figure 1.2 (b) (S= 0.50, T = 0 K, $\omega_j = 50\ cm^{-1}$, $\gamma_j = 5\ cm^{-1}$) but calculated at T = 30 K and 120 K. Figure 1.5 shows the rise of the hot bands, the intensity loss of the ZPL, and the PSB intensity increase due to the temperature increase. However, the integrated intensity of the whole profile does not depend on temperature (in the Condon approximation) [43-45]:

$$I_{ZPL}(T) + I_{PSB}(T) = \text{constant}, \tag{1.72}$$

where $I_{ZPL}(T)$ is integrated intensity of the ZPL and $I_{PSB}(T)$ is that of the PSB. Thus, Eq. (1.72) tells us that the lost intensity from the ZPL has been transferred to the PSB. Assigning the same width to all the bands is unphysical because it does not take into account pure electronic dephasing. Furthermore, the homogeneous width of the ZPL is independent of the phonons relaxations. The same width has been assigned to all the bands here only to simplify explaining what physically takes place when one raises the temperature. However, this problem will be resolved (see Eq. (27) of Chapter 3) with examples and applications given in Chapter 3.

In light of the above, it is seen that in the linear coupling approximation ZPL gets very weak as temperature increases, and is hardly observed for S >> 1 at T = 0 K (see Figure 1.3). Therefore, one can conclude that only the PSB is governed by the linear coupling approximation. Furthermore, electron-phonon scattering causes pure electronic dephasing (optical coherence loss) and if $S_j = 0$, there will be no dephasing according to the linear coupling approximation. It will be shown below that this is not physical unless higher order coupling terms are taken into account. Next the diagonal quadratic electron-phonon coupling is discussed.

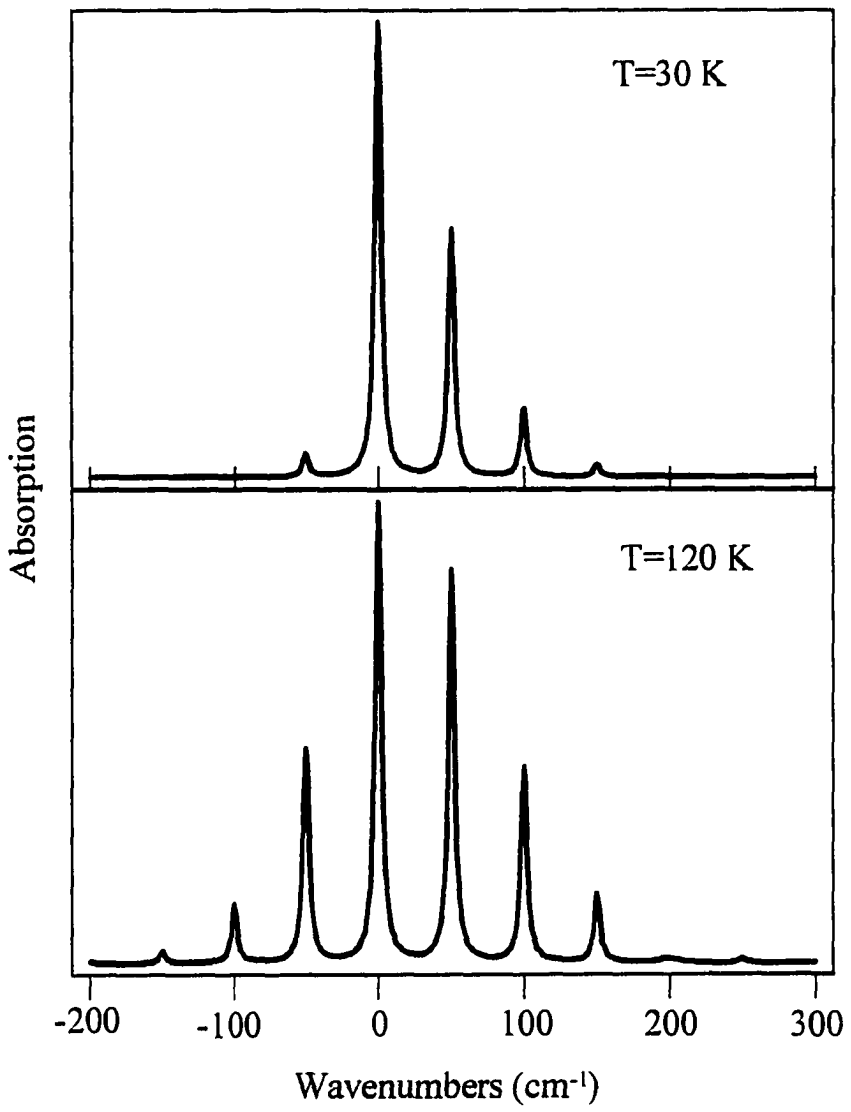

Figure 1.5 Single-site absorption spectra same as in Figure 1.2 (b) at finite temperatures calculated using Eq. (1.52) by replacing the delta functions with normalized lorentzians. Note the presence of the hot bands on the low energy side, the intensity loss of the ZPL, and the PSB intensity increase as the temperature increases. ($e^{-S\coth(\beta\hbar\omega_1/2)} = 0.55$ and 0.18 for T = 30 and 120 K). The intensity lost from the ZPL is transferred to the PSB intensity according to the conservation law.

1.2.2 Quadratic Coupling

Figure 1.3 indicates that when S_j increases the PSB predominates the entire absorption profile while the ZPL contributes insignificantly. Therefore, we can conclude that the linear coupling approximation is not sufficient for studying the homogeneous broadening of the ZPL (pure electronic dephasing). While linear electron-phonon coupling does not contribute to pure electronic dephasing, quadratic coupling does, *vide infra.* In other words, quadratic coupling can be neglected when considering the PSB, but not when considering the ZPL [43-45]. This is reminiscent of the three important findings by Small and co-workers when studying the ZPL dynamics in polymers and glasses [46, 47]. The first finding was that the exchange coupling mechanism [48, 49], which originates from quadratic electron-phonon coupling, often accounts for pure electronic dephasing at higher temperatures. (Above about 15 K the pure electronic dephasing becomes dominated by quadratic electron-phonon coupling, which gives rise to exchange coupling mechanism involving a low frequency pseudo-localized vibrational mode associated with the probe molecule.) The second finding was that the phonon modes exhibit negligible linear electron-phonon coupling (which means if we limit our system to only linear coupling, there will be no optical coherence loss, *vide infra*). The last finding was that the linearly coupled modes contribute appreciably to the PSB and negligibly to the ZPL. As a result, Small and co-workers [46, 47] concluded that neglecting quadratic coupling in liquids is questionable. In the limit where $S_j \rightarrow 0$, $g_j(t;T)$ of Eq. (1.51b), Eq. (24) of Chapter 3, or the one generated by the multi-mode Brownian oscillator (MBO) $\rightarrow 0$ [3]. Thus, when linear coupling vanishes ($S_j \rightarrow 0$), there is no optical coherence loss. This is unphysical as recognized by Fleming and co-workers [50]. However, inclusion of quadratic coupling leads to optical coherence loss (even when $S_j \approx 0$).

Of course, quadratic coupling contributes to PSB. However this coupling can never considerably increase the intensity of a PSB [44, 45] because FC factors dictate that quadratic coupling contributes to the phononic transitions with creation and annihilation of an even

number of phonons. Since the FC factors for any n → m transition for only quadratic coupling do not seem to be available in a closed form, they are only given here for the 0 → m (cold transitions) transition [38]:

$$|\langle m|0\rangle|^2 = 2\frac{(m-1)!!}{m!!}\frac{\sqrt{\Theta}}{(1+\Theta)}\left(\frac{\omega''-\omega'}{\omega''+\omega'}\right)^m \qquad m \equiv \text{even}$$
$$= 0 \qquad m \equiv \text{odd} \tag{1.73}$$

where $\Theta \equiv \omega''/\omega'$. Note that the final vibrational state m must be even due to the definite parity of the harmonic oscillator eigenstates (unlike the linear coupling), otherwise the overlap integral will be zero because the integrand is odd. It would be more instructive if we write out the FC factor for the ZPL,

$$|\langle 0|0\rangle|^2 = 2\frac{\sqrt{\Theta}}{(1+\Theta)}, \tag{1.74}$$

which means that the integrated intensity of the PSB generated by the quadratic coupling is $\left(1-2\sqrt{\Theta}/(1+\Theta)\right)$. Recall, only even transitions contribute to that PSB. For instance, if ω"= 30 cm^{-1} and ω' = 25 cm^{-1}, then FC factors for (0,0), (2,0), (4,0) transitions are 0.994, 0.0060, 0.000056, respectively. In general, $[(\omega''-\omega')/(\omega''+\omega')]^m$ for m ≥ 2 can never exceed unity. Thus, the ZPL dominates the entire profile under consideration (e.g., hole-burning, photon echo, or linear absorption) and the PSB contributes negligibly to that profile. Therefore, the contribution of quadratic coupling to the PSB, as a rule, is negligible [43-45].

The problem of handling quadratically coupled modes will be treated in Chapter 3 where pure electronic dephasing is taken into account and because of the approximation made (Eq. (1.57)) results are obtained that are valid for up to about 30% change of frequency. Furthermore, the only transition is seen at T = 0 K is the (0,0) transition (ZPL) but as the

temperature increases only the sequence transitions start to arise (e.g., (1,1), (2,2), etc.), see Figures 2 and 5 of Chapter 3. Figure 5 of Chapter 3 shows that the quadratic coupling shifts and thermally broadens the ZPL.

1.2.3 Linear and Quadratic Coupling

Modes that are both linearly and quadratically coupled are infrequently encountered and, for completeness, some of the most relevant features that may arise in spectroscopy will only be briefly pointed out. The reorganizational energy, λ, in harmonic systems whose modes exhibit both linear and quadratic electron-phonon coupling is equal to $S\omega'^2/\omega''$ (see Eq. (1.55)), which will lead to a different vertical transition frequency Ω_v (the sum of the adiabatic gap and λ, as shown in Eq. (1.59c)) from that one for the linear coupling case. The fact that λ for both linear and quadratic coupling case has changed is a direct signature that FC factors will change accordingly, and be different from the linear coupling ones. This is because of the following. As can be seen from Figure 1.1 the vertical line, Ω_v, starts from the equilibrium nuclear separation (where the probability distribution function is maximum) of the initial vibration state and reaches the most probable vibration state in the upper electronic state where this probability is larger at the classical turning points. Since FC factors tell us which transitions are the most probable ones (strongest transitions) in a spectrum, they must change in accordance with Ω_v (Franck-Condon principle) because they both lead to the most probable transitions. Hence, the upper vibrational state that the vertical line intersects will be the most intense member of the progressions. Furthermore, the centroid (λ) of the PSB will change as well causing all the absorption spectrum peaks to be shifted to the left $(\omega'-\omega'')/2$ cm^{-1}. The fact that we have two different fundamental frequencies (ω' and ω''), at high enough temperature, the bands attributed to ω'', its multiples, assuming $\omega' < \omega''$, and the multiple of the difference of the two fundamental frequencies start to appear and this will lead to non-constant splittings between the bands, unlike linear coupling. The difference of the two fundamental frequencies and its multiples give rise to

quantum beats in time-domain, which will be discussed in Chapter 2 with examples given in Chapter 4. To this end we just give the FC factor for the ZPL [38, 51-53,],

$$|\langle 0|0\rangle|^2 = 2\frac{\sqrt{\omega''\omega'}}{(\omega''+\omega')}\exp(-2S\omega'/(\omega''+\omega')) \tag{1.75}$$

In Chapter 3 approximate FC factors will be obtained, which are adequate up to ~ 30% frequency change. They are derived from the Fourier transform of J(t;T) obtained from our approximate excited state vibrational Hamiltonian. For more extensive details on FC factors for both linear and quadratic electron-phonon coupling with and without anharmonicity see Ref. [38].

1.3 Dissertation Organization

This dissertation contains the candidate's original work on theoretical development of temperature dependent linear and non-linear spectroscopy for condensed phase systems. Chapter 1 provides a general background on classical and quantum correlation functions, optical linear response functions, and harmonic electron-phonon coupling and the relevant Franck-Condon factors. Chapter 2 gives a background on applying optical non-linear response functions approach to photon echo spectroscopy. Chapter 3 and Chapter 4 are submitted papers on optical linear and non-linear response functions for condensed systems with linear and quadratic electron-vibration coupling. Chapter 3 contains an approximate linear response function for both linear and quadratic electron-phonon coupling, its associted Franck-Condon factors, and a linear response function that describes the pure electronic dephasing (homogeneous broadening of the zero-phonon line) for only linearly coupled modes. Chapter 4 is an extension and applications of the formalism developed in Chapter 3 to non-linear spectroscopy (photon echo). Concluding remarks are given in Chapter 5. Three

appendices are given at the end of the dissertation: Appendix A provides a spectral analysis of the multi-mode Brownian oscillator model. Appendix B gives a mathematical proof of the equivalence of Eq. (27) of Chapter 3 to Eq. (17) of Hayes et al [42]. Derivation of Eq. (29) from Eq. (27) of chapter 3 is given in Appendix C

1.4 References

1. A. S. Davydov, Theory of Molecular Excitons (Plenum Press, New York, 1971).
2. J. V. Kranedonk and J. E. Sipe, *in Progress in Optics* XV, edited by E. Wolf (North-Holland, Amsterdam, 1977).
3. S. Mukamel, *Principles of Nonlinear Optical Spectroscopy* (Oxford University Press, New York, 1995).
4. R. Kubo, *Statistical Mechanics* (North-Holland, Amsterdam, 1971).
5. M. Weissbluth, *Photon-Atom Interactions* (Academic Press, New York, 1989).
6. D. A. McQuarrie, *Statistical Mechanics* (Harper & Row, New york, 1976).
7. D. Chandler, *Introduction to Modern Statistical Mechanics* (Oxford University Press, New York, 1987).
8. K. Blum, *Density Matrix Theory and Applications* (Plenum Press, New York, 1981).
9. R. Reif, *Fundamentals of Statistical and Thermal Physics* (McGraw-Hill, 1965).
10. R. Gordon, Adv. Mag. Resonance, **3**, 1 (1968).
11. W. H. Louisell, *Quantum Statistical Properties of Radiation* (J. Wiley, New York, 1973).
12. R. Kubo, *In Lectures in Theoretical Physics*, Vol. 1, 120 (Wiley, Wiley, New York, 1958).
13. N. N. Bogolubov and N. N. Bogolubov Jnr, *Introduction to Quantum Statistical Mechanics* (Gordon and Breach Science, 1994).
14. C. C-Tannoudji, B. Diu, anf F. Laloe, *Quantum Mechanics* (Wiley, New York, 1977).

15 R. Loudon, *The Quantum Theory of Light* (Clarendon Press, Oxford, 1983).

16. A. D. davydov, *Quantum Mechanics* (Prgamon Press, 1965).

17. B. H. Bransden and C. J. J. Joachain, Physics of Atoms and Molecules (J. Wiley & Sons, New York, 1990).

18. C. C-Tannoudji, J. Dupont-Roc, and G. Grynberg, *Atom-Photon Interactions*(Wiley New York, 1989).

19. P. Meyster and M. Sargent, *Elements of Quantum Optics* (Springr-Verlag, Berlin, 1990).

20. L. E. Ballentine, *Quantum Mechanics* (Prentive Hall, New Jersey, 1990).

21. M. Sargent III, M O. Scully, W E.Lamb, Jr., *Laser Physics* (Addison-Wesley, London, 1974).

22. H. Goldstein, Classical Mechanics (Addison-Wesley, London, 1981).

23. H. B. Levine and D. A. McQuarrie, J. Chem. Phys. **49**, 4181 (1968).

24. D. B. DuPr'e and J. P. Tague, J. Chem. Phys. **50**, 2024 (1969).

25. R. G. Gordon, J. Chem. Phys. **42**, 3658 (1965).

26 R. G. Gordon, J. Chem. Phys. **43**, 1307 (1965).

27. R. G. Gordon, J. Chem. Phys. **44**, 3083 (1966).

28. S. L. Brenner and D. A. McQuarrie, Can. J. Phys. **49**, 837 (1971).

29. A. G. Redfield, Adv. Mag. Reson. **1**, 1 (1965).

30. R. G. Breen, *Theories of Spectral Lineshapes* (Wiley, York, 1981).

31 C. E. Porter, *Statistical Theory of Spectra: Fluctuations* (Academic Press, New York, 1965).

32. I. S. Osad'ko and M. V. Stashek, JETP **79**, 293 (1994).

33. B. B. Laird, J. Budimir, and J. Skinner, J. Chem. Phys. **94**, 4391 (1991).

34. G. Ficsher, *Vibronic Coupling* (Academic Press, London, 1984).

35. B. Sharf and B. Huang, Chem. Phys. Lett. **7**, 132 (1970).

36. G. J. Small, J. Chem. Phys. **54**, 3300 (1971).

37. W. Kaplan, *Advanced Calculus* (Addison-Wesley, London, 1984).

38. R. Englman, Non- Radiative Decay of Ions and Molecules In Solids (North-Holland, Amsterdam, 1979).

39. J. Freund and R. Walpole, *Mathematical Statistics* (Prentice-Hall, New Jersey, 1987).

40. K. Huang and A. Rhys, Proc. Roy. Soc. (London), **204A**, 406 (1950).

41. S. I. Pekar, Zh. Eksp. Teor. Fiz. **20**, 510 (1950).

42. J. M. Hayes, P. A. Lyle, and G. J. Small, J. Phys. Chem. **98**, 7337 (1994).

43. I. S. Osad'ko, *Spectroscopy and Excitation Dynamics of Condensed Molecular Systems*, edited by V. M. Agranovich and R. M. Hochstrasser (North-Holland, Amsterdam, 1983) p. 437.

44. I. S. Osad'ko and M. V. Stashek, J. Lumin. **64**, 25 (1995).

45. I. S. Osad'ko, Adv. Poly. Sci. **114**, 125 (1994).

46. T. Reinot, W.-H. Kim, J. M. Hayes, and G. J. Small, J. Chem. Phys. **104**, 793 (1996).

47. T. Reinot, W.-H. Kim, J. M. Hayes, and G. J. Small, J. Chem. Phys. **106**, 457 (1997).

48. R. M. Shelby, C. B. Harris, and P. A. Cornelius, J. Chem. Phys. **70**, 34 (1979).

49. B. Jackson and R. Silbey, Chem. Phys. Lett. **99**, 331 (1983).

50. Y. Nagasawa, S. A. Passino, T. Joo, and G. R. Fleming. **106**, 4840 (1997).

51. C. Manneback, Physica **17**, 1001 (1951).

52. M. G. Prais, D. F. Heller and K. F. Freed, Chem. Phys. **6**, 331 (1974).

53. D. F. Heller, K. F. Freed, and W.M. Gelbart, J. Chem. Phys. **56**, 2309 (1972).

CHAPTER 2. NONLINEAR OPTICAL SPECTROSCOPY FOR CONDENSED PHASE SYSTEMS

2.1 Introduction

Linear optical experiments cannot extract structural and dynamical information about molecular systems in condensed phases because they are usually hidden underneath a broad inhomogeneous distribution due to a variation in transition frequencies for different molecules, as a result of different local environments. This is typical for linear spectra in solutions, liquids, glasses, proteins, polymers and molecular crystals. However, non-linear optical techniques such as hole-burning [1-7], photon echoes [8-31], pump-probe absorption [8-10, 32-40], and fluorescence line narrowing [41-46] can extract this information by eliminating the inhomogeneous broadening. Those techniques require going to higher order optical response functions, i.e., non-linear response functions.

In hole-burning and fluorescence line narrowing techniques, the elimination of inhomogeneous broadening involves a selective narrow band excitation of a subgroup of molecules, and then following its subsequent dynamics by measuring the change in the absorption of a probe (hole-burning) or the spontaneous emission (fluorescence line narrowing). Only a small fraction of molecules within the inhomogeneous distribution is selectively probed in this case resulting in a partial elimination of the inhomogeneous broadening effect. On the contrary, the pulsed excitation process in photon echo spectroscopy is non-selective and the entire inhomogeneous distribution is excited. The ability of photon echo technique to eliminate the inhomogeneous broadening from the signal is the result of two propagation periods in which the inhomogeneous broadening has an opposite effect (the depahsing in the first period is followed by rephasing in the second) which exactly cancels.

In light of the above, hole-burning and fluorescence line narrowing techniques are based on frequency selection of chromophores by preparing a small homogeneous fraction of molecules (chromophores). Therefore, both emitted light and burned hole reflect a spectral width close to that in the single-site absorption/fluorescence spectra. On the other hand, photon echo spectroscopy is a kinetic type of spectroscopy. The photon echo methods are based on the temporal evolution of the chromophores dipole moments. This can be more easily seen using the wave function approach or the Bloch vector model [13, 15], *vide infra*.

The importance of optical polarization in spectroscopy was established in the previous Chapter. Since optical polarization is the only material quantity that appears in Maxwell's equation (Eq. (1.1)), it carries a complete microscopic information about the system. It was also pointed out that the non-linear third-order polarization, $P^{(3)}(\mathbf{r},t)$, is a key quantity in the interpretation of 4-wave mixing experiments (4WM) such as photon echoes, fluorescence line narrowing, hole-burning, and pump-probe spectroscopies. For example, when three incident pulses are applied to a sample, they interact with it to generate a new field (e.g., echo field in photon echo measurements). Here we limit the application of third-order polarization, which is expressed in terms of non-linear third-order response function as $P^{(1)}(\mathbf{r},t)$ was expressed in terms of linear response function $S^{(1)}(t)$ in Chapter 1, to photon echo spectroscopy. More extensive applications of non-linear third-order response function in non-linear spectroscopy can be found in [8].

2.2 Non-Linear Optical Response Function Description of $P^{(3)}(\mathbf{r},t)$

The non-linear third-order response function governes all the non-linear optical measurements. Equations (1.35) and (1.36) indicate that the polarization of the medium can be written as a convolution of the response function and the electric field(s). Following the same procedure that was adopted to calculate $P^{(1)}(\mathbf{r},t)$, $P^{(3)}(\mathbf{r},t)$ can be calculated by

substituting Eq. (1.44d) for n = 3 in Eq. (1.48) and changing the integration variables as shown in Chapter 5 of Ref. [8], this yields

$$P^{(3)}(\mathbf{r},t) = \int_0^\infty dt_1 \int_0^\infty dt_2 \int_0^\infty dt_3 S^{(3)}(t_3,t_2,t_1) E(r,t-t_3) \times E(r,t-t_3-t_2) E(r,t-t_3-t_2-t_1), \tag{2.1}$$

where the non-linear response function is

$$S^{(3)}(t_3,t_2,t_1) = -2\hbar^{-3}\theta(t_1)\theta(t_2)\theta(t_3)\,\mathrm{Im}\sum_{\alpha=1}^{4} R_\alpha(t_3,t_2,t_1), \tag{2.2}$$

where $R_\alpha(t_3,t_2,t_1)$ are the non-linear correlation functions, $\theta(t_n)$ is the Heavyside step function, and t_1, t_2, and t_3 are the time intervals between successive interactions with the radiation field. The $R_\alpha(t_3,t_2,t_1)$ terms represent only the homogeneous part (the dynamical contributions) of $S^{(3)}(t_3,t_2,t_1)$. $R_\alpha(t_3,t_2,t_1)$ factors are given by [8, 38]

$$\begin{aligned} R_1 &= Tr[G_{eg}(t_3)G_{ee}(t_2)G_{eg}(t_1)\rho_g], \\ R_2 &= Tr[G_{eg}(t_3)G_{ee}(t_2)G_{ge}(t_1)\rho_g], \\ R_3 &= Tr[G_{eg}(t_3)G_{gg}(t_2)G_{ge}(t_1)\rho_g], \\ R_4 &= Tr[G_{eg}(t_3)G_{gg}(t_2)G_{eg}(t_1)\rho_g]. \end{aligned} \tag{2.3}$$

It is assumed that the system is initially in thermal equilibrium in the electronic ground state and its nuclear density operator is ρ_g. Tr denotes a quantum mechanical trace over the nuclear degrees of freedom. The coherence time evolution operator (off-diagonal Green's function) is defined by its action on an arbitrary operator A:

$$G_{nm}(t) = \exp(-iH_n t/\hbar) A \exp(iH_m t/\hbar), \quad n,m = e,g \tag{2.4}$$

where H_g and H_e are the adiabatic nuclear Hamiltonians of the molecular system in the electronic states $|g\rangle$ and $|e\rangle$, respectively. (Note that $G_{mm}(t_2)$ (diagonal Green's function) describes the time evolution of the molecular nuclear degrees of freedom in the electronic state m and has a well-defined classical analog. On the other hand, the off-diagonal Green's function, $G_{nm}(t)$ with $n \neq m$, describes the molecular dynamics in an optical coherence (electronic dephasing) during t_1 and t_3 periods, which is purely quantum mechanical.

Using the form of Eq. (2.3), the non-linear response function may be given the following interpretation: The system is initially at thermal equilibrium in the electronic ground state $\rho_g(-\infty)$ before applying the radiation field. When the field is turned on, the system interacts with the field three different times. Figure 2.1 shows that the first interaction (takes place at time $\varphi_1 = t - t_1 - t_2 - t_3$) prepares the system in an optical coherence, the system then evolves for a period t_1. The second interaction (takes place at time $\varphi_2 = t - t_2 - t_3$) converts the system coherence state into a population state. The system then evolves for t_2 period as Figure 2.1 shows. Finally, the third interaction (occurs at time $\varphi_3 = t - t_3$) sets up again an electronic coherence in the system that evolves for t_3. At time t > t_3 the optical polarization is calculated by taking the trace. (Recall that $P^{(3)}(\mathbf{r},t) = Tr\{v\rho^{(3)}(t)\}$ (Eq. (1.48)) where $\rho^{(3)}(t)$ is given by Eq. (1.44d).) Therefore, one can conclude that t_1 and t_3 govern the dephasing times as described by $G_{nm}(t)$ and t_2 governs the population time in accordance with $G_{mm}(t_2)$.

The structural heterogeneity of the environment causes a variation in electronic transition frequencies, Ω, of the guest molecules which gives rise to inhomogeneous broadening. As a result, the inhomogeneous broadening need to be included in the response function, Eq. (2.2). Upon evaluating the ensemble average of Eq. (2.3) over the distribution of Ω (ZPL frequencies) one gets the following inhomogeneously broadened non-linear correlation function [8]

$$R_\alpha(t_3,t_2,t_1)\chi(t_3 \pm t_1), \tag{2.5}$$

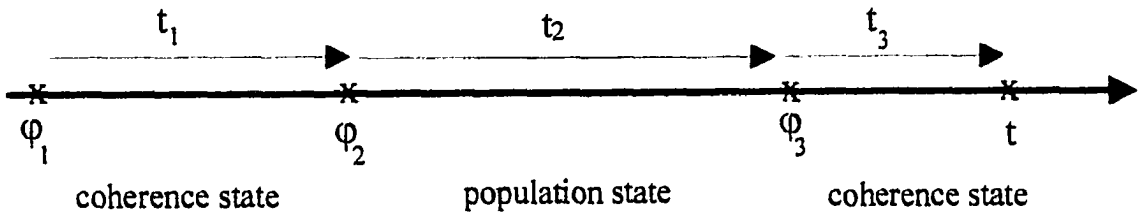

Figure 2.1 The time arguments in Eq. (2.1). The three interactions of the system with the radiation field take place at times φ_1, φ_2, and φ_3. The polarization is then calculated at time t; t_1, t_2, and t_3 are the time intervals between the radiative interactions.

where the χ function represents the inhomogeneous dephasing in time domain. $\chi(t_3 \pm t_1)$ comes from the ensemble average of the $\exp[-i\Omega(t_3 \pm t_1]$ factor which appears in $R_\alpha(t_3,t_2,t_1)$ (see Eq. (8.15) on p. 213 of Ref. [8]). That equation clearly shows the dependence of R_1 and R_4 on $\exp[-i\Omega(t_3 + t_1)]$ and R_2 and R_3 on $\exp[-i\Omega(t_3 - t_1)]$ and, therefore, R_1 and R_4 will select $\chi(t_3 + t_1)$ and R_2 and R_3 will select $\chi(t_3 - t_1)$. Combining Eq. (2.2) with Eq. (2.5), one obtains [8]

$$\begin{aligned} S^{(3)}(t_3,t_2,t_1) = \left(\frac{i}{\hbar}\right)^3 \theta(t_1)\theta(t_2)\theta(t_3)\{&[R_2(t_3,t_2,t_1) + R_3(t_3,t_2,t_1)]\chi(t_3 - t_1) \\ &+ [R_1(t_3,t_2,t_1) + R_4(t_3,t_2,t_1)]\chi(t_3 + t_1)\}. \end{aligned} \tag{2.6}$$

The radiation field $E(\mathbf{r},t)$ for a general 4WM process can be decomposed into three components:

$$E(\mathbf{r},t) = E_1(t+\tau'+\tau)\exp(i\mathbf{k}_1.\mathbf{r} - i\omega_1 t) + E_2(t+\tau)\exp(i\mathbf{k}_2.\mathbf{r} - i\omega_2 t) + E_3(t)\exp(i\mathbf{k}_3.\mathbf{r} - i\omega_3 t) + c.c.. \quad (2.7)$$

where, for example, E_1, E_2, and E_3 would determine the temporal shapes of the pulses centered at $t = -(\tau' + \tau)$, $t = -\tau$, and $t = 0$, respectively. Here, τ' is defined as the delay between the first (E_1) and second (E_2) pulses while τ is the delay between the second and third (E_3) pulses, while ω_j denotes the incident pulse mean frequency. Those pulses will interact with the medium to generate a new field with $\mathbf{k}_s$ and ω_s, where $\mathbf{k}_s$ can be any combination of the incoming wave vectors, $\mathbf{k}_s = \pm\mathbf{k}_1 \pm \mathbf{k}_2 \pm \mathbf{k}_3$ and $\omega_s = \pm\omega_1 \pm \omega_2 \pm \omega_3$. The various types of 4WM experiments differ by the choice of $\mathbf{k}_s$, ω_s, and the temporal characteristics of the incoming pulses [8, 17, 36, 38, 47]. Substituting Eqs. (2.7) and (2.6) in Eq. (2.1) yields extremely complicated expression for $P^{(3)}(\mathbf{r},t)$ with highly oscillatory terms, see Refs. [8, 17, 36, 38, 47, 48] for more details on selecting $\mathbf{k}_s$ and ω_s. However, $P^{(3)}(\mathbf{r},t)$ can tremendously be simplified if the pulses are infinitely short, resulting in $P^{(3)}(\mathbf{r},t) \sim S^{(3)}(t,\tau,\tau')$, *vide infra.*

2.3 The Non-Linear Response Function for Photon Echo Spectroscopy

Invoking the rotating wave approximation (by neglecting the highly oscillatory terms), in addition to the to the assumptions made in Refs. [8, 9, 17, 38, 47, 48] regarding the sums and differences of the electronic transition frequencies and the fields, leads to gratings with wave vectors $\pm(\mathbf{k}_2 - \mathbf{k}_1)$ created by E_1 and E_2 interactions [8, 9, 17, 38, 47]. As a result, the four dominant wave mixing signals show up in four possible directions: $\pm\mathbf{k}_3 \pm (\mathbf{k}_2 - \mathbf{k}_1)$. Thus, the remaining components of non-linear third-order polarization are given by [8, 9, 48]

$$P^{(3)}(\mathbf{k}_a,t)=\left(\frac{i}{\hbar}\right)^3\int_0^\infty dt_3\int_0^\infty dt_2\int_0^\infty dt_1[R_2(t_3,t_2,t_1)+R_3(t_3,t_2,t_1)]$$
$$\times\chi(t_3-t_1)\,E_3(t-t_3)\,E_2(t+\tau-t_3-t_2)\,E_1^*(t+\tau'+\tau$$
$$-t_3-t_2-t_1)\exp[i(\omega_3+\omega_2-\omega_1)t_3+i(\omega_2-\omega_1)t_2-i\omega_1t_1], \qquad (2.8)$$

and

$$P^{(3)}(\mathbf{k}_b,t)=\left(\frac{i}{\hbar}\right)^3\int_0^\infty dt_3\int_0^\infty dt_2\int_0^\infty dt_1[R_1(t_3,t_2,t_1)+R_4(t_3,t_2,t_1)]$$
$$\times\chi(t_3+t_1)\,E_3(t-t_3)\,E_2^*(t+\tau-t_3-t_2)\,E_1(t+\tau'+\tau$$
$$-t_3-t_2-t_1)\exp[i(\omega_3-\omega_2+\omega_1)t_3+i(\omega_2-\omega_1)t_2+i\omega_1t_1], \qquad (2.9)$$

where $\mathbf{k}_a=\mathbf{k}_3+\mathbf{k}_2-\mathbf{k}_1$ and $\mathbf{k}_b=\mathbf{k}_3-\mathbf{k}_2+\mathbf{k}_1$. The other components ($-\mathbf{k}_a$ and $-\mathbf{k}_b$) are obtained by taking the complex conjugate since $[P^{(3)}(\mathbf{k},t)]^*=P^{(3)}(-\mathbf{k},t)$.

The wave vector which an echo experiment selects is [8, 9, 17, 47] $\pm\mathbf{k}_a=\pm(\mathbf{k}_3+\mathbf{k}_2-\mathbf{k}_1)$ which, by Eq. (2.9) , selects $R_2(t_3,t_2,t_1)$ and $R_3(t_3,t_2,t_1)$ factors. Recall that $R_2(t_3,t_2,t_1)$ and $R_3(t_3,t_2,t_1)$ factors select its static (inhomogeneous) contribution as $\chi(t_3-t_1)$, and $\chi(t_3+t_1)$ is selected by $R_1(t_3,t_2,t_1)$ and $R_4(t_3,t_2,t_1)$ factors, *vide supra.* Note that if $\chi(t_3-t_1)$ is the inhomogeneous contribution, a strong peak (echo) will appear at $t_1=t_3$. The $\chi(t_3+t_1)$ factor, which is associated with $R_1(t_3,t_2,t_1)$ and $R_4(t_3,t_2,t_1)$, could only peak at $t_1=t_3=0$ (since t_1 and t_3 are positive) and will not contribute to the echo. This rules out the direction $\pm\mathbf{k}_b$ of the signal leaving $\pm\mathbf{k}_a$ as the only echo direction. Therefore the polarization of any echo signal is given by Eq. (2.8).

The time arguments of E_j in Eq. (2.8) can physically be justified based on the above physical interpretation of the non-linear response function. E_1 occurs at $t=-(\tau'+\tau)$ and interacts with the medium (as first interaction) at time $\varphi_1=t-t_1-t_2-t_3$ and, therefore, the time argument of E_1 becomes $E_1(\varphi_1+\tau+\tau')$. Similarly, E_2 takes place at $t=-\tau$ and interacts with the medium (as second interaction) at time $\varphi_2=t-t_2-t_3$ and, therefore, the

time argument of E_2 becomes $E_2(\varphi_2 + \tau)$. Finally, E_3 comes at t = 0 and given that the third interaction happens at time $\varphi_3 = t - t_3$, so E_3 would naturally depend on time φ_3 only as shown in Eq. (2.8).

2.3.1 Three-Pulse Photon Echo: Dephasing and rephasing processes

Consider the stimulated photon echo (SPE) in which three short laser pulses with wave vectors $\mathbf{k}_1$, $\mathbf{k}_2$, and $\mathbf{k}_3$ are sequentially applied to the system. Assuming that the form of the external field is as given in Eq. (2.7), which shows that the delay between the first (E_1) and second (E_2) pulses is τ' and τ is the delay between the second and third (E_3) pulses. while ω_j denotes the incident pulse mean frequency, *vide supra*. The stimulated echo, which centers around $t = \tau'$ after the interaction of the third pulse with the material, appears in the direction $\mathbf{k}_a = \mathbf{k}_3 + \mathbf{k}_2 - \mathbf{k}_1$. The integrated intensity of the stimulated photon echo signal, S_{SPE}, is given by [8, 9]

$$S_{SPE} = \int_0^\infty dt |P^{(3)}(\mathbf{k}_a, t)|^2 \tag{2.10}$$

In the impulsive limit, the laser pulses are infinitely short, that is

$$\begin{aligned} E_1(t) &= \delta(\varphi_1 + \tau + \tau'), \\ E_2(t) &= \delta(\varphi_2 + \tau), \\ E_3(t) &= \delta(\varphi_3), \end{aligned} \tag{2.11}$$

where $\varphi_1 = t - t_1 - t_2 - t_3$, $\varphi_2 = t - t_2 - t_3$, and $\varphi_3 = t - t_3$, and well separated, and τ' and τ are very large compared to the pulse widths. Thus, the lower limits of the triple-integral in Eq. (2.8) may be replaced by $-\infty$ and , then, the integration can trivially be carried out using the following relationship

$$\int_{-\infty}^{\infty} f(x)\delta(x-a)dx = f(a) \tag{2.12}$$

Upon the substitution of Eq. (2.11) into Eq. (2.10), one obtains

$$S_{SPE}(\tau',\tau) = \int_{0}^{\infty} dt\,|[R_2(t,\tau,\tau') + R_3(t,\tau,\tau')]|^2\,\chi(t-\tau') \tag{2.13}$$

Note that the time dependent exponentails do not show up in Eq. (2.13) because they become unity after taking modulus squared (e.g., $|e^{i\varphi}|^2 = 1$).

We shall now discuss how the present formalism (Eq. (9)) describes the *impulsive* echo formation through the rephasing processes of the individual dipoles. The SPE mechanism becomes governed by the response functions $\langle G_{eg}(\tau')G_{ee}(\tau)G_{ge}(\tau')\rangle$ and $\langle G_{eg}(\tau')G_{gg}(\tau)G_{ge}(\tau')\rangle$. At time t = – (τ' + τ), the pulse $E_1 = \delta(t+\tau+\tau')$ excites the system from the electronic ground state ρ_{gg} ($|g\rangle\langle g|$) to set up an optical coherence state ρ_{ge} ($|g\rangle\langle e|$) (a superposition state involving the ground (g) and the excited (e) electronic states), which then evolves for a period τ' as described by $G_{ge}(\tau')$. At the time t = –τ, the system interacts with $E_2 = \delta(t+\tau)$ and is converted to either the electronic ground population state ρ_{gg} or the electronic excited population state ρ_{ee}. These non-equilibrium population states evolve freely under $G_{gg}(\tau)$ and $G_{ee}(\tau)$, respectively, for a period τ until t = 0 when the system interact with $E_3 = \delta(t)$. The third pulse prepares the system in an optical electronic coherence again and the system emits a fourth radiation field called stimulated photon echo from the rephasing processes governed by $G_{eg}(t)$. The form of the inhomogeneous broadening χ(t–τ') indicates that the maximum of the echo is at t = τ'. For t > τ', the echo decays exponentially with time constant T_2, due to electronic dephasing. The key event to notice here is that the first dephasing of the molecules has taken place during τ' and the echo formation has reached its maximum at t = τ' indicating that the third pulse has rephased the

molecules during τ' as well. The selective elimination of inhomogeneous dephasing (inhomogeneous broadening in the frequency domain) by rephasing processes is the essential ingredient of photon echo experiments (i.e., the presence of two propagation periods $\langle G_{eg}(\tau')G_{ge}(\tau')\rangle$, in which dephasing and rephasing processes occur, respectively). It is important to note that T_2 must be long compared to τ' and τ for photon echo to be observed. The same constraint must be applied to T_1, which governs the population of the upper state. This implies that the laser pulse must have sufficient intensity to populate the upper state before there is any appreciable decay.

It is important to bear in mind that the remarkable phenomenon of phase reversal after a system has been dephased by inhomogeneous broadening does not apply to homogeneous dephasing; that is homogeneous broadening is not reversible. The reversible character of the inhomogeneous dephasing enables us to measure the extent of the homogeneous dephasing time contributing to the echo decay; because the part of the decay that can not be reversed is then attributed to homogeneous dephasing. This may be better understood when the two-pulse photon echo is discussed, *vide infra*, because it involves only two pulses.

Equation (2.13) tells us that the inhomogeneous broadening is eliminated at t = τ' (which generates the echo). However, the signal still has contribution at all times t, the inhomogeneous broadening is not completely eliminated. Assuming that the inhomogeneous broadening is very large, whereby inhomogeneous dephasing time compared to all the timescales of the system, we have $\chi(t-\tau') \sim \delta(t-\tau')$. The stimulated photon echo is then

$$S_{SPE}(\tau',\tau) = \left|R_2(\tau',\tau,\tau') + R_3(\tau',\tau,\tau')\right|^2, \tag{2.14}$$

whereby the inhomogeneous broadening has been eliminated completely at all times.

2.3.2 Two-Pulse Photon Echo (PE)

We start this subsection by describing the two-pulse photon echo experiment using the wave function approach, Bloch vector model, and, finally, the non-linear response function; more physical insight can be gained this way because of the simplicity of the two-pulse photon echo. For a two-pulse photon echo measurement, the first pulse ($\pi/2$ pulse) with a wave vector $\mathbf{k}_1$ creates an electronically coherent state of the chromophores. The ground and excited states of all the molecules are placed in a coherent superposition states with a well-defined phase relationships. The phase relationships are lost due to homogeneous (pure dephasing caused by dynamical interactions of the chromophores with the environment) and inhomogeneous broadening. After a time τ', the chromophores are subjected to another pulse (π pulse) with a wave vector $\mathbf{k}_2$ that switches the phase associated with each coherent superposition state by π with respect to that of the first optical coherent states. This starts a rephasing process. A time τ' still later (at $t = 2\tau'$), the inhomogeneous dephasing is eliminated (by being rephased) due to the rephasing process, and a macroscopic polarization (the echo field) is emitted by the sample in the direction $\mathbf{k}_a = 2\mathbf{k}_2 - \mathbf{k}_1$, *vide infra*. The echo reaches its maximum at $t = \tau'$. Since only the static inhomogeneous (reversible) dephasing is rephased at $t = 2\tau'$, then the signal is a measure of the homogeneous (irreversible) dephasing that has occurred between $t = 0$ and $2\tau'$. For $t > \tau'$, the echo decays due to the electronic dephasing. (Again, T_2 and T_1 must be long compared to τ' for the echo to be observed).

The PE process can be described mathematically using the wave function approach. Assuming that, at time $t = -0$, where $t = -0$ is used to indicate the time just before the first pulse arrives, the chromophores are in the ground electronic state $|g\rangle$. At $t = 0$, the $\pi/2$ pulse prepares the chromophores in a coherent superposition (non-stationary) quantum state

$$|\Psi(0)\rangle = \frac{1}{\sqrt{2}}(|g\rangle + |e\rangle), \tag{2.15}$$

where $|e\rangle$ is the excited electronic state. At time t = τ' – (just before the arrival of the π pulse), the wave function, $|\Psi(0)\rangle$, evolves under the time evolution operator as

$$|\Psi(\tau'-)\rangle = \frac{1}{\sqrt{2}}\left[\exp(-iE_g\tau'/\hbar)|g\rangle + \exp(-iE_e\tau'/\hbar)|e\rangle\right], \tag{2.16}$$

where E_g and E_e are energies of the ground and excited electronic states, respectively. Applying the second pulse at t = τ' , yields

$$|\Psi(\tau')\rangle = \frac{1}{\sqrt{2}}\left[\exp(-iE_e\tau'/\hbar)|g\rangle + \exp(-iE_g\tau'/\hbar)|e\rangle\right], \tag{2.17}$$

where the phase has been reversed in the wave function. During the time interval τ_1, the temporal evolution of chromophore wave function is given by

$$|\Psi(\tau'+\tau_1)\rangle = \frac{1}{\sqrt{2}}\left[\exp(-iE_e\tau'/\hbar - iE_g\tau_1/\hbar)|g\rangle + \exp(-iE_g\tau'/\hbar - iE_e\tau_1/\hbar)|e\rangle\right]. \tag{2.18}$$

The polarization of the medium can be calculated by evaluating the expectation value of the electronic transition dipole moment and is given in Ref. [12, 13]. Since an expression for the PE process polarization will be obtained through the non-linear response function approach, the polarization expression resulting from evaluating the expectation value of the electronic transition dipole moment will not be given here (see Ref. [12, 13]). For equal time intervals $\tau_1 = \tau'$, the polarization of the chromophore quantum state evolves radiating the echo field. Basically the second pulse, which acts as a phase reversing tool, subtracts the time development (in the wave function phases, i.e., the exponentials) during

the interval τ' such that the chromophores arrive back at their time t = 0 states at $t = \tau' + \tau_1$. For example, at $\tau_1 = \tau'$, Eq. (2.18) becomes

$$|\Psi(2\tau')\rangle = \frac{1}{\sqrt{2}}\left[\exp(-i(E_e + E_g)\tau'/\hbar)|g\rangle + \exp(-i(E_g + E_e)\tau'/\hbar)|e\rangle\right], \qquad (2.19)$$

which shows that both electronic states of the chromophores have the same phase. This is the case for the wave function at t = 0 (just like Eq. (2.15)). As a matter of fact, setting τ' equal to zero yields back Eq. (2.15). In other words, things have been restored.

The PE process can be visualized with the help of Bloch vector model using the construction of Figure 2.2, which shows the temporal evolution of the dipoles. The chromophores are initially in the ground electronic state in Figure 2.2 (a), where the Bloch vector, **u**, is pointing in the negative z-direction. Applying the first pulse at time t = 0 rotates the vector **u** $\pi/2$ radians up to the positive y-direction (Figure 2.2 (b)). Now the molecules (chromophores) are in a coherent superposition state, which is represented by Eq. (2.15), with a well-defined phase. Afterward, the molecules in Figure 2.2 (c) acquire different processional frequencies and are no longer in phase (the dipoles fan out in the xy-plane) due to the medium inhomogeneities; the higher frequency members will be ahead in phase and the lower frequency members will be behind in phase. The numbers label the positions of the dipoles as to which is ahead of the other, e.g., dipole labeled "+2" is ahead the rest and "–2 " is falling behind. At time $t = \tau'$, the molecules in Figure 2.2 (d) are subjected to a second pulse which rotates the vector **u** about the x-axis π radians up to the negative y-direction resulting in the reversal of the relative phases among the dipoles causing the members with higher frequencies that are ahead an amount η to suddenly be behind η (e.g., member "+2" is now behind and "-2" is ahead). In Figur 2.2 (e) the dipoles continue to precess about the z-axis in the same sense so that the faster dipoles can catch up with slower ones and eventually they add up constructively and the system rephases at $t = 2\tau'$, yielding a macroscopic

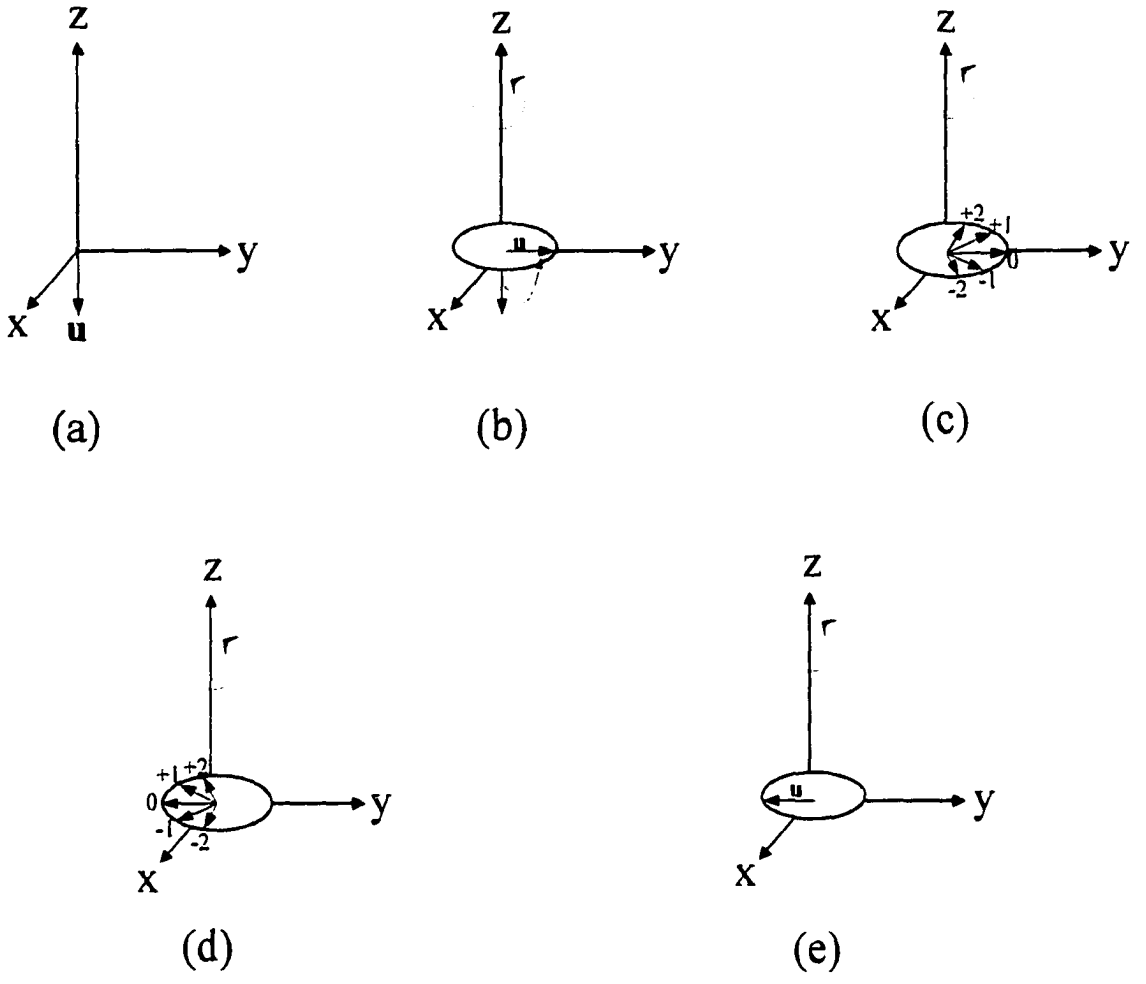

Figure 2.2 Bloch vector model for photon echo development. (a) For molecules initially in the ground electronic state, the Bloch vector **u** consists of one component pointing in the negative z-axis. (b) A $\pi/2$ pulse, rotates **u** up to positive y-axis. (c) The individual dipoles fan out due to the inhomogeneous broadening of the medium. (d) Another pulse rotates the dipoles π radians resulting in phase reversal among the dipoles. (e) Precessional motion continues about the z-axis in the same sense such that the faster dipoles can catch up with the slower ones allowing the system to rephase and eventually radiate an echo.

polarization that radiates an echo field. Since the homogeneous dephasing is irreversible (not rephased at t = 2 τ'), and only the inhomogeneous dephasing has been eliminated (rephased), the echo must then decay due to the homogeneous electronic dephasing. Therefore, the echo signal is a measure of the extent the homogeneous dephasing (homogeneous broadening in the frequency domain) between t = 0 and 2 τ'.

The two-pulse photon echo (PE) is a special case of the SPE in which pulses 2 and 3 are coincident ($\mathbf{k}_2 = \mathbf{k}_3$). The PE signal, S_{PE}, is generated in the direction $\mathbf{k}_a = 2\mathbf{k}_2 - \mathbf{k}_1$ and it is obtained by setting $E_2(t) = E_3(t)$, $\omega_2 = \omega_3$, $\mathbf{k}_2 = \mathbf{k}_3$, and $\tau = 0$, i.e., Eq. (2.13) gives

$$S_{PE}(\tau') = \int_0^\infty dt \left| R_2(\tau', 0, \tau') + R_3(\tau', 0, \tau') \right|^2 \chi(t - \tau'), \tag{2.20}$$

and very large inhomogeneous broadening, $\chi(t - \tau') \sim \delta(t - \tau')$, Eq. (2.20) yields

$$S_{PE}(\tau') = \left| R_2(\tau', 0, \tau') + R_3(\tau', 0, \tau') \right|^2 \tag{2.21}$$

2.3.3 Dynamical Considerations

A 4-point correlation function, $F(\tau_1, \tau_2, \tau_3, \tau_4)$, for a system whose modes are both linearly and quadratically coupled will be calculated in Chapter 4 using the excited state vibrational Hamiltonian, H_e, in Eq. (1.57). The associated $R_2(t_3, t_2, t_1)$ and $R_3(t_3, t_2, t_1)$ can be obtained from $F(\tau_1, \tau_2, \tau_3, \tau_4)$ using Eq. (4) of Chapter 4. $F(\tau_1, \tau_2, \tau_3, \tau_4)$ and its associated $R_2(t_3, t_2, t_1)$ and $R_3(t_3, t_2, t_1)$ for only linear coupling can then be obtained by setting ω' = ω". Our attention here will be focused on linearly coupled modes only. The response functions can be calculated from the line broadening function, $g(t;T)$, which is a complex quantity. As Fleming and co-workers [26] point out, the real part of $g(t;T)$ describes the line broadening via fluctuations , while the imaginary part describes the longer

time dynamics such as spectral diffusion. $g(t;T)$ is as important in non-linear spectroscopy as it is in linear measurements. In linear spectroscopy, the correlation function is (Eq. (1.58))

$$J\ (t;T), = \exp[-g(t;T) - i\Omega t], \tag{2.22}$$

while in non-linear spectroscopy the photon echo correlation functions, *vide supra*, are

$$\begin{aligned} R_2(t_3,t_2,t_1) &= \exp[-i\Omega(t_3 - t_1) - g^*(t_3;T) - g^*(t_1;T) + \\ &\quad g(t_2;T) - g(t_2 + t_3;T) - g^*(t_1 + t_2;T) + g^*(t_1 + t_2 + t_3;T)], \\ R_3(t_3,t_2,t_1) &= \exp[-i\Omega(t_3 - t_1) - g(t_3;T) - g^*(t_1;T) + \\ &\quad g^*(t_2;T) - g^*(t_2 + t_3;T) - g^*(t_1 + t_2;T) + g^*(t_1 + t_2 + t_3;T)]. \end{aligned} \tag{2.23}$$

Equation (2.23) can account for structural and dynamical information (e.g., pure electronic dephasing, quantum beats and spectral diffusion) about the system. In order to obtain this valuable information, one need to use the appropriate $g(t;T)$. Currently, we are aware of four mathematical forms of $g(t;T)$ with each form operating at a different level of physical sophistication: One form was given in Eq. (1.59b) and requires a simple damping constant in order to calculate spectra. Although it is unphysical because it yields a spectrum with a ZPL carrying a width that depends on the phonons damping (γ_j), it shows a reasonable structure for the vibrational progression members. Another form of $g(t;T)$ was obtained by Mukamel and co-workers using the multi-mode Brownian oscillator (MBO) model (see Chapter 8 of Ref. [8]). The MBO model has an advantage because it assigns different damping constants to different modes, and provides folding of the progression members which takes place in mixed crystals at liquid helium temperature [49, 50]. However, it yields the incorrect homogeneous width and intensity for the ZPL. (See Appendix A on p. 146 for more details.) The third form was obtained by Osad'ko [11, 13, 14]. Although it does not seem to have any

damping constants, it is set up such that the electronic pure dephasing can easily be taken into account by applying a damping constant, γ_{el}, for the homogeneous broadening of the ZPL and a damping constant, γ_j, for damping of the phonons. The last form, which we have developed (see Eq. (25) of Chapter 3), is given by

$$g(t;T) = \gamma_{el}(T)|t|/2 + S_j\{\coth(\beta\hbar\omega_j/2) - e^{-\gamma_j|t|/2}[\coth(\beta\hbar\omega_j/2)\cos(\omega_j t) - i\sin(\omega_j t)]\}, \tag{2.24}$$

where the first term is the electronic part, $g(t;T)^{el}$, and the second one is the phononic contribution, $g(t;T)^{ph}$, see Sec. IIB of Chapter 3 for more details. However, Osad'ko's and our $g(t;T)$ provide the most physical spectral or temporal profiles. As can be seen from Eq. (2.24), at high temperature $g(t;T)$ is dominated by its real part. The imaginary part of $g(t;T)$ is independent of temperature and , therefore, it dominates at low temperature. In the limit T $\rightarrow$ 0 K, $g(t;T)$ becomes

$$g(t) = \gamma_{el}|t|/2 + S_j(1 - e^{-\gamma_j|t|/2 - i\omega_j t}). \tag{2.25}$$

Suppose that g(t) = γ t, for illustration, which can be substituted in Eq. (2.14) to obtain S_{SPE},

$$S_{SPE}(\tau,\tau') = \exp(-4\gamma\tau'), \tag{2.26}$$

where γ is just a simple damping constant that measures half-width at half maximum (hwhm). Equation (2.26) shows the decay of the SPE signal at large τ' and that the echo drops to 1/e of its initial value at $t = T_2/4$ ($\gamma = 1/T_2$) [51]. This implies that the optical pulse should be shorter than $T_2/4$ to time resolve the echo decay. Equation (2.26) is a common

expression used by experimentalists to fit their data to obtain the slope which represents the depahsing time. Substituting Eq. (2.23) into Eqs. (2.13) or (2.14) yields the whole SPE profile that accounts for pure electronic dephasing, quantum beats and spectral diffusion. While the period τ' measures the fast dynamics (electronic dephasing), τ reflects longer time population dynamics and spectral diffusion (time dependent spectral shifts), *vide infra.*

Normally, the electronic dephasing rate can be extracted from the slope of the echo signal as a function of τ' [51, 52, 53]; alternatively, if the echo decays within the time resolution of the experiment, the dephasing can be obtained from the echo peak shift [26, 31, 54, 55]. The echo peak shift in a SPE signal is a measure of the difference between the signal decay on the rephasing side and that non-rephasing side. Thus the peak shift reflects the extent of the system ability to rephase (to generate the echo), i.e., the system's ability to retain memory of its electronic transition frequency after spending time, τ, in a population state. As Mukamel and co-workers point out [37], during the delay period τ (waiting time), the spectrum changes (both shifts and broadens) due to nuclear diffusive motions that are slow compared with the inverse line width, and that change the inhomogeneous distribution of the nuclear configurations. This time dependent process is called spectral diffusion [2-4, 6, 7, 28, 56-58] in which the linewidth changes with time. Spectral diffusion processes that occur during τ change the dephasing rate due to the change of the chromophore environment. During the time period τ, vibrational coherences may be observed (i.e., quantum beats) in the ground or the excited states and pure population relaxation in the excited state. This period represents the nuclear motions in an electronic state (see Eq. 2.27)) where the system does not acquire any phase and therefore no dephasing processes can take place during τ (τ is equivalent to t_2, where only nuclear dynamics may be probed). The absence of nuclear dynamics during τ' makes it impossible to probe population dynamics and spectral diffusion (τ' is equivalent to t_1 and t_3 intervals, where only dephasing processes can be measured, *vide supra*). The fact that the diagonal Green's function, $G_{mm}(t_2)$, governs the time evolution of

population states during t_2 indicates that only nuclear motions may be studied. This can be seen from the mathematical structure of $G_{mm}(t_2)$,

$$G_{mm}(t) = \exp(-iH_m t/\hbar) A \exp(iH_m t/\hbar). \tag{2.27}$$

Equation. (2.27) is a clear representation of one nuclear Hamiltonian of an electronic state (g or e) and therefore only vibrational states can be probed. For applications of measuring population dynamics and spectral diffusion using non-linear response functions in SPE experiments see [8-10, 17, 26, 31, 37, 38].

In a PE experiment, pulse 2 coincides with pulse 3 ($\tau = 0$) and thus the PE signal does not contain contributions from shift in energy of the excited state (i.e., population state) resulting from Stokes shift or spectral diffusion (because the response function, in the impulsive limit, becomes $\langle G_{eg}(\tau')G_{ge}(\tau')\rangle$ and $\langle G_{eg}(\tau')G_{ge}(\tau')\rangle$, in which dephasing is right followed by a rephasing process without a waiting time (τ) to allow for longer time dynamics to take place). On the other hand, the SPE contains the τ (the coherence information storage interval) interval that can be utilized to probe energy shift of the excited state, *vide supra.* (The reader is reminded that while pure electronic dephasing processes do not involve energy change, clearly population relaxations do).

The impulsive PE signal with finite inhomogeneous broadening can be calculated using Eqs. (2.20), (2.23), and (2.24). This yields

$$\begin{aligned} S_{PE}(\tau';T) = &\int_0^\infty dt \exp[-w^2(t-\tau')^2] \\ &\times \exp\{-2\,\mathrm{Re}[2g(t;T) + 2g(\tau';T) - g(t+\tau';T)]\}, \end{aligned} \tag{2.28}$$

where a Gaussian distribution has been used for the inhomogeneous broadening with w^2 being the variance. Note that only the real part contributes to the PE signal. Equation (2.28)

accounts for inhomogeneous dephasing, electronic dephasing (homogeneous broadening of the ZPL), and quantum beats, *vide infra*. Equation (2.28) generates a PE signal with an initial fast non-exponential decay that reflects the PSB contribution, periodic vibrational oscillations (quantum beats) signifying the coupling between nuclear motions and electronic coherence (interference between the ZPL and the multi-phonon transitions), and a slow exponential decay component due to the ZPL, *vide infra*. See Figures 3, 4, 5, and 6 of Chapter four for examples.

Quantum beats constitute the simplest example of quantum mechanical interference. When two levels are excited coherently and emit to a common final level, the emission spectrum oscillates with the two-level frequency. For example, suppose that the molecules are excited to a superposition of two closely spaced levels $|a\rangle$ and $|c\rangle$ by a pulse. One then observes that the emission intensity is modulated at the splitting ω_{ac} and varies periodically with the frequency ω_{ac} (for examples of quantum beats showing up in spectroscopy see Refs. [8-10, 12-14, 18-20, 29, 33, 38, 51-55, 59]). (Shank and co-workers [51] performed femtosecond echo experiments where quantum beats were due to the coupling of the nuclear motions to the electronic coherence between two electronic states). Quantum beats in time-domain experiments correspond to Franck-Condon progressions in the frequency-domain. Several examples of quantum beats showing up in two cases will be given in Chapter 4. The first case illustrates an impulsive SPE signal, which involves both linearly and quadratically coupled mode, due the vibrational frequency change upon electronic excitation which leads to a superposition of waves of two different frequencies, which gives rise to quantum mechanical interference (beats) with intensity that varies periodically with the frequency difference. The second case has to do with impulsive PE signals for only linearly coupled modes, where the quantum beats appear as underdamped vibrational oscillations, due to quantum mechanical interference between the ZPL and the multi-phonon transitions with intensity that varies periodically with the mode frequency ω_j modulated by the ZPL

frequency Ω (basically, the periodic position of the fundamental transition and its overtones in the frequency-domain). If Ω is set equal to zero, then the quantum beats are periodic only with the mode frequency ω_j. This quantum mechanical interference between the ZPL and the underdamped vibrational frequencies can easily be seen by using Eqs. (2.29) and (2.25) as follows:

$$\begin{aligned} J(t) &= \exp[-i\Omega t - \gamma_{el}|t|/2 + S_j(1 - e^{-\gamma_j|t|/2 - i\omega_j t})] \\ &= \exp(-i\Omega t)\exp(-S_j - \gamma_{el}|t|/2)\sum_{m=0}^{\infty} S_j^m \exp(-im\omega_j t - m\gamma_j|t|/2)/m! \\ &= \exp(-S_j - \gamma_{el}|t|/2)\{\exp(-i\Omega t) + S_j \exp(-i(\Omega+\omega_j)t - \gamma_j|t|/2) + \\ &\frac{1}{2!}S_j^2 \exp(-i(\Omega+2\omega_j)t - \gamma_j|t|) + \frac{1}{3!}S_j^3 \exp(-i(\Omega+3\omega_j)t - 3\gamma_j|t|/2) + \cdots\cdots, \end{aligned} \tag{2.29}$$

where the first term shows the frequency of the ZPL, and the terms thereafter show the frequencies of the fundamental peak and its overtones modulated by the ZPL frequency. which gives rise to quantum beats (Franck-Condon progressions in the frequency-domain) due to electron phonon coupling.

One can see what happens to the beats when the nuclear motions (phonons) are decoupled from the electronic transition (ZPL) by setting $S_j = 0$ in Eq. (2.29), $J(t)$ becomes

$$J(t) = \exp(-i\Omega t - \gamma_{el}|t|/2). \tag{2.30}$$

Equation (2.30) tells us that the beats have vanished and the ZPL represents the entire profile. Fourier transforming Eq. (2.30) yields a single-site absorption spectrum with one sharp band which is the ZPL with FC factor $e^{-S_j} = 1$

The mechanics that have been carried out in Eq. (2.29) should provide an insight about how the ZPL frequency modulates the mode frequency ω_j and its multiples. Of

course, in order to get the whole PE signal one needs to go through Eq. (2.28). However, PE decay measurements are linear absorption measurement hidden underneath a broad inhomogeneous distribution, and the homogeneous optical band is related to the PE signal [11, 13, 14, 29, 60] in which each component of the absorption lineshape is related to the temporal behavior of the echo decay function over the relevant time scales [11, 13, 14, 19, 20].

2.4 References

1. *Persistent Spectral Hole Burninig:* Sience and Applications, edited by W. E. Moerner (Springer, New York, 1987), Vol. 44.
2. R. Jankowiak, J. M. Hayes, and G. J. Small, Chem. Rev. **93**, 1471 (1993).
3. G. J. Small, *Spectroscopy and Excitation Dynamics of Condensed Molecular Systems*, edited by V. M. Agranovich and R. M. Hochstrasser (North-Holland, Amsterdam, 1983) p. 437.
4. G. Shulte, W. Grond, D. Harrer, and R. J. Silbey, J. Chem. Phys. **88**, 679 (1988).
5. S. Völker. *Relaxation Processes in Molecular Excited States*, edited by J. Fünfschilling (Kluwer, Dordrecht, 1989), p. 113.
6. J. Friedrich and D. Harrer, J. Chem. Phys. **76**, 61 (1982).
7. J. Friedrich and D. Harrer, Angewandte Chemie, Int. Ed. **23**, 113 (1984).
8. S. Mukamel, *Principles of Nonlinear Optical Spectroscopy* (Oxford University, New York, 1995).
9. Y. J. Yan and S. Mukamel, J. Chem. Phys. **94**, 179 (1991).
10. W. B. Bosma, Y. J. Yan, and S. Mukamel, Phys. Rev. A. **42**, 9620 (1990).
11. I. S. Osad'ko, *Spectroscopy and Excitation Dynamics of Condensed Molecular Systems*, edited by V. M. Agranovich and R. M. Hochstrasser (North-Holland, Amsterdam, 1983) p. 437.

12. I. S. Osad'ko and M. V. Stashek, J. Lumin. **64**, 25 (1995).

13. I. S. Osad'ko, Adv. Poly. **114**, 125 (1994).

14. I. S. Osad'ko and M. V. Stashek, JETP **79**, 293 (1994).

15. I. S. Osad'ko and S. N. Gladenkova, Chem. Phys. Lett. **198**, 531 (1992).

16 I. S. Osad'ko, M. A. Mikhailov and S. N. Gladenkova, Chem. Phys. Lett. **270**, 183 (1992).

17. R. F. Loring and S. Mukamel, Chem. Phys. Lett. **114**, 426 (1985); J. Chem. Phys. **83**. 2116 (1985).

18. S. Saikan, A. Imaoka, Y. Kanematsu, K. Sakoda and T. Kishida, Chem. Phys. Lett. **162**, 217 (1989).

19 S. Saikan, T. Nakabayashi, Y. Kanematsu, N. Tato, Phys. Rev. B. **38,** 7777 (1988).

20. S. Saikan, A. Imaoka, Y. Kanematsu, K. Sakoda, K. Kominami, M. Iwamoto, Phys. Rev. B. **41,** 3185 (1990).

21. S. Saikan, Y. Kanematsu, R. Shiraishi, T. Nakabayashi, T. Kushida, J. Luminescence. **38**, 15 (1987).

22. S. Saikan, J. W-I Lin, H. Nemoto, Phys. Rev. B. **46**, 11125 (1992).

23. S. Asaka, H. Nakatsuka, M. Fujiwara, M. Matsuka. Phys. Rev. A. **29**, 2286 (1984).

24. C. J. Bardeen, G. Cerullo, C. V. Shank, Chem. Phys. Lett. 280, 127 (1997).

25. P. Schellenberg, R. J. W. Louwe, S. Shochat, P. Gast, and T. J. Artsma, J. Phys. Chem. B. **101**, 6786 (1997).

26. Y. Nagasawa, S. A. Passino, T. Joo, and G. R. Fleming. **106**, 4840 (1997).

27. W. P. de Boeij, M. S. Pshenichnikov, K. Duppen, and D. A. Wiersma, Chem. Phys. Lett. **138**, 1 (1995).

28. L. R. Narashiman, K. A. Littau, D. W. Pack, Y. S. Bai, A. Elschner, and M. D. Fayer, Chem. Rev. **90**, 439 (1990).

29. W. H. Hesselink and D. A. Wiersma, *Spectroscopy and Excitation Dynamics of Condensed Molecular Systems*, edited by V. M. Agranovich and R. M. Hochstrasser (North-Holland, Amsterdam, 1983) p. 249.

30. R. L. Shoemaker, Annu. Rev. Phys. Chem. **30**, 239 (1979).

31. T. Joo, Y. Jia, J-Y. Yu, M. J. Lang, and G. R. Fleming, J. Chem. Phys. **104**, 6089 (1996).

32. K. A. Nelson and E. P. Ippen, Adv. Chem. Phys. **75**, 1 (1989).

33. J. Chesnoy and A. Mokhtari, Phys. Rev. A **38**, 3566 (1988).

34. W. S. Warren and A. H. Zewail, J. Chem. Phys. **78**, 2279 (1983).

35. N. F. Scherer, L. D. Ziegler, and G. R. Fleming, J. Chem. Phys. **96**, 5544 (1992).

36. R. F. Loring, Y. J. Yan, and S. Mukamel, J. Chem. Phys. **87**, 5840 (1987).

37 Y. J. Yan and S. Mukamel, Phys. Rev. A **41**, 6485 (1990).

38. S. Mukamel, Annu. Rev. Phys. Chem. **41**, 647 (1990); Adv. Chem. Phys. **70**, 165 (1988).

39. H. L. Fragnito, J. Y. Bigot, P. C. Becker, and C. V. Shnak, Chem. Phys. Lett. **160**, 101 (1989).

40. S. Saikan, Phys. Rev. A **38**, 4669 (1988); S. Saikan, T. Nakabayashi, Y. Kanematsu, and A. Imaoka, J. Chem. Phys. **89**, 4609 (1980).

41. B. M. Kharlamov, R. I. Personov, and L. A. Bykovskaya, Opt. Commun. **12**, 191 (1974).

42. Y. T. Mazurenko and V. S. Udaltsov, Opt. Spectrosc. **44**, 417 (1977).

43. M. J. Weber, J. Lumin. **36**, 179 (1987).

44. R. I. Personov, *Spectroscopy and Excitation Dynamics of Condensed Molecular Systems*, edited by V. M. Agranovich and R. M. Hochstrasser (North-Holland, Amsterdam, 1983) p. 555.

45. R. Jankowiak and G. J. Small, Anal. Chem. **61**, 1023A (1989).

46. R. Jankowiak and G. J. Small, Chem. Res. Toxicol. **4**, 256 (1991).

47. S. Mukamel and R. F. Loring, J. Opt. Soc. Am. B **3**, 595 (1986).

48. Y. J. Yan and S. Mukamel, J. Chem. Phys. **89**, 5160 (1988).

49. R. L. Beckman and G. J. Small, Chem. Phys. **30**, 19 (1978).

50. G. Fischer, Chem. Phys. Lett. **20**, 569 (1973).

51. P. C. Becker, H. L. Fragnito, J. Y. Bigot, C. H. Cruz, R. L. Fork, and C. V. Shank, Phys. Rev. Lett. **63**, 505 (1989).

52. W. Hesselink and D. A. Wiersma, Phys. Rev. Lett. **73**, 1991 (1979).

53. R. W. Schoenlein, D. M. Mittleman, J. J. Shiang, A. P. Alivisatos, and C. V. Shank, Phys. Rev. Lett. **70**, 1014 (1993).

54. A. M. Weiner, S. De Silvestri, and E. P. Ippen, J. Opti. Soc. Am. B **2**, 654 (1985).

55. R. Kaarli and M. Rätsep, Laser Phys. **2**, 517 (1992).

56. E. J. Nebbering, D. A. Wiersma, and K. Duppen, Chem. Phys. **183**, 167 (1994).

57. D. Thorn Leeson, O. Berg, and D. A. Wiersma, J. Phys. Chem. **98**, 3913 (1994).

58. L. R. Narashiman, Y. S. Bai, M. A. Dugan, and M. D. Fayer, Chem. Phys. Lett. **176**, 335 (1991).

59. M. J. Rosker, F. W. Wise, and C. L. Tang, Phys. Rev. Lett. **57**, 321 (1986).

60. P. Vöhringer, D. C. Arnett, T. -S. Yang, and N. F. Scherer, Chem. Phys. Lett. **237**, 387 (1995).

CHAPTER 3. OPTICAL RESPONSE FUNCTIONS FOR CONDENSED SYSTEMS WITH LINEAR AND QUADRATIC ELECTRON-VIBRATION COUPLING

A paper submitted to the Journal of Chemical Physics

Mohamad Toutounji and Gerald J. Small
Department of Chemistry, Iowa State University, Ames, IA 50011

Shaul Mukamel
Department of Chemistry, University of Rochester, Rochester, NY 14627

ABSTRACT

Understanding the similarities and differences between optical coherence loss of electronic transitions of chromophores in glasses and in the glass forming solvent requires, in part, linear response (2-point correlation) functions, J(t;T). An approximate excited state vibrational Hamiltonian (H_e) which accounts for both linear and quadratic electron-phonon coupling is derived that is acceptable for mode frequency changes smaller than 30%. The associated linear response function for the case of no damping is obtained. A response function that includes damping is proposed for systems whose modes are either linearly or quadratically coupled. It is the product of three response functions, two of which are phononic and associated with linear and quadratic modes. The third response function is electronic with a dephasing frequency γ_{el} that is the width of the zero-phonon line. The total response function yields single-site absorption spectra in which folding of the widths of multi-phonon and sequence transitions occurs. Applications of the new response functions are made to the temperature dependence of single site absorption and hole-burned spectra of the special pair band of the bacterial reaction center and the temperature dependence of the single site absorption spectrum of Al-phthalocyanine tetrasulphonate in glassy ethanol.

I. INTRODUCTION

Recently, there has been considerable activity in the use of femtosecond photon echo spectroscopies to study how nuclear (vibrational) motions lead to coherence loss of optical transitions of solute chromophores in liquids at room temperature.[1-12] Of particular interest has been the role of inertial (librational) intermolecular modes ("phonons") which couple linearly to the electronic transition and lead to optical dephasing on a timescale shorter than 1 ps. (Such modes lead to multi-phonon transitions in the $S_1 \leftarrow S_0$ absorption spectrum.) One reason for this interest is that the inertial modes may set the stage for longer timescale, larger amplitude nuclear solvent dynamics which are the rate limiting step in condensed phase electron-transfer reactions. The multi-mode Brownian oscillator (MBO) model[13-15] has often been used in interpretation of the data. In this model the linearly coupled modes are the primary BOs which, along with the bath oscillators, are taken to be harmonic. The coupling between a primary BO and the bath modes is linear in the BO displacement which results from electronic excitation of the chromophore. This coupling gives rise to a damping constant, $\gamma_j(\omega)$, for BO j of frequency ω_j. This gives rise to an effective frequency-dependent damping ($\gamma_j(\omega_j)$) for the jth BO where the frequency dependence arises from the spectral distribution of the BO's coupling to the bath oscillators. $\gamma_j(\omega)$ enters into the optical response function (see p. 227 of ref. 15). In applications of the MBO model the frequency dependence of γ_j is commonly neglected which amounts to a white spectrum for the bath (known as Ohmic dissipation). In the case of underdamping ($\gamma_j < \omega_j$), this leads to a width for the zero-phonon line (ZPL) of $2S_j(2\bar{n}_j + 1)\gamma_j$, where S_j is the Huang-Rhys factor and $\bar{n}_j$ the thermal occupation number of BO j. Thus, incorporation of pure electronic dephasing associated with the width (γ_{el}) of the ZPL in realistic host media at low temperatures requires different mechanisms that cannot be represented by the MBO model.

As discussed in refs. 16,17, hole burning and photon echo spectroscopies have been used to study pure electronic dephasing of the ZPL of chromophores in glasses and polymers

at low temperatures since the early 1980s (see refs. 18,19 for reviews). At temperatures lower than about 10 K the homogeneous width of the ZPL is determined by the tunneling dynamics of the bistable configurations or two-level systems of the glass. Above about 15 K the dephasing is dominated by quadratic electron-phonon coupling of the type identified earlier for chromophores in host crystals. The studies of the ZPL in glasses and polymers led to three important findings. The first is that the exchange coupling dephasing mechanism,[20,21] which stems from diagonal quadratic electron-phonon coupling, often accounts for the homogeneous width of the ZPL at higher temperatures. This coupling leads to a change in the frequency of a pseudo-localized phonon upon electronic excitation of the chromophore. The second finding is that these dephasing phonons are Franck-Condon (FC) inactive, i.e. exhibit negligible linear electron-phonon coupling. The third finding is that the linearly coupled modes responsible for multi-phonon transitions appear to be infrequently involved in pure electronic dephasing. The last two findings suggest that the system phonons can often be divided into two subsets, one associated with linear coupling and the other with quadratic coupling. The most detailed studies which support the above findings involved spectral hole burning experiments on Al-phthalocyanine tetrasulphonate (APT) in hyperquenched glassy films of water,[16] ethanol and methanol[17] which were performed over a very wide temperature range, 5- ~ 130 K. In the case of water, the exchange coupling modes correlated with the 50 and 180 cm^{-1} transverse and longitudinal acoustic modes of liquid water. For ethanol, the exchange coupling mode frequency is ~ 50 cm^{-1}, close to the first maximum in the spectral density of liquid ethanol. High resolution hole-burned spectra proved that these modes exhibit little if any FC activity. For water, ethanol and methanol the FC activity by intermolecular modes is dominated by phonons at 38, 26 and 17 cm^{-1}, respectively. They were assigned as modes mainly associated with APT librational motion. In the case of glassy water, characterization and determination of the electron-phonon coupling parameters (including the Huang-Rhys factor and shape of the one-phonon profile

for the linearly coupled mode at 38 cm^{-1}) and static inhomogeneous broadening associated with the pure electronic transition at lower temperatures led to calculated hole burned spectra for higher temperatures in good agreement with the experimental spectra.[16] The frequency domain hole burning theory of Hayes et al.[22-24] was used for the calculations. The results indicate that the above inhomogeneous broadening is constant over the temperature range used in the experiments. Given the good agreement, the same experimentally determined parameters were used to calculate the width of APT's origin absorption band in water at room temperature. The value of 500 cm^{-1} obtained differs by only 10 cm^{-1} from the experimental value. It was suggested that the combination of temperature dependent hole-burning and photon echo studies above and below the glass transition of the solvent should provide new insights on optical coherence loss of chromophores in liquids (see also refs. 25,26).

We present here linear response or 2-point correlation functions, J(t;T), which do yield single-site absorption and hole burned spectra at finite temperature that describe the essential features of experimental spectra. (The harmonic approximation is assumed for the optically active modes.) The response functions are appropriate for modes which are underdamped, $\gamma_j < \omega_j$.[27] The cases of critically damped and overdamped modes are treated in Chap. 8 of ref. 15. The case of linear electron-phonon coupling is considered first. The form of J(t;T) yields, for example, widths (fwhm) of $\gamma_{el}(T) + n_j \gamma_j(T)$ for members of the cold absorption progression (n_j=0,1,...) associated with mode j with $\gamma_{el}(T)$ the contribution from pure electronic dephasing. The linear dependence (folding) on n_j is valid for any relaxation mechanism of the active phonon that is linear in its coordinate. Insofar as the temperature dependencies of γ_{el} and γ_j are concerned, one need consider different mechanisms and feed their T-dependencies into J(t;T), which is standard procedure. J(t;T) or, equivalently the lineshape function g(t;T), allows for straightforward evaluation of the 4- and higher-point correlation functions associated with photon echo spectroscopies. Next, we consider the case where the active modes exhibit diagonal quadratic electron-phonon coupling which results in

mode frequency changes upon electronic excitation of the chromophore. An approximate excited state vibrational Hamiltonian, H_e, is derived which is shown to be adequate for a mode frequency change smaller than about 30%. (Off-diagonal quadratic electron-phonon coupling or the Duschinsky effect is neglected since it is expected to be unimportant for strongly allowed electronic transitions of dye molecules.[28] Such a change may be considered to be large for low frequency modes of condensed phase systems. An expression for the linear response function is derived for the case of no damping. A linear response function with damping is given for a system whose modes are either linearly or quadratically coupled (see preceding paragraph for motivation). The response function is the product of three response functions, two of which are associated with a phononic contribution, one from linearly coupled modes and the other from quadratically coupled modes. the third response function is associated with pure electronic dephasing.

Applications of the new response functions include the single-site absorption and hole-burned spectra of the special pair band of the bacterial reaction center which previous studies had shown to be characterized by linearly coupled modes at 30 and 120 cm^{-1} [29] and the temperature dependence of the single-site absorption spectrum of Al-phthalocyanine tetrasulphonate in glassy ethanol.

II. THEORY AND CALCULATED SPECTRA

A. Approximate excited state vibrational Hamiltonian H_e and linear response function J(t;T) with no damping.

Consider absorption from the ground electronic state (g) to an excited electronic state (e) and let ω'' and ω' be, respectively, the ground and excited state frequencies of a vibrational mode. Let q be the dimensionless normal coordinate of this mode for the ground electronic state. It is related to the mass-weighted coordinate, Q, by $q = (\omega''/\hbar)^{1/2}Q$. Similarly, we define d as the dimensionless translational displacement between the potential

energy minima of the two electronic states. For linear and diagonal quadratic electron-phonon coupling the excited state vibrational Hamiltonian is given exactly by[30]

$$H_e = H_g + \frac{\hbar\omega''}{2}[(r^2-1)q^2 + 2r^2 qd + r^2 d^2] + \hbar\Omega, \tag{1}$$

where $r = (\omega'/\omega'')$. $\hbar\Omega$ is the adiabatic electronic energy gap. The r^2d^2 term multiplied by $\hbar\omega''/2$ is the optical reorganization energy. Thus,

$$\Omega_v = \Omega + \omega'' r^2 d^2/2, \tag{2}$$

where Ω_v is the vertical (Condon) frequency gap. When $\omega' = \omega''$, the optical reorganization energy is $S\omega''$, with $S = d^2/2$ being the familiar Huang-Rhys factor. In Eq. (1), H_g is the vibrational Hamiltonian for the ground state:

$$H_g = \hbar\omega''(a^+a + 1/2), \tag{3}$$

with a^+ and a the raising and lowering operators for the ground state, i.e. $q = 2^{-1/2}(a^+ + a)$. For a multi-mode system one need only sum Eq. (1) over all modes. When dealing with fluorescence or resonance Raman, one should interchange e and g, ω' and ω'' and associate q with the normal coordinate of the excited state (e.g. d would now equal $(\omega'/\hbar)\Delta Q$ rather than $(\omega''/\hbar)\Delta Q$). The reader is referred to ref. 31 for further (and simple) discussion.

Exact solutions to the problem of determining the Franck-Condon factors associated with Eq. (1) have been available for many years.[32-35] Thus, calculation of "stick" linear absorption spectra, $\sigma(\omega)$, is routine. One can introduce shapes to the sticks and calculate the temperature dependencies of the integrated absorption intensities of the vibronic (phononic)

transitions. However, doing the equivalent of this in the time domain with Eq. (1) is both difficult and impractical, especially when one is interested in nonlinear spectroscopies such as the 2-pulse and 3-pulse stimulated photon echo since they involve 4-point correlation functions. It is essential, therefore, to approximate Eq. (1). In what follows we derive an expression for H_e which is adequate for $r \gtrsim 0.7$ (without loss generality we take $\omega' < \omega''$).

Our approach involves a first-order Taylor series expansion of the $r^2 - 1$ and r^2 terms in Eq. (2) about r = 1 (e.g., $r^2-1 \approx 2r-1$). When it is recognized that H_g of Eq. (3) is exactly equivalent to

$$H_g = \hbar\omega'(a^+a + 1/2) - \hbar\omega''(r-1)a^+a - \hbar\omega''(r-1)/2, \tag{4}$$

it follows easily that

$$H_e \approx \hbar\omega'\left[\left(a^+a + \frac{1}{2}\right) + (2-r^{-1})d(a^+ + a)/\sqrt{2} + (2-r^{-1})d^2/2\right] + \hbar\Omega \tag{5}$$

when the term $2^{-1}\,\hbar\,\omega'(1 - r^{-1})\,(a^{+2} + a^2)$ is dropped. *It is the elimination of this term that leads to the desired simplification.* The $(a^{+2} + a^2)$ operator brings intensity, in first order, to phononic transitions for which the quantum number n changes by ±2. However, the contributions from that operator to such transitions which carry sufficient intensity from linear coupling to be relevant to linear and nonlinear optical experiments are small for $r \gtrsim 0.7$. The effect of the $(a^{+2} + a^2)$ operator on transitions for which the quantum number change is odd is also small for such r-values (see below for supportive results). The vertical transition frequency from Eq. (5) is

$$\Omega_v = \Omega + \omega'(2 - r^{-1})d^2/2 \tag{6}$$

The most important effect from quadratic coupling for systems of the type we are interested in has to do with sequence structure in the absorption spectrum, i.e. n'' = n' transitions which carry different frequencies, one result of which could be beats in photon echo decays. The relative intensities of such transitions depend, of course, on temperature. Importantly, the expression for H_e given by Eq. (5) retains the sequence structure.

We turn next to the two-point correlation function J(t) whose Fourier transform yields the linear absorption spectrum. In the Heisenberg picture,[15]

$$J(t;T) = \left\langle e^{iH_g t/\hbar}\, v(q)\, e^{-iH_e t/\hbar}\, v(q)\, \rho_g \right\rangle \tag{7}$$

with $\rho_g = \exp(-\beta H_g)/\mathrm{Tr}[\exp(-\beta H_g)]$, $\beta = (kT)^{-1}$. <···> denotes quantum mechanical trace (Tr) over the nuclear degrees of freedom. Because we are in the Heisenberg picture, the electronic transition dipole moment operator v(q) is time-independent. In the Condon approximation, which we employ,[36] the dependence of v on the vibrational coordinates q is lost, i.e. v(q) = v(0), a constant whose magnitude squared contains the square of the pure electronic transition dipole. Setting $|v(0)|^2$ multiplied by other constants equal to 1 for convenience, we are left with

$$J(t;T) = \left\langle e^{iH_g t/\hbar}\; e^{-iH_e t/\hbar}\; \rho_g \right\rangle \tag{8}$$

to evaluate with H_g and H_e given by Eqs. (3) and (5). In doing so we employed coherent states for the phonon field rather than number states. The reader is referred to refs. 39-42 for discussions on advantages gained in utilization of coherent states as a complete basis set. Appendix A reviews some basic properties of coherent states, including their evolution under

the time-evolution operator. We mention here only that a coherent state $|z\rangle$ is an eigenvector of the non-hermitian lowering operator a,

$$a|z\rangle = z|z\rangle, \tag{9}$$

where the eigenvalue z can be complex, that $|z\rangle$ can be expressed as a superposition of phonon number states and that coherent states obey a special type of closure relationship:

$$\frac{1}{\pi}\int d^2z \frac{|z\rangle\langle z|}{\langle z|z\rangle} = 1, \tag{10}$$

where $d^2z = d(\text{Re } z)\, d(\text{Im } z)$. It is the elimination of the a^{+2} and a^2 operators from H_e that allows for relatively straightforward evaluation of J(t;T). The result is[43]

$$J(t;T) = \frac{1}{\pi}\int \frac{d^2z}{\langle z|z\rangle}\langle z|e^{iH_g t/\hbar}\, e^{-iH_e t/\hbar}\, \rho_g|z\rangle \tag{11}$$

$$= \frac{C}{Q}\left(\frac{1}{f_1}\right)\exp\left[\frac{f_2}{f_1} + f_3\right] \tag{12}$$

where $Q \equiv \text{Tr}(\exp(-\beta H_g)]$ is the canonical partition function,

$$Q = [2\sinh(\beta\hbar\omega''/2)]^{-1}, \tag{13}$$

and

$$C \equiv e^{-\beta\hbar\omega''/2}\, e^{-i(\omega'-\omega'')t/2}\, e^{-i\Omega_v t} \tag{14a}$$

$$f_1 \equiv 1 - e^{\beta\hbar\omega'' + i(\omega''-\omega')t} \tag{14b}$$

$$f_2 \equiv S_{eff}\, e^{-\beta\hbar\omega'' + i\omega'' t}\,(e^{-i\omega' t} - 1)^2 \tag{14c}$$

$$f_3 \equiv iS_{eff}\omega' t + S_{eff}\,(e^{-i\omega' t} - 1). \tag{14d}$$

The derivation of Eq. (12) leads to $S_{eff} = (2-r^{-1})^2 d^2/2$ which contains a term of higher order than should be retained. For this reason and because the first term of Eq. (14d) should cancel out the contribution to Ω_v from the optical reorganization energy in the last exponential of Eq. (14a), we use in what follows

$$S_{eff} \equiv (2 - r^{-1})d^2 / 2. \tag{15}$$

With this equation and Eq. (6), Eqs. (14a) and (14d) become

$$C \equiv e^{-\beta\hbar\omega''/2}\; e^{-i(\omega'-\omega'')t/2}\; e^{-i\Omega t} \tag{14a)'}$$

and

$$f_3 \equiv S_{eff}\,(e^{-i\omega' t} - 1). \tag{14d)'}$$

At this point it is important to establish the reliability of J(t;T) as given by Eq. (12); i.e., one need check the Franck-Condon (FC) factors. The easiest way to do this is to Fourier transform J(t;T) to obtain the linear absorption spectrum:

$$\sigma(\omega;T) = \frac{1}{2\pi}\int_{-\infty}^{+\infty} J(t;T)\, e^{i\omega t}\, dt \tag{16}$$

The result is (Appendix B):

$$\sigma(\omega;T) = 2^{-1}(1-e^{-\beta\hbar\omega''})\, e^{-S_{eff}} \sum_{q=0}^{\infty} \frac{(S_{eff})^q}{q!} \sum_{n''=0}^{\infty} e^{-n''\beta\hbar\omega''}\, n''!$$

$$\times \left\{ \sum_{m=0}^{n''} \sum_{\ell=0}^{m} (-1)^{m+\ell}\, 2^{-2m}\, \frac{(4\,S_{eff})^m\,(2m)!\,\varepsilon_\ell}{(m!)^2\,(n''-m)!\,(m+\ell)!\,(m-\ell)!} \right\}$$

$$\times [\delta(\tilde{\omega} - \ell\omega') + \delta(\tilde{\omega} + \ell\omega')] \qquad (17)$$

where ε_ℓ is the von Neumann symbol ($\varepsilon_0 = 1$, $\varepsilon_\ell = 2$ for $\ell \geq 1$) and

$$\tilde{\omega} = \omega - \Omega - q\omega' + (\omega'' - \omega')(n'' + 1/2). \qquad (18)$$

S_{eff} is defined by Eq. (15). In Eq. (17) n" is the initial state quantum number of the absorption transition. We performed calculations which confirmed that Eq. (17) and the numerical Fourier transform (FT) of Eq. (12) yield identical spectra. Franck-Condon factors for n"→n' transitions can be obtained from Eq. (12) by setting the value of n" and the value of ω for the n"→n' transition of interest. One then sets the (1 – exp(–βħω")) and exp(–n"βħω") terms equal to unity and adds the terms in Eq. (17) whose delta functions give the correct ω-value. All appropriate delta functions are then set equal to unity. This procedure is somewhat cumbersome for hot transitions. For cold transitions, n" = 0, it is simple because q in Eq. (17) is n' and m and ℓ are zero. Table I compares our approximate FC factors for a few transitions with the exact FC factors calculated using harmonic oscillator wavefunctions with Mathematica 2.2. (We confirmed that, for pure linear coupling, Eq. (17) gives FC factors in exact agreement with the values calculated using the latter method.) The results given in Tables I and II are for r = 0.7 and 0.8 and S = 0.8 (Table I) and 2.0 (Table II) with $S = d^2/2$. S_{eff} in Eq. (17) is determined using Eq. (15). Overall, the agreement between the approximate and exact FC factors may be said to be quite satisfactory. (The agreement for

r = 0.8 is better than for r = 0.7.) As expected, the agreement for small FC factors worsens. However, the associated transitions would contribute relatively weakly to the absorption spectrum. Furthermore, for small FC factors anharmonic or even Duschinsky contributions to the intensities can be expected to be non-negligible. Also included in the tables are approximate FC factors calculated using the bottom equation on p. 121 of Englman[35] which is restricted to cold transitions. We conclude that for r $\gtrsim$ 0.7, the excited state vibrational Hamiltonian given by Eq. (5) for linear and quadratic coupling is a useful approximation for condensed phase phononic transitions which contribute significantly to the absorption spectrum. Condensed phase systems which exhibit r-values smaller than 0.7 for the intermolecular modes should be rare.

B. A Linear Response Function for a Multi-Mode System with Linear Electron-Phonon Coupling

The response function for the case of linear coupling only is obtained from Eq. (12) by setting $\omega' = \omega''$. For the multi-mode system

$$J_\ell(t;T) = \exp[-g(t;T)], \tag{19}$$

where the line-shape function

$$g(t;T) = \sum_j g_j(t;T), \tag{20}$$

with j labeling the mode and

$$g_j(t;T) = S_j\left[\coth(\beta\hbar\omega''_j/2)\left(1-\cos(\omega''_j t)\right) + i\sin(\omega''_j t)\right]. \tag{21}$$

Equation (21) is a well-known result (for convenience we set the adiabatic electronic energy gap, Ω, equal to zero). Since damping isn't included, the FT of $J_\ell(t;T)$ yields an absorption spectrum consisting of delta-function peaks, see Eq. (17). The problem, therefore, is to introduce damping(s) in a way that yields physically acceptable spectra.

The linear response and lineshape functions which follow stem from our study of the consequences of the MBO model (see Chap. 8 of ref. 15) for linear absorption and hole burned spectra (unpublished results). We propose a phononic contribution to $J_\ell(t;T)$ of the form

$$J_\ell^{ph}(t;T) = \exp[-g^{ph}(t;T)], \tag{22}$$

where

$$g^{ph}(t;T) = \sum_j g_j^{ph}(t;T) \tag{23}$$

and

$$g_j^{ph}(t;T) = S_j\left\{\coth(\beta\hbar\omega_j/2) - e^{-\gamma_j|t|/2}[\coth(\beta\hbar\omega_j/2)\cos(\omega_j t) - i\sin(\omega_j t)]\right\}. \tag{24}$$

Here, γ_j is the damping constant of mode j and S_j and ω_j are its Huang-Rhys factor and frequency. The FT of $\exp[-g_j^{ph}(t;T)]$ yields a delta-function lineshape for the ZPL and, for example, widths (fwhm) of $n_j'\gamma_j$ for the "cold" phonon transitions, $n_j'' = 0 \rightarrow n_j' = 1,\ldots,$ *vide infra*. The linear dependence of the width on n_j' is expected for a decay mechanism of mode j that is linear in its coordinate. Let γ_{el} be the actual width of the ZPL. The response function

$$\tilde{J}_\ell(t;T) = J_\ell^{ph}(t;T)\cdot J^{el}(t;T), \tag{25}$$

with $J_{\ell}^{ph}(t;T)$ given by Eq. (22) and

$$J^{el}(t;T) = \exp(-\gamma_{el}(T)|t|/2), \tag{26}$$

yields a ZPL with a width of γ_{el}. (We remind the reader that the temperature dependencies of γ_{el} and the γ_j's depend on the mechanisms of dephasing.) For the $n_j'' = 0 \rightarrow n_j' = 0,1,\ldots$ progression, the widths of the members are $\gamma_{el} + n_j'\gamma_j$. Clearly the addition of γ_{el} to the widths of the cold multi-phonon transitions has a physical basis.

The FT of Eq. (25) for mode j is (Appendix C):

$$\sigma_j(\omega_j;T) = \exp[-S_j \coth(\beta\hbar\omega_j/2)] \sum_{m=-\infty}^{\infty} \sum_{\ell=0}^{\infty} \left\{ \frac{\left(S_j \operatorname{csch}(\beta\hbar\omega_j/2)\right)^{m+2\ell}}{\ell!\,\Gamma(m+\ell+1)2^{(m+2\ell)}} \exp(m\beta\hbar\omega_j/2) \right.$$
$$\left. \times \frac{(\gamma_{el} + (m+2\ell)\gamma_j)/2\pi}{(\omega - m\omega_j)^2 + \left((\gamma_{el} + (m+2\ell)\gamma_j)/2\right)^2} \right\}, \tag{27}$$

where Γ is the gamma function. This equation describes the absorption spectrum associated with mode j. As expected from Eq. (24) and Eq. (26), the last term in Eq. (27) leads to Lorentzian lineshapes for all bands. Unfortunately, the complexity of Eq. (27) does not lend itself to ready visualization of the absorption spectrum. The presence of $(m+2\ell)\gamma_j$ in the Lorentzian suggests that there can be negative contributions to σ_j. However, the properties of the Γ function are such that $\Gamma(m+\ell+1) = \pm\infty$ for $(m+2\ell) \leq 0$ so that negative contributions do not arise. Figure 1 shows a spectrum calculated with Eq. (27) for $\omega_j = 25$ cm^{-1}, $S_j = 1.8$, $\gamma_j = 3$ cm^{-1}, $\gamma_{el} = 1$ cm^{-1} and $T = 50$ K. The spectrum calculated by taking the numerical FT of the response function is identical. The sharp ZPL appears superimposed on the broader

(1,1) and (2,2) transitions. The effects of folding, which lead to larger widths for higher quantum number transitions, are also apparent. Further discussion of folding is given later.

In Appendix C we show that with $\gamma_{el} = \gamma_j = 0$, one recovers the well-known frequency domain result (see, e.g., Eq. (8.43) of ref. 15):

$$\sigma_j(\omega;T) = \exp\left[-S_j \coth\left(\frac{\beta\hbar\omega_j}{2}\right)\right] \sum_{m=-\infty}^{\infty} \exp(m\beta\hbar\omega_j/2)\, I_m(z_o)\, \delta(\omega - m\omega_j), \tag{28}$$

where $z_o = S_j \,\mathrm{csch}(\beta\hbar\omega_j/2)$ and $I_m(z_o)$ are modified Bessel functions. We have also proven that[43] Eq. (27) is mathematically equivalent to Eq. (17) of Hayes et al.,[24] an equation whose structure is quite different than that of Eq. (27). In that paper, Eq. (17) is the basis for a frequency domain theory of hole burned spectra. By setting $\coth(\beta\hbar\omega_j/2) = 1$ in Eq. (24) and taking the FT of $\tilde{J}_\ell(t)$, Eq. (25), one obtains for the T = 0 K spectrum:

$$\sigma_j(\omega) = \exp(-S_j) \sum_{m=0}^{\infty} \frac{S_j^m}{m!} \left\{ \frac{(\gamma_{el} + m\gamma_j)/2\pi}{\omega - m\omega_j)^2 + \left((\gamma_{el} + m\gamma_j)/2\right)} \right\}, \tag{29}$$

with { } a normalized Lorentzian with widths given by

$$(fwhm)_m = \gamma_{el} + m\,\gamma_j \tag{30}$$

for the progression members, m=0,1,.... Here, the nature of the folding is clear and one has the desired result that γ_{el}, from pure electronic dephasing, adds to the widths of the multi-phonon transitions. Equation (27), with its Poisson distribution for the Franck-Condon factors, can also be obtained starting with Eq. (27). The derivation is quite lengthy and will be given elsewhere.[43]

In summary the postulated response function $\tilde{J}_\ell(t;T)$ of Eq. (25), with J_ℓ^{ph} and J^{el} defined by Eqs. (22) and (26), leads to a frequency domain expression for the absorption spectrum, Eq. (27), which yields physically reasonable spectra, as will become more apparent. Thus, single site absorption and hole-burned spectra at finite temperature can be conveniently calculated by numerically Fourier transforming $\tilde{J}_\ell(t;T)$, see subsection D. As written, $\tilde{J}_\ell(t;T)$ yields Lorentzian lineshapes for all transitions. The modifications necessary to introduce different lineshapes are discussed in the final section of the paper.

C. A Linear Response Function for a System whose Modes are Either Linearly or Quadratically Coupled

As pointed out in the Introduction, there appear to be a number of systems of chromophores in amorphous solids where modes are either linearly or quadratically coupled. We consider first pure quadratic (q) coupling. The linear response function for the case of no damping is given by Eq. (12) with S_{eff} set equal to zero. Guided by the mathematical insights gained in the development of $\tilde{J}_\ell(t;T)$, Eq. (25), we were led to the following expression as a potentially useful response function which includes damping (dephasing) of the phonons and pure electronic dephasing (γ_{el}):

$$\tilde{J}_q(t;T) = J_q^{ph}(t;T) \cdot J^{el}(t;T), \tag{31a}$$

with J^{el} defined by Eq. (26) and the phononic (ph) contribution to the response function given by

$$J_q^{ph}(t;T) = \prod_j J_{q.j}^{ph}(t;T), \tag{31b}$$

with

$$J^{ph}_{q,j}(t;T) = \frac{(1-e^{-\beta\hbar\omega''_j})\, e^{-i(\omega'_j-\omega''_j)t/2}}{1-e^{-\beta\hbar\omega''_j-i(\omega'_j-\omega''_j)t-\gamma_j|t|/2}}. \tag{31c}$$

The FT of Eq. (31) yields a delta-function line shape for the ZPL ($n''_j = 0 \rightarrow n'_j = 0$ transition) and widths for the $n''_j \rightarrow n'_j = n''_j$ sequence transitions of

$$(fwhm)\, n''_j = n''_j \gamma_j \,;\, n''_j = 1,2,\ldots, \tag{32}$$

where γ_j is the width of the $n''_j = 1 \rightarrow n'_j = 1$ transition. For the sake of brevity we do not give the proof of Eq. (32), but see discussion of Fig. 2, *vide infra*. The FT of $J^{ph}_{q,j}(t;T)$ multiplied by $J^{el}(t;T)$ (Eq. (26)) yields a width of γ_{el} for the ZPL defined above. Equation (32) becomes

$$(fwhm)_{n''_j} = \gamma_{el} + n''_j \gamma_j \,;\, n''_j = 0,1,\ldots. \tag{33}$$

With the results of this and the preceding subsection, the response function for a system whose modes are either linearly or quadratically coupled can be written as

$$\tilde{J}_{\ell,q}(t;T) = J^{ph}_{\ell}(t;T) \cdot J^{ph}_{q}(t;T) \cdot J^{el}(t;T), \tag{34}$$

with the three terms on the R.H.S. defined by Eqs. (22), (31b) and (26). Equation (34) is the main result of this paper. Figure 2 shows the absorption spectrum calculated by taking the numerical FT of Eq. (34) for a model system consisting of one linearly (ℓ) mode and one quadratically (q) coupled mode. For the former, $\omega_\ell = 200$ cm^{-1}, $S_\ell = 0.70$, $\gamma_\ell = 5$ cm^{-1} and for the latter, $\omega''_q = 50$ cm^{-1}, $\omega'_q = 35$ cm^{-1} and $\gamma_q = 2$ cm^{-1}. γ_{el}, is set equal to 1 cm^{-1} and T = 100 K. The location of the ZPL at – 7.5 cm^{-1} is a zero-point energy effect due to the

quadratically coupled mode. The width of the ZPL in Fig. 2 is 1 cm^{-1}, as expected since γ_{el} = 1 cm^{-1}. The measured widths of the $(1,1)_q$ and $(2,2)_q$ sequence transitions to the left of the ZPL are 3 and 5 cm^{-1}, in accordance with Eq. (32). The cold $(1,0)_\ell$ transition due to the linearly coupled 200 cm^{-1} mode carries a width of 5 cm^{-1}, in accordance with Eq. (30). To the left of the $(1,0)_\ell$ band are the sequence transitions due to the quadratic mode. The measured width of the band to the immediate left of the $(1,0)_\ell$ band is 7 cm^{-1}, which is the sum of γ_{el} = 1 cm^{-1} and the phononic contributions to the widths of the $(1,1)_q$ and $(1,0)_\ell$ transitions.

D. Application to Real Systems

The lowest energy ($S_1(Q_y) \leftarrow S_0$ absorption band of the special BChl *a* pair (P) of the bacterial reaction center has been investigated in detail using hole burning spectroscopy.[29,44] For *Rb. sphaeroides* this so-called P-band is characterized by strong linear electron-coupling involving modes centered at ω_m = 30 cm^{-1} and ω_{sp} = 120 cm^{-1}. The former is most likely due to protein phonons. The Huang-Rhys factor S_m = 1.8 and the effective damping constant is γ_m ~ 30-40 cm^{-1}. In the calculations which follow a value of 20 cm^{-1} for γ_m was used in order to enhance the structure in the single-site absorption and hole burned spectra. The 120 cm^{-1} mode is referred to as the special pair marker mode. Its effective damping constant is γ_{sp} = 25 cm^{-1} and its Huang-Rhys factor is S_{sp} = 1.5. At sufficiently low temperatures the homogeneous width of the pure electronic transition is 5 cm^{-1} due to the 1 ps primary charge separation process that depopulates the excited state. The hole burning results indicate that the width of the ZPL remains constant at 5 cm^{-1} between 1.8 K and 15 K, at which temperature the ZPH is nearly Franck-Condon forbidden. Thus, over this temperature range the contribution to the homogeneous width of the ZPL from interaction with the bath modes is negligible.

The upper frame of Fig. 3 is the 0 K single-site absorption spectrum of the special pair calculated with Eq. (25). The parameter values given above were used. The spectrum is very similar to that calculated by Reddy et al.[45] in the frequency domain. The washing out of structure for the higher energy bands is due to folding. The spectrum for 15 K is shown in the bottom frame of Fig. 3. The most significant difference between the 0 K and 15 K spectra is that the ZPL of the latter is considerably weaker. This is due to a reduction in its FC factor stemming from the linearly coupled 30 cm^{-1} mode. Also, the lower frame shows a hot band at $\omega = -30$ cm^{-1} due to (0,1) transition.

We now extend the calculations to the hole burned spectrum of the P-band. The absorption spectrum following a burn for time τ is given by[22-24]

$$\sigma_\tau(\omega;T) = \int_{-\infty}^{+\infty} d\Omega\, \chi(\Omega - \nu_m)\, \tilde{J}_\ell(\omega - \Omega)\exp[-k\tilde{J}_\ell(\omega_B - \Omega)\tau], \tag{35}$$

where Ω is the frequency of the ZPL of a single absorber and ω_B is the burn frequency. $\chi(\Omega - \nu_m)$ is a Gaussian function, with variance w^2 centered at ν_m, which governs the distribution of ZPL frequencies due to structural heterogeneity. k is the product of three terms: the absorption cross-section, the laser burn flux and the quantum yield for hole-burning. $\tilde{J}_\ell(\omega - \Omega)$ is the absorption spectrum of a single site whose ZPL frequency is Ω. Note that for $\tau = 0$, Eq. (34) is the inhomogeneously broadened absorption spectrum. The hole-burned spectrum is defined here as $\sigma_\tau(\omega;T) - \sigma_0(\omega;T)$. The 0 K (upper frame) and 15 K (lower frame) hole burned spectra shown in Fig. 4 correspond to the single site absorption spectra of Fig. 3. The value for the standard deviation of $\chi(\Omega - \nu_m)$ used was 64 cm^{-1} [29] (ν_m was set equal to zero with ω_B set equal to ν_m). $k\tau$ was set at 0.004. The calculation of $\sigma_\tau(\omega;T)$ involved[46] taking the numerical Fourier transform of Eq. (25). The agreement between the 0 K hole burned spectrum of Fig. 4 and the experimental spectrum[29] as well as the

spectrum calculated using the frequency domain theory of Hayes et al.[24] (not shown) is good. Note the very weak intensity of the ZPH at ω_B which carries a width of $2\gamma_{el} = 10\ cm^{-1}$, as expected.[47] The weakness of the ZPH can be understood from its FC factor, $\bar{n}\ \exp[-2\{S_m(\bar{n}(\omega_m)+1)+S_{sp}(\bar{n}(\omega_{sp}+1)\}]$, where the $\bar{n}$'s are thermal occupation numbers. For T = 0 K, the FC factor is exp(−6.6) = 0.0014. Elevation of the temperature to 15 K is sufficient to significantly reduce the intensity of the ZPH, in agreement with experiment.[29] The effect of increasing γ_m from 20 cm^{-1} to 40 cm^{-1}, the value used in ref. 24, would be to significantly fill in the valley between the ZPH at ω_B and the phonon sideband hole at $\omega_B + \omega_m$, resulting in an apparent weakening of the ZPH.

As a final application we consider the chromophore APT in hyperquenched glassy films of ethanol which has been thoroughly studied by nonphotochemical hole burning spectroscopy.[17] This system is characterized by a linearly coupled mode with $\omega_\ell = 25\ cm^{-1}$, $S_\ell = 0.5$ and $\gamma_\ell \sim 10\ cm^{-1}$ and a quadratically coupled mode with $\omega_q'' = 50\ cm^{-1}$ which is responsible for dephasing of the zero-phonon transition. For the calculations we set $\omega_q' = 35\ cm^{-1}$ which represents a 30% frequency change. The temperature dependent data of ref. 17 indicate that $\gamma_{el}(T) = 8\ \bar{n}\ (\omega_q'')\ cm^{-1}$ and, furthermore, that $\gamma_q(T) = 5(\bar{n}(\omega_q'')+1)\ cm^{-1}$ when the theoretical model of Jackson and Silbey[21] is used. γ_ℓ is taken to be temperature independent. The single site absorption spectra for T = 15, 60 and 100 K shown in Fig. 5 were calculated by numerical FT of Eq. (34). In all three spectra the ZPL is located at −(50−35)/2 cm^{-1} relative to 0 cm^{-1} which would be the position in the absence of quadratic coupling. At 15 K (top frame) only the ZPL and cold $(1,0)_\ell$ transition is observed. At 60 K, the sequence $(1,1)_q$ transition and hot $(0,1)_\ell$ transition appear as well as the $(2,0)_\ell$ band. Structure is diminished at 100 K (bottom frame) due to the higher probability for multi-phonon transitions and sequence transitions with larger n" values as well as folding and the temperature dependencies imposed on γ_{el} and γ_q. At 300 K all structure is lost (result not shown).

III. CONCLUSIONS

This paper is the result of our interest in understanding the relationship and differences between the optical coherence loss of a chromophore in a glass and in the liquid phase of the glass forming solvent.[17] Linear response functions were presented which allow for a consistent approach to the calculation of single-site and inhomogeneously broadened absorption spectra and hole burned spectra. The response functions are appropriate for systems whose modes are underdamped. Two cases were treated: a system whose modes exhibit only linear electron-phonon coupling (Eq. (25)); and a system whose modes are either linearly or quadratically coupled (Eq. (31a)). The response functions take into account pure electronic dephasing, γ_{el}, which is responsible for the homogeneous width of the ZPL. Furthermore, γ_{el} adds to the widths of the multi-phonon transitions, a result which has a physical basis. As expected, the widths of the multi-phonon, sequence and combination transitions exhibit folding. The phononic contribution(s) to the response functions of Eqs. (25) and (31a) lead to folding of the widths of multi-phonon, sequence ($n_j^{''} = n_j^{'}$) and combination band transitions. For example, the widths of the cold multi-phonon progression, $n_j^{''} = 0 \rightarrow n_j^{'}$, are given by $\gamma_{el} + n_j^{'} \gamma_j$, where γ_j is the damping constant for mode j. The linear dependence on the excited state mode quantum number, $n_j^{'}$, is expected for damping mechanisms which are linear in the coordinate q_j of mode j. Mixed crystal spectra, taken at liquid helium temperatures, have shown this dependence (see, for example, refs. 31,53). Mechanisms that yield such a dependence include the Duschinsky effect where, in the excited state vibrational Hamiltonian, one has $q_j Q_\beta$ terms (with the Q_β's the bath coordinates), and anharmonic coupling terms that are linear in q_j. (The Duschinsky effect is actually the decay mechanism for the primary oscillators of the MBO model, see Chap. 8 of ref. 15).

From the properties of Fourier transforms, it follows that our response functions yield Lorentzian lineshapes for all phonon transitions. In amorphous hosts structural heterogeneity

can result in a distribution of frequencies for the primary oscillators. The modification of the response functions required to take into account such in homogeneity is straightforward. For example, if one desires Voigt profiles, one need only multiply $\exp(-\gamma_j|t|/2)$ in the response functions (see Eqs. (24) and (31c)) by $\exp(-\Delta_j^2 t^2/2)$, where Δ_j^2 is the variance of the distribution of ω_j frequencies. In the limit $\gamma_j << \Delta_j$, the folding of the aforementioned cold multi-phonon progression carries a $(n_j')^{1/2}$ -dependence, rather than an n_j-dependence.[17]

An approximate excited state vibrational Hamiltonian (H_e of Eq. (5)) which accounts for linear and quadratic electron-phonon coupling and is acceptable for mode frequency changes smaller than about 30% was derived as was the linear response function it gives rise to for the case of no damping (Eq. (12)). Inclusion of damping for a system whose modes are both linearly and quadratically coupled results in a complex linear response function. (The complexity is far greater for the non-linear response functions associated with photon echo spectroscopies.) Thus, we presented only the response function for a system whose modes are either linearly or quadratically coupled. Nevertheless, our approximate Hamiltonian should be useful in future studies devoted to derivation of linear and non-linear response functions for systems whose modes are both linearly and quadratically coupled.

As stated in the Introduction, the combination of temperature dependent hole-burning and photon echo studies above and below the glass transition of the solvent should provide new insights on optical coherence loss of chromophores in liquids. The results presented will be applied to photon echo spectroscopy in a subsequent publication.[48]

ACKNOWLEDGMENTS

Research at Iowa State University was supported by NSF grant DMR-9630781 and at the University of Rochester by grants from NSF CHE9526125 and AFOSR F49620-96-1-0030.

REFERENCES

1. Y. J. Yan and S. Mukamel, J. Chem. Phys. **94**, 179 (1991).

2. W. B. Bosma, Y. J. Yan, and S. Mukamel, Phys. Rev. A. 42, 9620 (1990).

3. M. Cho and G. R. Fleming, J. Chem. Phys. **98**, 2848 (1993).

4. P. Vöhringer, D. C. Arnett, R. A. Westervelt, M. J. Feldstein, and N. F. Scherer, J. Chem. Phys. **102**, 4027, (1995).

5. M. S. Pshenichnikov, K. Duppen, and D. A. Wiersma, Phys. Rev. Lett. **74**, 674 (1995).

6. W. P. de Boeij, M. S. Pshenichnikov, K. Duppen, and D. A. Wiersma, Chem. Phys. Lett. **138**, 1 (1995).

7. T. Joo, Y. Jia, J-Y. Yu, M. J. Lang, and G. R. Fleming, J. Chem. Phys. **104**, 6089 (1996).

8. G. R. Fleming and M. Cho, Annu. Rev. Phys. Chem. **47**, 109 (1996).

9. C. H. B. Cruz, R. L. Frork, W. H. Knox, and C. V. Shank, Chem. Phys. Lett. 132, 341 (1986).

10. W. P. de Boeij, M. S. Pshenichnikov, and D. A. Wiersma, J. Phys. Chem. **100,** 11806 (1996).

11. P. Vöhringer, D. C. Arnett, T. -S. Yang, and N. F. Scherer, Chem. Phys. Lett. **237**, 387 (1995).

12. C. J. Bardeen and C. V. Shank, Chem. Phys. Lett. 226, **310** (1994).

13. Y. J. Yan and S. Mukamel, Phys. Rev. A **41**, 6485 (1990); J. Chem. Phys. **94**, 179 (1991).

14. S. Mukamel, Annu. Rev. Phys. Chem. **41**, 647 (1990); Adv. Chem. Phys. **70**, 165 (1988).

15. S. Mukamel, *Principles of Nonlinear Optical Spectroscopy* (Oxford University, New York, 1995).

16. T. Reinot, W.-H. Kim, J. M. Hayes, and G. J. Small, J. Chem. Phys. **104**, 793 (1996).

17. T. Reinot, W.-H. Kim, J. M. Hayes, and G. J. Small, J. Chem. Phys. **106**, 457 (1997).

18. R. Jankowiak, J. M. Hayes, and G. J. Small, Chem. Rev. **93**, 1471 (1993).

19. L. R. Narashiman, K. A. Littau, D. W. Pack, Y. S. Bai, A. Elschner, and M. D. Fayer, Chem. Rev. **90**, 439 (1990).

20. R. M. Shelby, C. B. Harris, and P. A. Cornelius, J. Chem. Phys. **70**, 34 (1979).

21. B. Jackson and R. Silbey, Chem. Phys. Lett. **99**, 331 (1983).

22. J. M. Hayes and G. J. Small, J. Phys. Chem. **90**, 4928 (1986).

23. R. Jankowiak, J. M. Hayes, and G. J. Small, Chem. Rev. **93**, 1471 (1993)

24. J. M. Hayes, P. A. Lyle, and G. J. Small, J. Phys. Chem. **98**, 7337 (1994).

25. Y. Nagasawa, S. A. Passino, T. Joo, and G. R. Fleming. **106**, 4840 (1997).

26. C. J. Bardeen, G. Cerullo, C. V. Shank, Chem. Phys. Lett. **280**, 127 (1997).

27. An extensive review of low temperature absorption spectra of chromophore in host crystals and hole burned and fluorescence line narrowed of chromophores in amorphous hosts and proteins failed to reveal a clear cut case of overdamping. We note that the damping constants for the 50 and 180 cm^{-1} acoustic modes which dephase the pure electronic transition of APT in annealed glassy water correspond to widths of 17 and 15 cm^{-1}, respectively, at the glass transition temperature of 135 K.

28. G. J. Small, J. Chem. Phys. **54**, 3300 (1971).

29. P. A. Lyle, S. V. Kolaczkowski, and G. J. Small, J. Phys. Chem. **97**, 6924 (1993).

30. F. M. Fernández and E. A. Castro, Algebraic Methods in Quantum Chemistry and Physics (CRC Press, Boca Raton, 1995).

31. R. L. Beckman and G. J. Small, Chem. Phys. **30**, 19 (1978).

32. C. Manneback, Physica **17**, 1001 (1951).

33. M. G. Prais, D. F. Heller and K. F. Freed, Chem. Phys. **6**, 331 (1974).

34. D. F. Heller, K. F. Freed, and W.M. Gelbart, J. Chem. Phys. **56**, 2309 (1972).

35. R. Englman, Non- Radiative Decay of Ions and Molecules In Solids (North-Holland, Amsterdam, 1979).

36. See refs. 37 and 38 for an approach to evaluation of Eq. (7) with v(q) expressed as $v_0 \exp(cq)$ where c and v_0 are constants.

37. Y. Tanimura and S. Mukamel, J. Opt. Soc. Am. B. **10** , 2263 (1993)

38. V. Khidekel and S. Mukamel, Chem. Phys. Lett. **240**, 304 (1995).

39. R. J. Glauber, Phys. Rev. **131**, 2766, (1963).

40. J. R. Clauder and B-S. Skagerstam, *Coherent States- Applications in Physics and Mathematical Physics* (World Scientific Publishing Co. Pte. Ltd. 1985).

41. M. Weissbluth, *Photon- Atom Interactions (*Academic Press, New York, 1989).

42. W. H. Louisell, *Quantum Statistical Properties of Radiation* (J. Wiley, New York, 1973).

43. M. Toutounji, Ph.D. Dissertation, Iowa State University, 1998.

44. G. Small, Chem. Phys. **197**, 239 (1995) and Refs. therein.

45. N. R. S. Reddy, P. A. Lyle, and G. J. Small, Photosyn. Res. **31**,167 (1992).

46. A Mathematica program has been written such that the numerical FT of $\tilde{J}_\ell(t,T)$ was maintained in unevaluated form as a function of ω (via the set delay operator built into Mathematica). Then the program was instructed to substitute the evaluated numerical transform as a function of $\omega - \Omega$ or $\omega_B - \Omega$ in Eq. (35). The numerical integration was performed 1101 times to cover the frequency range shown in Fig. 4.

47. *Persistent Spectral Hole Burninig:* Sience and Applications, edited by W. E. Moerner (Springer, New York, 1987), Vol. 44.

48. M. Toutounji, S. Mukamel, and G. J. Small, to be submitted to J. Chem. Phys.

49. R. P. Feynman, Phys. Rev. **84**, 108 (1951).

50. W. Magnus, Commun. Pure Appl. Math. **7**, 649 (1954).

51. R. M. Wilcox, J. Math. Phys. **8**, 962 (1967).

52. M. Suzuki, Commun. Math. Phys. **57**, 193 (1977).

53. G. Fischer, Chem. Phys. Lett. **20**, 569 (1973).

APPENDIX A

Coherent states form a complete and non-orthogonal basis set. They are very useful in radiation theory and quantum optics. The coherent state $|z\rangle$ is an eigenvector of the non-hermitian operator a. The eigenvalue equation for the vector $|z\rangle$ is

$$a|z\rangle = z|z\rangle \tag{A1}$$

Thus z, which can be complex, is the eigenvalue of a. We can express $|z\rangle$ in terms of the number states $|n\rangle$ as

$$|z\rangle = C_0 \sum_{n=0}^{\infty} \frac{z^n}{\sqrt{n!}} |n\rangle \tag{A2}$$

One of the most appealing properties of coherent states is that they can be chosen to be unnormalized states by setting $C_0 = 1$. Since $|n\rangle$ can be written as

$$|n\rangle = \frac{(a^+)^n}{\sqrt{n!}} |0\rangle, \tag{A3}$$

where $|0\rangle$ is the vacuum state of the oscillator, Eq. (A2) becomes

$$|z\rangle = \exp(za^+)|0\rangle \tag{A4}$$

Applying a to Eq. (A2), one obtains

$$a|z\rangle = \sum_{n=0}^{\infty} \frac{z^n}{\sqrt{n!}} \sqrt{n}|n-1\rangle \tag{A6}$$

$$= z\sum_{n=0}^{\infty} \frac{z^{n-1}}{\sqrt{(n-1)!}}|n-1\rangle \tag{A7}$$

$$= z|z\rangle \tag{A8}$$

Equations (A7) and (A8) show that $|z\rangle$ is an eigenvector of a with eigenvalue z. Coherent states lack property of orthogonality because

$$\langle z|z'\rangle = \exp(z^* z') \neq 0. \tag{A9}$$

With Eq. (A1) one can show that

$$\exp(ca)|z\rangle = \exp(cz)|z\rangle \tag{A10}$$

where c is a constant, while with Eq. (A4) it follows that

$$\exp(ca^+)|z\rangle = |z+c\rangle. \tag{A11}$$

Note that $\exp(ca^+)$ acts as a translational operator in coherent state space with the translational parameter c.

We now show how a^+ acts on $|z\rangle$. By taking the hermitian conjugate of Eq. (A1), we obtain

$$|z\rangle a^+ = z^*\langle z| \tag{A12}$$

Using Eq. (A4),

$$a^+|z\rangle = a^+ \exp(za^+)|0\rangle \tag{A13}$$

$$= \partial/\partial z \exp(za^+)|0\rangle \tag{A14}$$

$$= \partial/\partial z |z\rangle. \tag{A15}$$

Recall that $\langle z|z\rangle \neq 1$. Equation (A15) confirms that exp(c a^+) is a translational operator.

We next show how $|z\rangle$ evolves in time under the time evolution operator exp(−iH_gt/$\hbar$).

$$\exp(-iH_g t/\hbar)|z(0)\rangle = |z(t)\rangle. \tag{A16}$$

Using Eq. (A2) one obtains

$$\exp(-iH_g t/\hbar|z(0)\rangle = \sum_{n=0}^{\infty} \frac{z^n}{\sqrt{n!}} \exp\left[-i\omega''\left(a^+a + \tfrac{1}{2}\right)t\right]|n\rangle \tag{A17}$$

$$= \exp(-i\omega'' t/2) \sum_{n=0}^{\infty} \frac{z^n}{\sqrt{n!}} \exp(-in\omega'' t)|n\rangle \tag{A18}$$

$$= \exp(-i\omega'' t/2) \sum_{n-0}^{\infty} \frac{[z\exp(-i\omega'' t)]^n}{\sqrt{n!}}|n\rangle \tag{A19}$$

$$= \exp(-i\omega'' t/2)\left|\exp(-i\omega'' t)\, z(0)\right\rangle \tag{A20}$$

$$= |z(t)\rangle \tag{A21}$$

To operate with exp(−iH_et/$\hbar$) on $|z(0)\rangle$, one of the following approaches may be used: Feynman's formula for non-commuting exponential operators,[49] Lie algebra for

disentangling non-commuting exponential operators,[30] or Inverse Campbell-Baker-Hausdorff formula (Zassenhause formula).[50-52] All three approaches worked equally well when we eliminated the a^2 and a^{+2} operators in H_e. The Lie algebra approach was found to be straightforward for pure quadratic coupling. We found that using the Zassenhause formula without eliminating a^2 and a^{+2} led to an unrecognized pattern of infinite terms which we were not able to simplify.

APPENDIX B

Here we provide a derivation of Eq. (17) starting with Eq. (12). We define $\alpha_1 \equiv \exp(f_3)$ (f_3 is given in Eq. (14d)), upon power series expansion we obtain,

$$\alpha_1 = \exp(-S_{eff}) \sum_{q=0}^{\infty} \frac{(S_{eff}\, e^{-i\omega' t})^q}{q!}. \tag{B1}$$

We have

$$\frac{C}{Q}\left(\frac{1}{f_1}\right) = \frac{e^{-i\Omega t}\, e^{-i(\omega'-\omega'')t/2}\, (1 - e^{-\beta\hbar\omega''})}{1 - e^{-\beta\hbar\omega'' + i(\omega''-\omega')t}}, \tag{B2}$$

where Ω is the adiabatic gap and, from Eq. (13), $Q = [2 \sinh(\beta\hbar\omega''/2)]^{-1} = \exp(-\beta\hbar\omega''/2) \cdot [1 - \exp(-\beta\hbar\omega'')]^{-1}$. For notational simplicity we define

$$f_2 = S_{eff}\, e^{-\beta\hbar\omega'' + i\omega'' t}\, (e^{-i\omega' t} - 1)^2 \equiv -\alpha_2 \alpha, \tag{B3}$$

where $\alpha_2 \equiv -S_{eff}\, e^{i\omega' t}\, (e^{-i\omega' t} - 1)^2$ and $\alpha \equiv e^{-\beta\hbar\omega'' + i\omega'' t - i\omega' t}$. With Eqs. (B1)-(B3), J(t) becomes

$$J(t) = \frac{C}{Q} \alpha_1 \frac{1}{1-\alpha} \exp\left[-\frac{\alpha_2 \alpha}{1-\alpha}\right]. \tag{B4}$$

With J(t) in this form, one can utilize the generating function for Laguerre polynomials:

$$\exp[-\alpha_2\alpha/(1-\alpha)]\left(\frac{1}{1-\alpha}\right) = \sum_{n''=0}^{\infty} L_n''(\alpha_2)\,\alpha^{n''}. \tag{B5}$$

With Eq. (B5), J(t) becomes

$$J(t) = \frac{C}{Q}\exp(-S_{eff})\sum_{q=0}^{\infty}\frac{(S_{eff}\,e^{-i\omega' t})^q}{q!}\sum_{n''=0}^{\infty} L_n''(\alpha_2)\,\alpha^{n''}. \tag{B6}$$

Equation (B6) needs further simplification which can be accomplished by noting that $\alpha_2 = 4S_{eff}\sin^2(\omega' t/2)$ and $L_{n''}(\alpha_2)$ can be rewritten as

$$L_n''(\alpha_2) = \sum_{m=0}^{n''}(-1)^m\binom{n''}{n''-m}\frac{\alpha_2^m}{m!}. \tag{B7}$$

J(t) can now be written as

$$J(t) = \frac{C}{Q}\exp(-S_{eff})\sum_{q=0}^{\infty}\sum_{n''=0}^{\infty}\frac{(S_{eff}\,e^{-i\omega' t})^q}{q!}\times\left\{\sum_{m=0}^{n''}(-1)^m\binom{n''}{n''-m}\frac{[4S_{eff}\sin^2(\omega' t/2)]^m}{m!}\right\}\alpha^{n''}. \tag{B8}$$

The $[\sin(\omega' t/2)]^{2m}$ factor can be dealt with using the following identity

$$\sin(\omega' t/2)^{2m} = 2^{-2m}(2m)!\sum_{\ell=0}^{m}\frac{(-1)^\ell\,\varepsilon_\ell\cos(2\ell\omega' t/2)}{(m+\ell)!\,(m-\ell)!}. \tag{B9}$$

Equations (B8) and (B9) lead directly to Eq. (17) via a straightforward Fourier transform.

APPENDIX C

This appendix shows the derivation of Eq. (27) and the recovery of Eq. (28). $\tilde{J}_\ell(t;T)$ for one mode is ($\Omega = 0$)

$$\tilde{J}_\ell(t;T) = \exp\left\{-\gamma_{el}|t|/2 - S_j \coth(\beta\hbar\omega_j/2) + S_j\, e^{-\gamma_j|t|/2}\left[\coth(\beta\hbar\omega_j/2)\cos(\omega_j t) - i\sin(\omega_j t)\right]\right\}, \tag{C1}$$

which can be rewritten as

$$\tilde{J}_\ell(t;T) = \exp[-\gamma_{el}|t|/2 - S_j \coth(\beta\hbar\omega_j/2)]\exp\left\{S_j\, e^{-\gamma_j|t|/2}\sqrt{\coth^2(\beta\hbar\omega_j/2) - 1}\cos(\omega_j t - \varphi_j)\right\}. \tag{C2}$$

Here,

$$\varphi_j = \arctan\left(\frac{-i}{\coth(\beta\hbar\omega_j/2)}\right) = -i\,\beta\hbar\omega_j/2 \tag{C3}$$

To proceed further, one needs to decompose Eq. (C2) by using the generating function for modified Bessel functions,

$$\begin{aligned}\tilde{J}_\ell(t;T) &= \exp[-\gamma_{el}|t|/2 - S_j \coth(\beta\hbar\omega_j/2)] \\ &\times \sum_{m=-\infty}^{\infty}\left\{I_m\left(S_j\,\mathrm{csch}(\beta\hbar\omega_j/2)\,e^{-\gamma_j|t|/2}\right)\exp(im\omega_j t - m\beta\hbar\omega_j/2)\right\}\end{aligned} \tag{C4}$$

The times dependent argument of I_m makes Fourier transform very difficult. However this is dealt with by using the definition of $I_m(W_j)$:

$$I_m(W_j) = \sum_{\ell=0}^{\infty} \frac{(W_j/2)^{m+2\ell}}{\ell!\,\Gamma(m+\ell+1)}, \tag{C5}$$

where

$$W_j \equiv S_j \,\mathrm{csch}(\beta\hbar\omega_j/2)\, e^{-\gamma_j|t|/2}. \tag{C6}$$

Substitution of Eq. (C5) into Eq. (C4) results in

$$\begin{aligned} \tilde{J}_\ell(t,T) = \exp\!\left[-S_j \coth(\beta\hbar\omega_j/2)\right] \sum_{m=-\infty}^{\infty}\sum_{\ell=0}^{\infty} \frac{\left[S_j \,\mathrm{csch}(\beta\hbar\omega_j/2)\right]^{m+2\ell}}{2^{m+2\ell}\,\ell!\,\Gamma(m+\ell+1)} \\ \times \exp(m\beta\hbar\omega_j/2)\exp\!\left[-im\omega_j t - \left((m+2\ell)\gamma_j + \gamma_{el}\right)|t|/2\right] \end{aligned} \tag{C7}$$

The Fourier transform of Eq. (C7) leads directly to Eq. (27). Note that we have switched the signs in $\exp(im\omega_j t - m\beta\hbar\omega_j/2)$ so that the high and low energy sides of the spectrum relative to the ZPL have positive and negative energies, respectively.

Finally, Eq. (28) is obtained from Eq. (C4) by setting $\gamma_{el} = \gamma_j = 0$:

$$\begin{aligned} J_\ell(t;T) = \exp[-S_j \coth(\beta\hbar\omega_j/2)] \sum_{m=-\infty}^{\infty} e^{m\beta\hbar\omega_j/2} \\ \times I_m[S_j \,\mathrm{csch}(\beta\hbar\omega_j/2)]\exp(-im\omega_j t). \end{aligned} \tag{C8}$$

Straightforward Fourier transformation of Eq. (C8) leads directly to Eq. (28).

Table 1. Franck-Condon factors for S = 0.8 and r = 0.7 and 0.8 (in parenthesis).

(n', n'')[a]	Equation (17)	Exact[b]	Englman[c]
(0, 0)	0.63 (0.55)	0.51 (0.49)	0.46 (0.45)
(1, 0)	0.30 (0.33)	0.40 (0.39)	0.28 (0.28)
(2, 0)	0.070 (0.10)	0.091 (0.11)	0.087 (0.089)
(3, 0)	0.010 (0.020)	0.0040 (0.013)	0.0200 (0.020)
(0, 1)	0.29 (0.33)	0.28 (0.31)	
(1, 1)	0.19 (0.088)	0.057 (0.040)	
(2, 1)	0.34 (0.32)	0.43 (0.37)	
(3, 1)	0.14 (0.19)	0.22 (0.24)	
(0, 2)	0.066 (0.10)	0.13 (0.14)	
(1, 2)	0.34 (0.32)	0.17 (0.21)	
(2, 2)	0.023 (0.00020)	0.00044 (0.013)	
(3, 2)	0.29 (0.21)	0.30 (0.23)	
(0, 3)	0.010 (0.020)	0.053 (0.048)	
(1, 3)	0.14 (0.19)	0.17 (0.19)	
(2, 3)	0.29 (0.21)	0.044 (0.068)	
(3, 3)	0.0035 (0.048)	0.055 (0.083)	

[a]n'' and n' are the initial and final electronic state vibrational quantum numbers. $r = \omega'/\omega''$.
[b]Calculated using Mathematica with exact harmonic oscillator wavefunctions.
[c]Calculated using the equation on p. 121 of ref. 35.

Table 2. Franck-Condon factors for S = 2.0 and r = 0.7 and 0.8 (in parentheses).

(n', n'')[a]	Equation (17)		Exact[b]		Englman[c]	
(0, 0)	0.32	(0.22)	0.19	(0.17)	0.14	(0.14)
(1, 0)	0.36	(0.33)	0.37	(0.33)	0.14	(0.14)
(2, 0)	0.21	(0.25)	0.30	(0.29)	0.068	(0.068)
(3, 0)	0.080	(0.13)	0.12	(0.15)	0.022	(0.022)
(0, 1)	0.36	(0.33)	0.26	(0.27)		
(1, 1)	0.0070	(0.056)	0.077	(0.10)		
(2, 1)	0.13	(0.042)	0.045	(0.017)		
(3, 1)	0.24	(0.19)	0.27	(0.20)		
(0, 2)	0.21	(0.25)	0.22	(0.24)		
(1, 2)	0.13	(0.042)	0.0024	(0.0012)		
(2, 2)	0.13	(0.17)	0.14	(0.15)		
(3, 2)	0.0061	(0.016)	0.016	(0.043)		
(0, 3)	0.080	(0.13)	0.15	(0.16)		
(1, 3)	0.24	(0.19)	0.068	(0.077)		
(2, 3)	0.0061	(0.016)	0.0610	(0.070)		
(3, 3)	0.17	(0.11)	0.046	(0.040)		

[a]n'' and n' are the initial and final electronic state vibrational quantum numbers. $r = \omega'/\omega''$.
[b]Calculated using Mathematica with exact harmonic oscillator wavefunctions.
[c]Calculated using the equation on p. 121 of ref. 35.

FIGURE CAPTIONS

Figure 1. Single-site absorption spectrum calculated with Eq. (27) for a model system: $\omega_j = 25$ cm^{-1}; $\gamma_j = 3$ cm^{-1}; $S_j = 1.8$; $\gamma_{el} = 1$ cm^{-1} and T = 50 K. The spectrum calculated by taking the numerical FT of Eq. (25) is identical.

Figure 2. Single-site absorption spectrum for T = 100 K calculated by taking the numerical FT of Eq. (34) for a two-mode system with one mode linearly coupled (ℓ) and the other quadratically coupled (q): $\omega_\ell = 200$ cm^{-1}; $S_\ell = 0.7$; $\gamma_\ell = 5$ cm^{-1}; $\omega_q'' = 50$ cm^{-1};
$\omega_q' = 35$ cm^{-1}; $\gamma_q = 2$ cm^{-1} and $\gamma_{el} = 1$ cm^{-1}.

Figure 3. Single-site absorption spectra for the special pair of the bacterial reaction center calculated with Eq. (25) at T = 0 K (top frame) and 15 K (bottom frame) with $\omega_m = 30$ cm^{-1}, $S_m = 1.8$, $\gamma_m = 20$ cm^{-1}, $\omega_{sp} = 120$ cm^{-1}, $S_{sp} = 1.5$, $\gamma_{sp} = 25$ cm^{-1} and $\gamma_{el} = 5$ cm^{-1}. γ_m for the bottom frame is 15 cm^{-1}; see text for more details.

Figure 4. Hole-burned spectra for the special pair band of the bacterial reaction center calculated with Eq. (35) for T = 0 K (top frame) and T = 15 K (bottom frame). $\omega = 62$ cm^{-1}, $\nu_m = \omega_B = 0$ cm^{-1} and $k\tau = 0.004$. Other parameter values are as given in the caption to Fig. 3.

Figure 5. Single-site absorption spectra of Al-phthalocyanine tetrasulphonate in glassy ethanol calculated by taking the numerical FT of Eq. (34) with $\omega_\ell = 25$ cm^{-1}, $S_\ell = 0.5$,
$\gamma_\ell = 10$ cm^{-1}, $\omega_q'' = 50$ cm^{-1}, $\omega_q' = 35$ cm^{-1}, $\gamma_q = 5\,(\bar{n}_q(\omega_q'') + 1)$ cm^{-1} and $\gamma_{el} = 8\ \bar{n}_q(\omega_q'')$ cm^{-1}. The top, middle, and bottom spectra are for T = 15, 60 and 100 K, respectively.

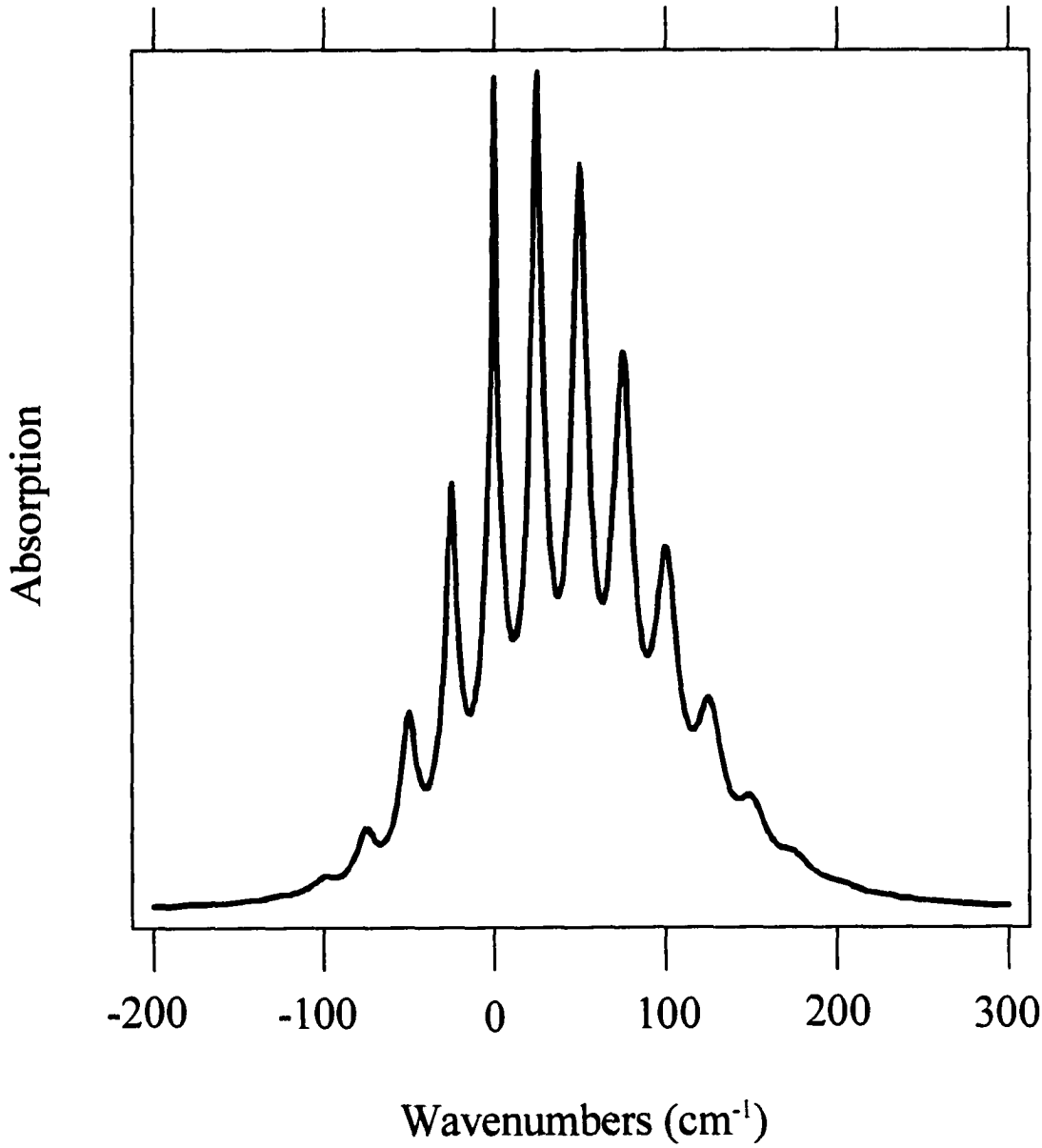

Figure 1

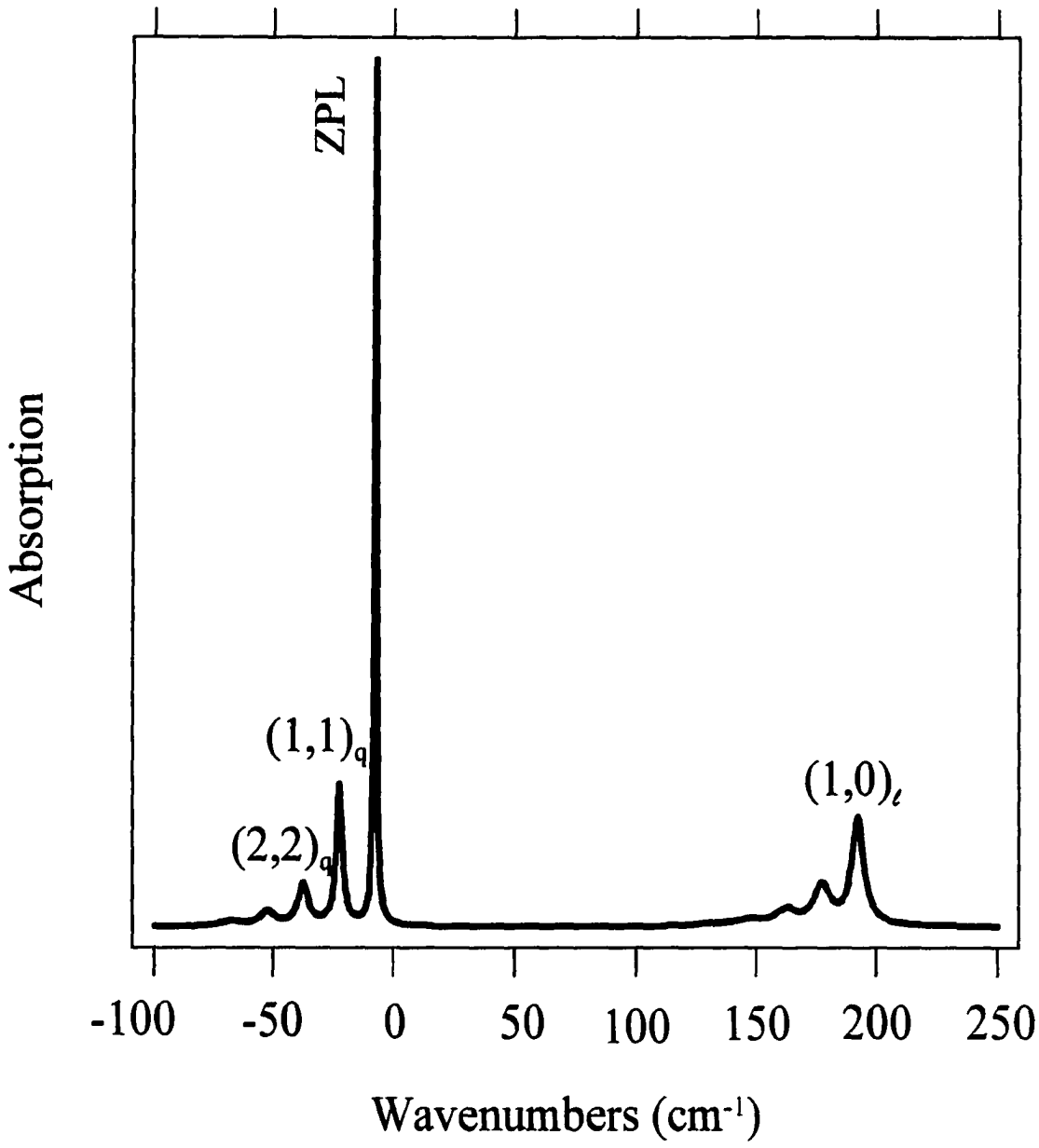
ZPL
(1,1)q
(2,2)q
(1,0)ℓ
Absorption
-100
-50
0
50
100
150
200
250
Wavenumbers (cm-1)

Figure 2

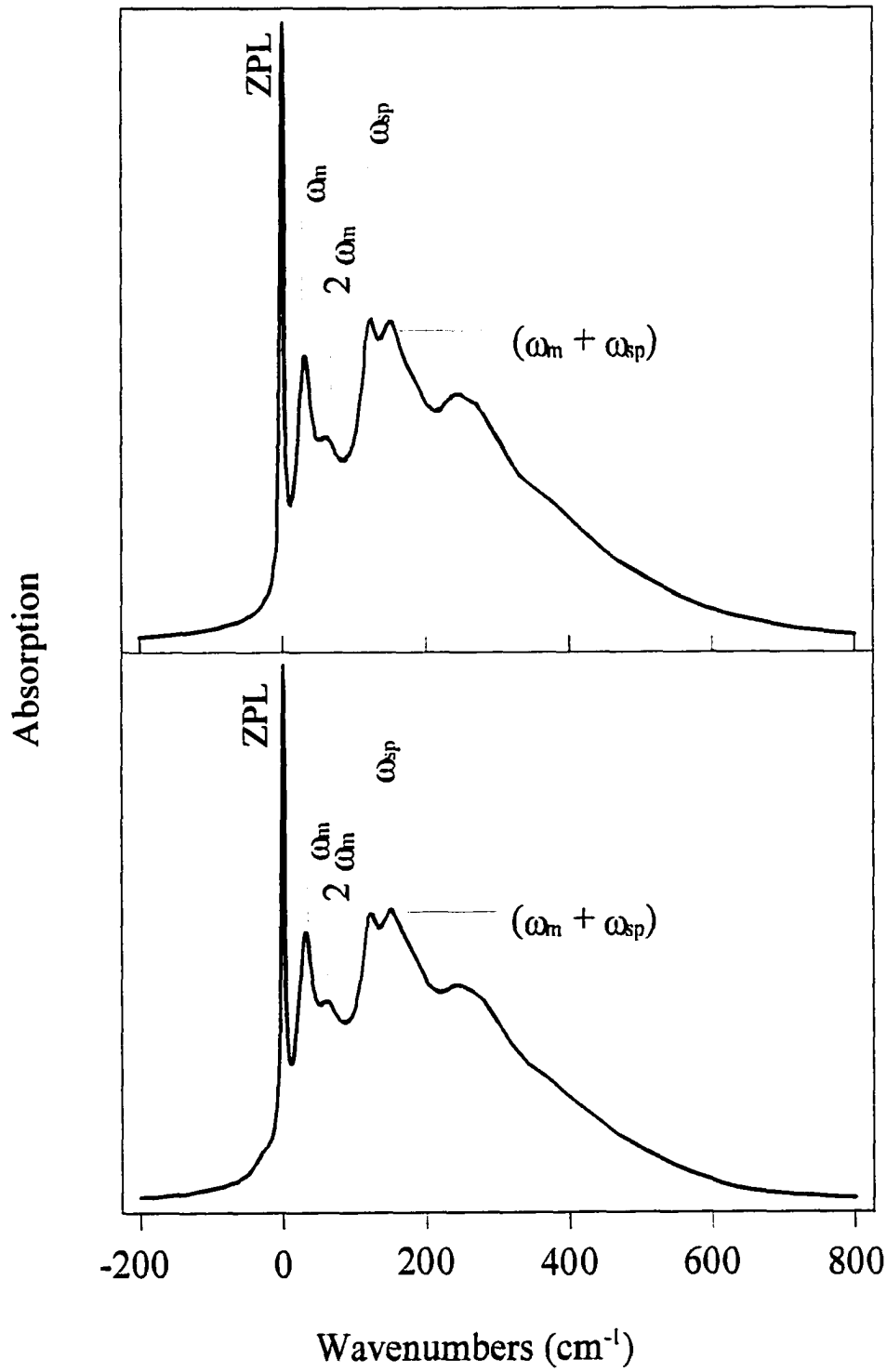
ZPL
ωsp
ωm
2 ωm
(ωm + ωsp)
ZPL
ωsp
ωm
2 ωm
(ωm + ωsp)
Absorption
-200
0
200
400
600
800
Wavenumbers (cm-1)

Figure 3

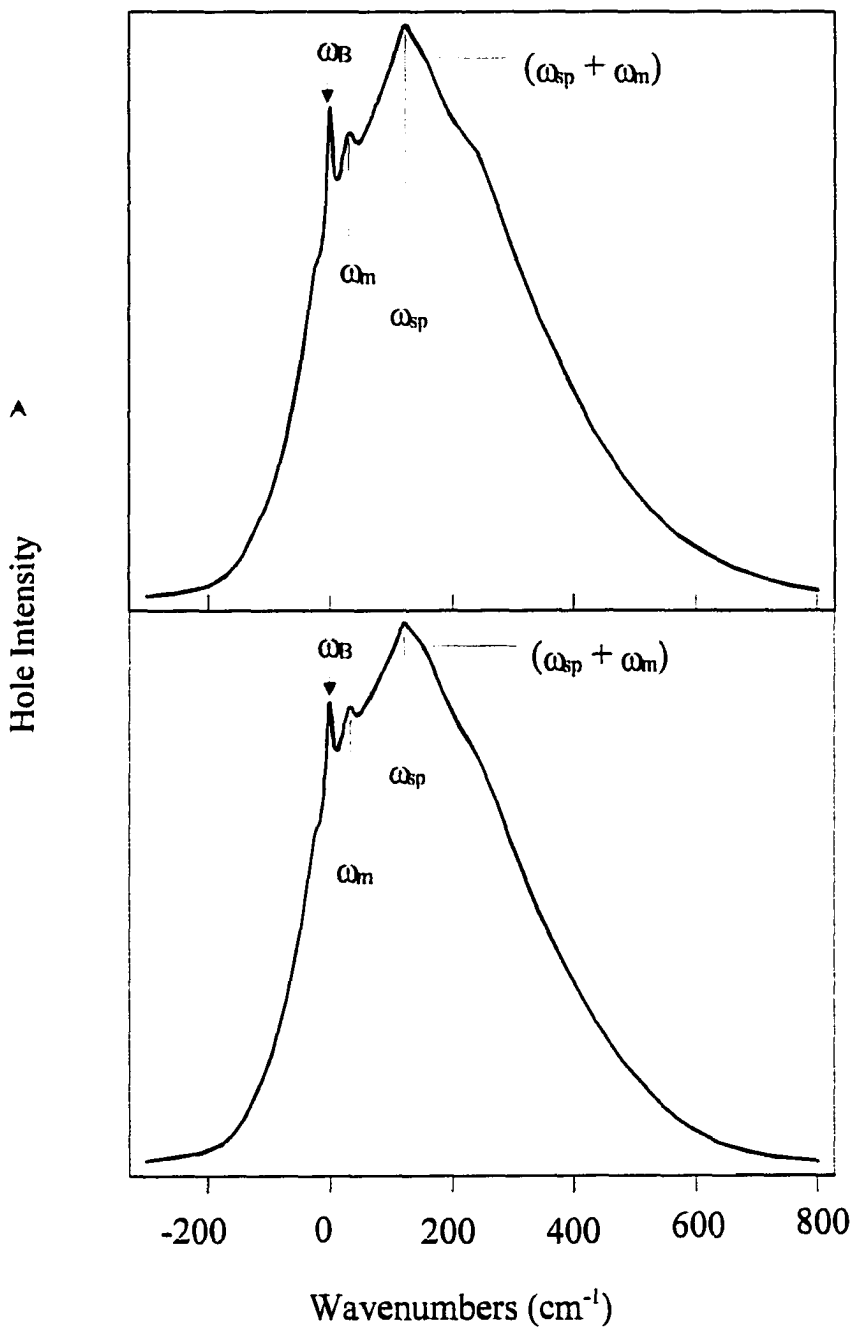
Hole Intensity
ωB
(ωsp + ωm)
ωm
ωsp
ωB
(ωsp + ωm)
ωsp
ωm
-200
0
200
400
600
800
Wavenumbers (cm-1)

Figure 4

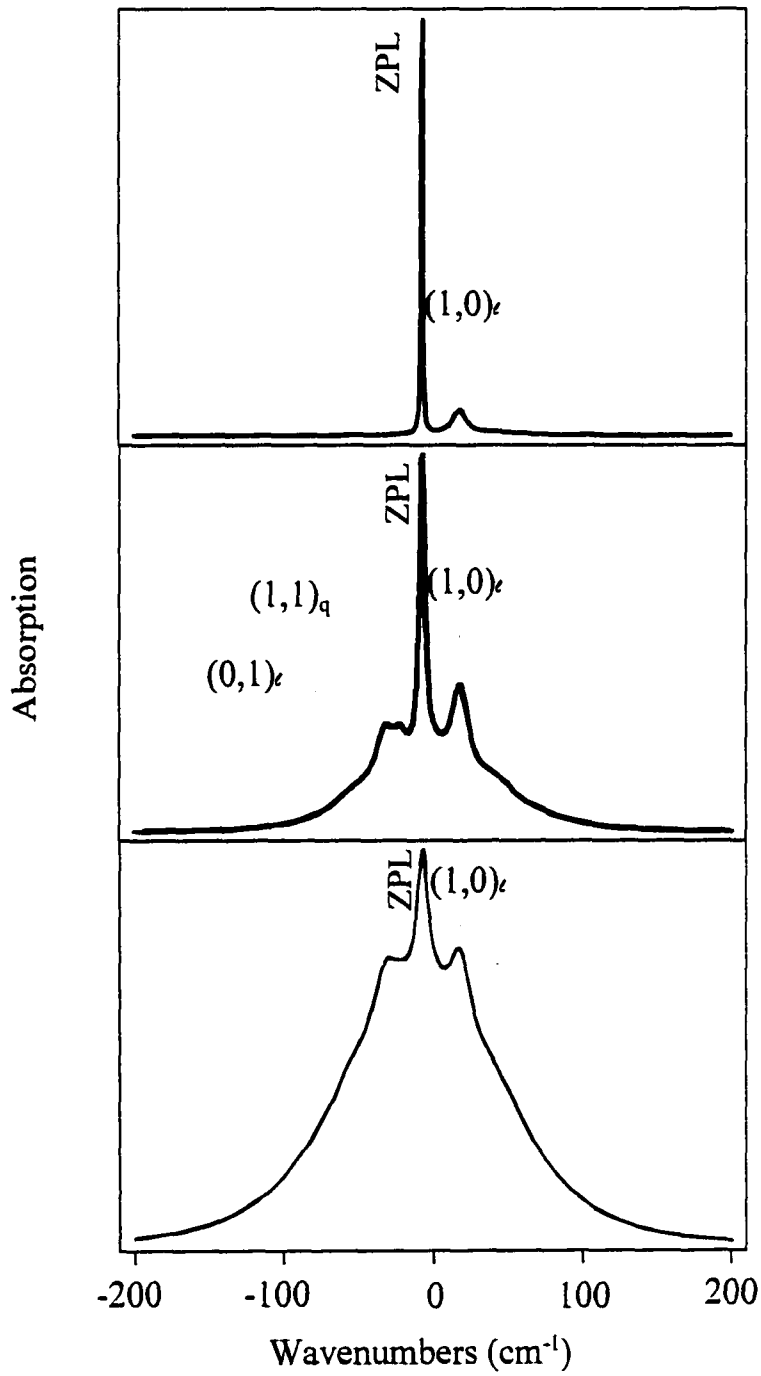
ZPL
(1,0)e
ZPL
(1,1)q
(1,0)e
(0,1)e
ZPL
(1,0)e
Absorption
-200
-100
0
100
200
Wavenumbers (cm-1)

Figure 5

CHAPTER 4. NON-LINEAR OPTICAL RESPONSE FUNCTIONS FOR CONDENSED SYSTEMS WITH LINEAR AND QUADRATIC ELECTRON-VIBRATION COUPLING

A paper submitted to the Journal of Chemical Physics

Mohamad Toutounji and Gerald J. Small
Department of Chemistry and Ames Laboratory–USDOE
Iowa State University, Ames, IA 50011
and
Shaul Mukamel
Department of Chemistry
University of Rochester, Rochester, NY 14627

ABSTRACT

A 4-point correlation function which is valid for finite temperature is derived using an approximate excited state vibrational Hamiltonian, H_e, for a system whose phonon modes exhibit both linear and diagonal quadratic electron-phonon coupling. The Hamiltonian is applicable for mode frequency changes due to quadratic coupling smaller than 30%. The non-linear response functions obtained from the correlation function are used to calculate the impulsive 3-pulse photon echo signal for a system exhibiting very large inhomogeneous broadening in order to reveal quantum beats due to the frequency change of a mode that accompanies electronic excitation. Damping of the phonons and pure electronic dephasing are not included in the 4-point correlation function. It was determined that their inclusion would lead to response functions of very considerable complexity. Thus, the remainder of the paper is concerned with the 4-point correlation function and echo response functions for systems whose modes are linearly coupled. The response functions are expressed in terms of the lineshape function g(t;T) of Toutounji (*J. Chem. Phys.*, submitted) which includes phonon damping and pure electronic dephasing. Applications of the theory are given for

impulsive 2-pulse photon echo signal, both time-integrated and as a function of the detection time t and pulse delay time τ'. Attention is focused on the dependence of the echo signals on the linear coupling strength for a fixed temperature and their dependence on temperature for a fixed coupling strength. The initial fast non-exponential decay (free-induction) due to all multi-phonon transitions, quantum beats and the slow decay component due to the zero-phonon line (pure electronic dephasing) are identified and correlated with features of the single-site absorption spectrum whose relationship to the hole burned spectrum is well understood. That pure electronic dephasing associated with the zero-phonon line contributes to the decay of the quantum beats is emphasized. It is suggested that this contribution may be non-negligible at high temperatures in certain systems. The final application is to the special pair absorption band of the bacterial reaction center.

I. INTRODUCTION

Recently, femtosecond photon echo spectroscopies have been used to study optical coherence loss of electronic transitions of molecular chromophores in liquids.[1-12] Of particular interest has been the dephasing due to inertial (librational) modes ("phonons") which couple linearly to the $S_1 \leftarrow S_0$ electronic transition. The damping of these Franck-Condon active phonons can lead to coherence loss on the femtosecond time scale. We recently suggested that[13,14] the study of optical coherence loss of chromophores in glasses and in the glass forming solvents could lead to a better understanding of the phononic contribution to dephasing in liquids. This suggestion stemmed from the results of persistent spectral hole burning studies of Al-phthalocyanine tetrasulphonate in glassy water[13] and ethanol[14] between 5 K and temperatures close to their glass transition temperature (T_g), 135 and 95 K, respectively. In the case of water it was shown that the values of the linear electron-phonon coupling parameters and inhomogeneous broadening of the zero-phonon line (ZPL, i.e. pure electronic transition), determined from the 5 K spectra, when used with

the expression of Hayes et al.[15] for the hole burned spectrum, provided a good accounting of the temperature dependence of APT's hole burned spectrum. The linear electron-phonon coupling is dominated by a 38 cm^{-1} phonon with a small Huang-Rhys factor of 0.55 (the width of the one-phonon profile associated with the 38 cm^{-1} phonon is 45 cm^{-1}).[16] The corresponding frequencies for glassy ethanol and methanol are 26 and 17 cm^{-1}, respectively.[17] The 38, 26 and 17 cm^{-1} phonons were assigned as pseudo-localized with amplitude centered on APT and nearest neighbor solvent molecules. The high resolution of the temperature-dependent hole spectra led to the conclusion that, at temperatures $\geq$ 15 K,[17] the dephasing of the ZPL is due to the exchange coupling mechanism associated with diagonal quadratic electron-phonon coupling.[18,19] the quadratic coupling gives rise to a mode frequency change upon electronic excitation of the chromophore. For glassy water the exchange coupling was found to be due to two phonons with frequencies of 50 and 180 cm^{-1} which correspond to the acoustic modes of water. For glassy ethanol, an exchange coupling mode of 50 cm^{-1} was identified which coincides with the lowest energy peak in the spectral density of liquid ethanol.

The combination of spectral hole burning and photon echo spectroscopies is well suited for determination of the similarities and differences between optical coherence loss in glasses and liquids which can be expected to depend on the liquid and the value of $T - T_g > 0$. Of particular interest would be identification of ultra-fast dynamics from inertial modes unique to the liquid. Interpretation of the results of such experiments, however, requires linear and nonlinear response functions for finite temperature that provide a consistent and physically acceptable description of the single-site absorption, hole-burned and photon echo spectra, as recently pointed out by Nagasawa et al.[20] and Bardeen et al.[21] in their studies of the temperature dependence of optical coherence loss of chromophores in polymers.

We recently derived an approximate excited state vibrational Hamiltonian (H_e) that, in addition to linear coupling, includes diagonal quadratic coupling.[22] This Hamiltonian, which is adequate for mode frequency changes smaller than 30%, was used to obtain the linear response or 2-point correlation function for the case of no damping that provides a good description of the temperature dependences of the ZPL, multi-phonon and sequence transitions. (Sequence transitions correspond to $n_j'' \rightarrow n_j' = n_j''$, where n_j'' and n_j' are the quantum numbers of mode j for the ground and exited electronic states, respectively.) A linear response function for finite temperature ($\tilde{J}_{l,q}(t;T)$) that includes damping was proposed for systems whose modes are either linearly (l) or quadratically (q) coupled since there appear to be many systems of this type. It is the product of three response functions, two of which are phononic with one associated with linear modes and the other with quadratic modes. Different modes (ω_j) can be assigned different damping constants, γ_j. (We adopt the convention that γ_j is the fwhm of the one-phonon absorption profile in the absence of pure electronic dephasing.) The third response function is electronic, $\exp(-\gamma_{el}|t|/2)$, with γ_{el} the width of the zero-phonon line. The total response function yields single-site absorption spectra in which folding of the widths of multi-phonon and sequence transition occurs. γ_{el} is included in the widths of those transitions. For example, the widths of the $n_j'' = 0 \rightarrow n_j'$ progression members are given by $\gamma_{el} + n_j' \gamma_j (n_j' = 0, 1, \ldots)$ where γ_j is the damping constant for phonon j. That γ_{el} adds to the widths of the multi-phonon transition has a physical basis.[22] The linear dependence on n_j' (folding) is valid for any phonon relaxation mechanism that is linear in the coordinate of the phonon. Such folding has been observed for chromophores in host crystals.[23,24] The structure of $\tilde{J}_{l,q}(t,T)$ is such that all transitions in the single-site absorption spectrum carry Lorentzian lineshapes. However, the modification required to account for a distribution of values for ω_j due to structural heterogeneity is straightforward. The new response functions were found, for example, to provide a good description of the temperature dependence of the hole-burned spectrum of the special pair

band of the bacterial reaction center. The response functions are applicable to systems whose phonons are underdamped, $\gamma_j < \omega_j$.

In this paper the temperature dependent 4-point correlation function, $F(\tau_1,\tau_2,\tau_3,\tau_4)$, for the aforementioned approximate Hamiltonian H_e is obtained for the case of no damping. In order to demonstrate quantum beats from quadratic coupling, it is used to calculate the impulsive stimulated photon echo signal in the limit of large inhomogeneous broadening for a linearly and quadratically coupled phonon. A 4-point correlation function which includes both phononic damping and pure electronic dephasing is derived for linear coupling only using the results of ref. 22 which include an expression for the phonon lineshape function, $g^{ph}(t;T)$. The 4-point correlation function defines the echo response functions which enter into the expression for the third-order polarization that describes all 4-wave mixing spectroscopies including the 3-pulse stimulated photon echo (SPE). Calculations based on our 4-point correlation function are restricted to impulsive echo spectroscopy because the computational time for pulses of finite width, relative to inhomogeneous broadening, is very long. Nevertheless, the results provide a clear picture of the basic aspects of the echo profile which include the faster and slower components of the echo decay due to the multi-phonon transitions (phonon sideband) and ZPL as well as the phonon-induced quantum beats.[25-29,30-34] Particular attention is given to the dependence of the 2-pulse echo signal for a fixed temperature on the value of the Huang-Rhys factor S of the active phonon, the dependence of the signal for fixed S on the temperature, the relationship between the integrated echo signal and the single-site absorption spectrum and the dynamical information contained in the quantum beat profiles. Consistent with the widths of the multi-phonon absorption transitions, *vide supra*, we find that the pure electronic dephasing (γ_{el}) contributes to the decay of the quantum beats. Finally, the 2-pulse PE signals are calculated in the low temperature limit for the special pair absorption band of the bacterial reaction center and compared with the results of recent accumulated photon echo experiments.[35]

II. THEORY

A. Background

We begin by reviewing the equations in the book by Mukamel[36] that form the basis for this work, the results of which are presented in the following three subsections.[37] The non-linear response function which governs 4-wave mixing (4WM) experiments is

$$S^{(3)}(t_3,t_2,t_1) = 2\hbar^{-3}\,\theta(t_1)\theta(t_2)\theta(t_3)\;Im\sum_{\alpha=1}^{4} R_\alpha(t_3,t_2,t_1), \tag{1}$$

where $\{R_\alpha(t_1,t_2,t_3)\}_{\alpha=1}^{4}$ are the non-linear correlation functions, $\theta(t_n)$ is the Heaviside step function, and t_1, t_2 and t_3 are the interaction intervals between the system and radiation field, *vide infra*. The R_α's are obtainable from the following 4-point correlation function

$$F(\tau_1,\tau_2,\tau_3,\tau_4) \equiv \left\langle V_{ge}(\tau_1)\,V_{eg}(\tau_2)\,V_{ge}(\tau_3)\,V_{eg}(\tau_4)\right\rangle \tag{2}$$

with

$$V_{ge}(\tau) = \exp\left(\frac{i}{\hbar}H_g\tau\right)V_{ge}\exp\left(-\frac{i}{\hbar}H_e\tau\right), \tag{3a}$$

$$V_{eg}(\tau) = \exp\left(\frac{i}{\hbar}H_e\tau\right)V_{eg}\exp\left(-\frac{i}{\hbar}H_g\tau\right). \tag{3b}$$

Here, V_{eg} is the electronic transition dipole moment which depends on the nuclear coordinates of the system. Later, we will employ the Condon approximation. H_g and H_e are the ground and excited state vibrational Hamiltonians. Using the fact that the correlation function is invariant under time translation, it can be shown that

$$R_1(t_3,t_2,t_1) = F(t_1,t_1+t_2,t_1+t_2+t_3,0)\,,$$

$$R_2(t_3,t_2,t_1) = F(0,t_1+t_2,t_1+t_2+t_3,t_1)\,,$$

$$R_3(t_3,t_2,t_1) = F(0,t_1,t_1+t_2+t_3,t_1+t_2)\,,$$

$$R_4(t_3,t_2,t_1) = F(t_1+t_2+t_3,t_1+t_2,t_1,0)\,. \qquad (4)$$

We mention for what follows that when the field is turned on, the first interaction takes place at time $t-t_1-t_2-t_3$ and creates an optical coherence which evolves for a period t_1. The second interaction occurs at time $t-t_2-t_3$ and converts the coherence state into a population state which evolves for a period t_2. The third interaction occurs at time $t-t_3$ and creates a second electronic coherence that evolves for time t_3. At times $t > t_3$ the optical polarization $P^{(3)}$ is calculated, *vide infra*.

We consider the stimulated photon echo in which three pulses with wavevectors $\mathbf{k}_1$, $\mathbf{k}_2$ and $\mathbf{k}_3$ are sequentially applied to the system. The external field $E(\mathbf{r},t)$ can be written as

$$E(\boldsymbol{r},t) = E_1(t+\tau'+\tau)\exp(i\boldsymbol{k}_1\cdot\boldsymbol{r}-i\omega_1 t) + E_2(t+\tau)\exp(i\boldsymbol{k}_2\cdot\boldsymbol{r}-i\omega_2 t)$$

$$+ E_3(t)\exp(i\boldsymbol{k}_3\cdot\boldsymbol{r}-i\omega_3 t) + c.c.\,. \qquad (5)$$

E_1, E_2 and E_3 determine the temporal shapes of the pulses centered at $t = -(\tau' + \tau)$, $-\tau$ and 0, respectively. Thus τ' is the delay between the first (E_1) and second (E_2) pulses and τ the delay between the second and third (E_3) pulses. As is well-known the stimulated echo is centered at τ' after the third. The echo direction of primary interest is $\mathbf{k}_a = \mathbf{k}_3 + \mathbf{k}_2 - \mathbf{k}_1$ (see pp. 297-298 of ref. 36 for discussion). The integrated intensity of the echo signal, S_{SPE}, is:

$$S_{SPE}(\tau',\tau) = \int_0^\infty dt \left| P^{(3)}(k_a,t) \right|^2 , \tag{6}$$

where $P^{(3)}(\mathbf{k}_a,t)$ third order polarization with wavevector $\mathbf{k}_a$ induced by the external fields. With the rotating wave approximation and the assumption of well-separated pulses one has

$$P^{(3)}(k_a,t) = \left(\frac{i}{\hbar}\right)^3 \int_0^\infty dt_3 \int_0^\infty dt_2 \int_0^\infty dt_1 \, \mathbf{R}(t_3,t_2,t_1)\, \chi(t_3-t_1)\, E_3(t-t_3)\, E_2(t+\tau-t_3-t_2)$$

$$\times E_1^*(t+\tau'+\tau-t_3-t_2-t_1)\exp[i(\omega_3+\omega_2-\omega_1)t_3 + i(\omega_2-\omega_1)t_2 - i\omega_1 t_1] \tag{7}$$

Here, $\mathcal{R}(t_3,t_2,t_1)$ is the echo response function defined as

$$\mathbf{R}(t_3,t_2,t_1) \equiv R_2(t_3,t_2,t_1) + R_3(t_3,t_2,t_1) . \tag{8}$$

While $\mathcal{R}(t_3,t_2,t_1)$ governs the homogeneous (dynamical) contribution to the dephasing, $\chi(t_3-t_1)$ governs the static inhomogeneous contribution. To relate the time arguments of E_j in Eq. (5) to those of E_j in $P^{(3)}(\mathbf{k}_a,t)$, one need recall that Eq. (7) must take into account that the first, second and third interactions occur at $t-t_1-t_2-t_3$, $t-t_2-t_3$ and $t-t_3$.

In the impulsive limit, the pulses are infinitely short and the temporal field functions E_j become delta functions in Eq. (7), e.g. $E_3(t-t_3) \rightarrow \delta(t-t_3)$. The integration is then straightforward and Eq. (6) becomes

$$S_{SPE}(\tau',\tau) = \int_0^\infty dt \left|\mathbf{R}(t,\tau,\tau')\right|^2 \left|\chi(t-\tau')\right|^2 . \tag{9}$$

The form of the inhomogeneous broadening term χ, *vide infra*, results in the maximum of the echo appearing at time $t = \tau'$ after the interaction with the third pulse which we can now consider to have occurred at $t = 0$. For $t > \tau'$, the echo decays due to electronic dephasing. If in the frequency domain the inhomogeneous broadening is far greater than the homogeneous broadening, $\chi(t-\tau')$ in Eq. (9) can be approximated by a delta function which results in

$$S_{SPE}(\tau',\tau) = \left|\mathbf{R}(\tau',\tau,\tau')\right|^2 . \tag{10}$$

We consider next the 2-pulse photon echo in which pulses 2 and 3 are coincident ($\tau = 0$) and $\mathbf{k}_2 = \mathbf{k}_3$, $E_2(t) = E_3(t)$ and $\omega_2 = \omega_3$. Utilization of these three equalities in Eq. (7) leads to the expression for the polarization of the 2-pulse echo. Under the assumption that pulses 2 and 3 are short relative to the nuclear dynamics, meaning that the population states do not evolve before creation of the last optical coherence, the integration over t_2 can be eliminated and t_2 set equal to zero. The result is:

$$P_{PE}^{(3)}(\boldsymbol{k}_a,t) = \left(\frac{i}{\hbar}\right)^3 \int_0^\infty dt_3 \int_0^\infty dt_1 \left[\mathbf{R}(t_3,0,t_1)\left|E_2(t-\tau')\right|^2 E_1^*(t-t_1)\,\chi(t_3-t_1)\exp[i\omega_1(t_3-t_1)\right] \tag{11}$$

where we have set $\omega_1 = \omega_2$. The integrated 2-pulse echo signal is given by

$$S_{PE}(\tau') = \int_0^\infty \left|P_{PE}^{(3)}(\boldsymbol{k}_a,t)\right|^2 . \tag{12}$$

In the calculations which follow a Gaussian profile is used for the inhomogeneous function χ:

$$\chi(t_3 - t_1) = \exp\left[-\frac{1}{2}w^2(t_3 - t_1)^2\right], \tag{13}$$

where the parameter w is related to the fwhm of the inhomogeneous profile in the frequency domain by fwhm = 2.35 w. For finite pulses, a Gaussian profile can be used, e.g.

$$E_2(t - \tau') = \frac{1}{\sqrt{2\pi\sigma^2}}\exp\left[-(t - \tau')^2 / 2\sigma^2\right], \tag{14}$$

where σ^2 is the variance.

B. Four-point Correlation Function for Both Linear and Quadratic Coupling

Consider a system with modes that exhibit both linear and diagonal quadratic electron-phonon coupling. Let ω'' and ω' be the ground and excited electronic state frequencies of such a mode. The dimensionless normal coordinate for the ground state is defined as q and the dimensionless linear displacement between the potential energy minima of the two states as d. The vibrational Hamiltonian for the ground state is

$$H_g = \hbar\omega''(a^+a + 1/2), \tag{15}$$

with a^+ and a the raising and lower operators, i.e. $q = 2^{-1/2}(a^+ + a)$. The exact Hamiltonian for the excited state, H_e, is given in ref. 22. We do not give it here, the reason being that even the expression for the 2-point correlation function it would give rise to is quite unwieldy. (It is the bilinear terms in H_e involving a^+ and a that are responsible for this.) For this reason we introduced the following approximate expression for H_e:[22]

$$H_e = \hbar\omega'\left[\left(a^+a+\frac{1}{2}\right)+(2-r^{-1})\,d\,(a^++a)/\sqrt{2}+(2-r^{-1})\,d^2/2\right]+\hbar\Omega \tag{16}$$

where $r = \omega'/\omega''$ and $\hbar\Omega$ is the adiabatic electronic energy gap. This Hamiltonian is adequate for $r \gtrsim 0.7$ (without loss of generality we take $\omega' < \omega''$). The adiabatic gap is related to the vertical gap by

$$\Omega_v = \Omega + S_{eff}\ \omega', \tag{17}$$

where

$$S_{eff} = (2-r^{-1})d^2/2 \tag{18}$$

with S_{eff} an effective Huang-Rhys factor that equals $S = d^2/2$ when $\omega' = \omega''$. The approximate H_e was used in ref. 22 to obtain the linear response (2-point correlation) function, J(t;T), for the case of no phonon damping. Coherent states, rather than number states, were used in the derivation. We have used the same approach to obtain the temperature dependent 4-point correlation function ($F(\tau_1,\tau_2,\tau_3,\tau_4)$ for the case of no damping, Eq. (A4) of Appendix A. It can be used to obtain the echo response functions $\left\{R_\alpha(t_3,t_2,t_1)\right\}_{\alpha=1}^{4}$, Eq. (4), which can be used to calculate the third order polarization for any 4-wave mixing experiment.

C. Four-point Correlation Function with Damping for Linear Coupling

The correlation function given by Eq. (A4) is a new result which we use in section III to demonstrate the quantum beats that arise from quadratic as well as linear coupling. Unfortunately, inclusion of phonon damping and pure electronic dephasing would lead to a very complicated correlation function which, from a computational point of view, is

impractical. This is not the case for linear coupling only. By setting $\omega' = \omega''$ in Eq. (A4) one obtains

$$F(\tau_1,\tau_2,\tau_3,\tau_4) = \exp[-g(\tau_1-\tau_2)+g(\tau_1-\tau_3)-g(\tau_2-\tau_3)-g(\tau_1-\tau_4) + g(\tau_2-\tau_4)-g(\tau_3-\tau_4)], \tag{19}$$

which is identical to Eq. (8.14) of ref. 36. At this point we use the expression for the lineshape function g(t;T) from ref. 22 which is the sum of a phononic (ph) and electronic contribution:

$$g(t;T) = g^{ph}(t;T) + g^{el}(t;T), \tag{20}$$

where

$$g^{ph}(t;T) = \sum_{j=1}^{N} g_j^{ph}(t;T), \tag{21}$$

$$g_j^{ph}(t;T) = S_j\left\{\coth(\beta\hbar\omega_j/2) - e^{-\gamma_j|t|/2}\left[\coth(\beta\hbar\omega_j/2)\cos(\omega_j t) - i\sin(\omega_j t)\right]\right\}, \tag{22}$$

and

$$g^{el}(t;T) = \gamma_{el}|t|/2. \tag{23}$$

Insofar as the temperature dependencies of γ_j and γ_{el} are concerned, one need consider different mechanisms and feed their temperature dependencies into the lineshape functions, which is standard procedure.

We note that the lineshape function, g(t;T) defined by Eq. (20) and the equations that follow yield a single-site absorption spectrum, which is given by

$$\sigma(\omega;T) = \frac{1}{\pi}\mathrm{Re}\int_0^\infty dt\, \exp[-g(t;T) + i\omega t], \tag{24}$$

for which the ZPL and multi-phonon transitions carry Lorentzian profiles. In amorphous hosts structural heterogeneity can result in a distribution of frequencies for a Franck-Condon active phonon. The modification of the lineshape function required to take into account such inhomogeneity is straightforward. For example, if one desires Voigt profiles, one need only multiply $\exp(-\gamma_j|t|/2)$ in Eq. (22) by $\exp(-\Delta_j^2\, t^2/2)$, where Δ_j^2 is the variance of the distribution of ω_j frequencies.

The impulsive 2-pulse echo (IPE) can be calculated by setting $\tau = 0$ in Eq. (9). Using the echo response function, $\mathcal{R}(\tau',0,\tau')$, obtained from Eq. (19) in Eq. (9) yields the impulsive 2-pulse echo signal,[36] $S_{IPE}(\tau';T)$,

$$S_{IPE}(\tau';T) = \int_0^\infty dt\, \exp[-w^2(t-\tau')^2]\exp\{-2\,\mathrm{Re}[2\,g(t;T) + 2\,g(\tau';T) - g(t+\tau';T)]\}. \tag{25}$$

whose polarization is given by

$$P_{IPE}^{(3)}(t,\tau';T) = \exp[-w^2(t-\tau')^2]\exp\{-2\,\mathrm{Re}[2\,g(t;T) + 2\,g(\tau';T) - g(t+\tau';T)]\}. \tag{26}$$

III. RESULTS OF CALCULATIONS

Figure 1 shows an impulsive SPE signal at 300 K for a linearly and quadratically coupled mode defined by $\omega'' = 200\ \mathrm{cm}^{-1}$, $\omega' = 150\ \mathrm{cm}^{-1}$ and $S = 2$. It was calculated using

Eqs. (A4), 8 and 10. (Again, τ' is the delay between the first and second pulses and τ the delay between the second and third.) Although damping is not included, Fig. 1 reflects an important feature due to quadratic electron-phonon coupling; namely, quantum beats due to interference of the ground and excited state phonon waves. This is more easily seen by looking at a slice in the frequency domain obtained from Fig. 1. Figure 2 was obtained by performing a Fourier transform of Eq. (10) with $\tau = 1$ fs as follows

$$S_{SPE}(\omega) = \frac{1}{\pi} \mathrm{Re} \int_0^\infty d\tau' \, S_{SPE}(\tau') \exp[(i\omega - \gamma)\tau']. \tag{27}$$

(To avoid delta functions, a uniform damping, γ, of 3 cm^{-1} was introduced.) In addition to the ground and excited state fundamentals ω'' and ω', one observes their difference frequency, $\Delta\omega = 50$ cm^{-1} and its multiple $2\Delta\omega = 100$ cm^{-1}. The latter two are responsible for the quantum beats indicated by the arrow in Fig. 1. Note that in the absence of temperature dependent data the features in Fig. 2 might be incorrectly assigned to three or four distinct linearly coupled modes.

The remainder of this section is concerned with *impulsive* 2-pulse photon echo (IPE) results for systems with finite inhomogeneous broadening and modes that exhibit linear coupling only. Phonon damping (γ_j) and pure electronic dephasing (γ_{el}) are taken into account.

Figure 3 shows 0 K results for a linearly coupled mode ($\omega_j = 30$ cm^{-1}, $\gamma_j = 20$ cm^{-1}, $\gamma_{el} = 2.5$ cm^{-1} and $w = 64$ cm^{-1}) for three values of S, 0.01, 0.1 and 0.5 Integrated IPE signals calculated with Eq. (25) are given in the left panel and the corresponding single-site absorption spectra calculated with Eq. (24) in the right panel. For $S = 0.01$, the ZPL of a width 2.5 cm^{-1} dominates the absorption spectrum as expected for such a small S-value. Correspondingly, multi-phonon transitions make a negligible contribution to the echo signal

which is dictated by the ZPL. The decay of the echo signal is single-exponential according to $\exp(-2\gamma_{el}\tau')$, where τ' is the time delay, and $\gamma_{el}(s^{-1}) = 2\pi c\, \gamma_{el}(cm^{-1})$ with $\gamma_{el}(cm^{-1}) = 2.5$.[38] For S = 0.1, the (1,0) phonon transition appears in the single-site absorption spectrum. Its appearance is reflected by that of the fundamental beat at 1.1 ps which is the period (ϕ_j) for $\omega_j = 30\ cm^{-1}$. Increasing S to 0.5 results in resolution of the beat due sharpening of the feature labeled as PSB (phonon sideband). This sharpening or faster decay (free-induction) which precedes the echo is due to the increase in the Franck-Condon factors of multi-phonon transitions. (The contribution from the slowly decaying ZPL component to the signal at ~ 0 ps is negligible.) One-half the inverse of the width of the PSB is an effective or average width for the overall profile of the multi-phonon transitions that contribute to the absorption band, *vide infra*. The lineshape function g(t;T) of Eq. (20) leads to widths for the cold phonon absorption progression $n_j'' = 0 \rightarrow n_j' = 0,1,\ldots$ of $\gamma_{el} + n_j'\gamma_j$.[39] The (1,0) absorption transition of Fig. 3 should carry a width of 22.5 cm^{-1}. This was confirmed by "ruler" measurement of the (1,0) band for S = 0.5.[40] Because the resolved fundamental beat in the echo signal for S = 0.5 corresponds to the (1,0) absorption transition, the width of the beat profile is inversely proportional to the width of the (1,0) transition. Since we have defined γ_{el} and γ_j as fwhm contributions, the width $\Gamma(s)$ of the beat equals $2^{-1}(\gamma_{el} + \gamma_{ph})^{-1}$, the inverse of the decay constant for the beat, where the unit of γ_{el} and γ_j is circular frequency. Thus, $2^{-1}\Gamma^{-1}$ is the width of the (1,0) absorption transition, as confirmed by ruler measurement. (To convert to cm^{-1} one need multiply $2^{-1}\Gamma^{-1}$ by $(2\pi c)^{-1}$.) That γ_{el} adds to the homogeneous widths of the multi-phonon transition has a physical basis which is that the phonon levels build on the zero-point vibrational level. Thus, phononic transitions cannot be sharper than the ZPL. The question arises as to when the contribution from γ_{el} is negligible. For typical dye molecules in amorphous solids at liquid helium temperatures it is, since $\gamma_{el} << 1\ cm^{-1}$ ($T_2^* >> 10$ ps).[41,42] However, this situation may not hold at high temperatures. For example, the dependence of $\gamma_{el}(T_2^*)$ on temperature (5-100 K) for APT in glassy water[13] and

glassy ethanol[14] was satisfactorily explained using the exchange coupling model of Jackson and Silbey.[19] Theoretical extrapolation to room temperature yielded an estimate of ~ 0.3 fs for T_2^* for both systems. However, the frequency of the exchange coupling mode for both systems is ~ 50 cm^{-1}, which is considerably higher than observed for dye/polymer and dye/protein systems. Thus, it is possible that, in certain systems, T_2^* could approach 0.1 fs, which is comparable to the timescales for optical coherence loss and solvation dynamics due to low frequency modes that have been reported for dyes in liquids at room temperature.

Figure 4 is a continuation of Fig. 3 with S = 1.7, which corresponds to strong coupling. The 3-D graph calculated with Eq. (26) shows the behavior of the echo along the $t = \tau'$ diagonal. Following the rapid decay of the intense PSB features associated with the overall profile of the multi-phonon transitions, the fundamental beat at 1.1 ps and its first overtone at 2.2 ps are observed. (Since the FC progression in the frequency domain is periodic in ω_j, the beat pattern is periodic with features at ϕ_j, $2\phi_j$,... where ϕ_j is the period of the fundamental beat, 1.1 ps for the case at hand. The time-integrated IPE signal calculated with Eq. (25) is given in the bottom frame. The width of the PSB is ~ 160 fs which corresponds to a multi-phonon profile width of 65 cm^{-1} which can be compared with $S\omega_j = 51$ cm^{-1}, where $S\omega_j$ is approximately the expected width.[43] Insert A is the single-site absorption spectrum (Eq. (24)) with a and b the one- and two-phonon transitions. The second overtone also appears. Folding of the widths of the phonon transitions is apparent. The time-integrated signal with the PSB cutoff is shown in insert B. The correspondence between the ZPL and the beats and the ZPL and multi-phonon transitions in absorption is clear.

We turn next to the temperature dependence of the IPE signal. Figure 5 calculated with Eq. (26) shows results for a model system with $\omega_j = 25$ cm^{-1}, S = 0.30, $\gamma_j = 10$ cm^{-1}, $w = 64$ cm^{-1} and $\gamma_{el}(T) = 8\,\bar{n}(\omega''_q)$ cm^{-1}, where $\omega''_q = 50$ cm^{-1} is the ground state frequency of the exchange coupling mode responsible for the pure electronic dephasing. $\bar{n}(\omega''_q)$ is the thermal occupation number $[\exp(\hbar\omega''_q / kT) - 1]^{-1}$. This model system mimics quite closely

APT in glassy ethanol.[14] The top, middle and bottom graphs correspond to 15, 25 and 100 K, respectively. (Note the changes in time scales.) For comparison of the three t,τ′ graphs it is useful to know the values of the ZPL FC factor which is given by $\exp[-S(2\bar{n}(\omega_j)+1]$. They are 0.70, 0.50 and 0.18 for 15, 25 and 100 K.

At 15 K the ZPL is strongly allowed and $\gamma_{el} = 0.07$ cm^{-1} which corresponds to an echo decay constant of (38 ps)$^{-1}$. The contribution dominates the signal seen in the top graph of Fig. 5. Because of the time scale the PSB appears as a sharp spike near $t = \tau' = 0$. At 25 K, the FC factor of the ZPL has decreased by 30% and its width is $\gamma_{el} = 0.50$ cm^{-1}. Its echo decay constant is (5.3 ps)$^{-1}$. Following the decay of the PSB, whose amplitude and width have increased, one observes the one-quantum beat at 1.3 ps which is the period of $\omega_j = 25$ cm^{-1}. Its overtone is also visible and is followed by the relatively slowly decaying ZPL component. At 50 K the ZPL is barely observable on the scale used in Fig. 5 (results not shown). By 100 K, the FC factor of the ZPL is only 0.18 and $\gamma_{el} = 7.6$ cm^{-1}. Its echo decay constant is (0.35 ps)$^{-1}$ which means that the ZPL component of the decay should appear near the tail of the PSB. However it, as well as the beats, are too weak to be observable in the bottom graph of Fig. 5. The physics conveyed by Fig. 5 has been observed by Saikan et al. in their accumulated photon echo (APE) studies of octaethylporphine in polystyrene.[34]

As a final application we present results for the special pair absorption band (P870) of the bacterial reaction center of *Rhodobacter sphaeroides*. Photochemical hole burning studies of P870 revealed that[44] it is characterized by strong electron-phonon coupling involving two modes with frequencies $\omega_m = 30$ cm^{-1} and $\omega_{sp} = 120$ cm^{-1} and Huang-Rhys factors of $S_m = 1.8$ and $S_{sp} = 1.5$ (sp denotes special pair and m the mean frequency of low frequency protein phonons). Based on the results of ref. 22 we used $\gamma_{sp} = 25$ cm^{-1}, $\gamma_m = 20$ cm^{-1} and $w = 64$ cm^{-1} for the calculations. More recently, Schellenberg et al.[35] reported the results of APE experiments performed on P870 at 1.4 K. Following a fast

($\lesssim$ 100 fs) initial decay due to multi-phonon excitation (our PSB), they observed a much weaker decay due to the ZPL with a decay constant determined by the primary charge separation time of 1.9 ps. This time corresponds to γ_{el}= 2.5 cm^{-1} which was used in our calculations. An effective S-value of 1.7 was determined which most likely corresponds to the 30 cm^{-1} protein phonons identified by hole burning. Quantum beats were not observed in ref. 35 and, thus, a mode frequency(ies) could not be determined. Thus, except for γ_{el} = 2.5 cm^{-1}, we used the hole burning values for all parameters.

The results are shown in Fig. 6. The 3-D graph calculated according to Eq. (26) shows five features, a-e, plus the relatively slowly decaying ZPL but note that feature a. due mainly to the PSB, is cut off. The periods of ω_{sp} = 120 cm^{-1} and the combination band $\omega_{sp} + \omega_m$ = 150 cm^{-1} are 277 and 220 fs. Thus, they are buried by the PSB. The signal in the lower frame with the feature at $t \approx 0$ labeled as PSB is time-integrated (Eq. (25)). The width of the PSB is 54 fs which corresponds to a width of 196 cm^{-1} for the multi-phonon profile in the frequency domain. This value is close to the anticipated approximate value of $S_m\omega_m + S_{sp}\omega_{sp}$ = 231 cm^{-1}. Features b-d can be assigned as follows: b, c and e are the first, second and fourth overtones of the fundamental quantum beat of the special pair mode while beat d is due to both the fundamental beat of the 30 cm^{-1} mode with a period of 1.1 ps and the third harmonic of the special pair fundamental beat (see inset of bottom frame). With Fig. 6 the difficulty in observing the ZPL decay component and the quantum beats for strong electron-phonon coupling is apparent (see also Fig. 5). As mentioned, Schellenberg et al. were able to detect the relatively very weak ZPL component. However, quantum beats are not evident in their time-integrated echo signal whereas Fig. 6 indicates that if the ZPL component is observed, quantum beats should also be observed. A likely reason for the discrepancy is that in the APE experiment ~ 100 fs pulses with a width of ~ 7 nm were used to pump P870 considerably to the red of its absorption maximum where the probability of exciting the 120 cm^{-1} special pair mode is low. This would significantly suppress the

quantum beats seen in Fig. 6. In addition, it has been suggested that the one-phonon absorption due to a single mode at 120 cm^{-1} could be due to two or more modes in the vicinity of 120 cm^{-1}.[45,46] This would have the effect of washing out the structure especially if the damping constants were significantly less than 25 cm^{-1}.

III. CONCLUSIONS

New 4-point and non-linear response functions $\left(\{R_\alpha\}_{\alpha=1}^{4}\right)$ for finite temperatures were obtained for a system whose phonon modes exhibit linear electron-phonon coupling only. The lineshape function g(t;T) from ref. 22 used in the response functions includes phonon damping (γ_j) and pure electronic dephasing (γ_{el}). In that paper it was shown that g(t;T) yields physically reasonable single-site absorption and hole burned spectra in which γ_{el} contributes to the widths of the phononic transitions and folding of the widths of phonon progression members occurs. Applications of the non-linear response functions were confined to the impulsive 2-pulse photon echo (IPE) because of computational considerations. Calculated IPE signals for model systems and the special pair band of the bacterial reaction clearly revealed the initial fast decay due to the envelope of multi-phonon transitions, quantum beats and the decay of the fundamental beat and the decay due to dephasing of the ZPL and how these features depend on the strength of the electron-phonon coupling and temperature. Based on the results of ref. 22 it was expected that pure electronic dephasing would contribute to the decay of the quantum beats and such was confirmed. It was suggested that this contribution could be significant at room temperature for systems whose modes are sufficiently underdamped. The features of the echo profiles/signals were correlated with those of single site absorption spectra which are closely related to hole burned spectra. The correlations illustrate the complementarity of photon echo and hole burning spectroscopies.

As discussed in refs. 13, 14 and 20, the combination of temperature dependent hole burning and echo studies of optical coherence loss of chromophores in glasses and their liquids should lead to a much better understanding of the inertial modes of liquids responsible for ultra-fast dephasing. In this regard, we believe our response functions can play an important role. The question arises as to what types of chromophores are best suited for such studies. The answer is rigid molecules devoid of Franck-Condon active low frequency *intramolecular* modes that can interfere with the low frequency inertial (librational) modes of interest. In addition, the linear electron-phonon coupling of such a chromophore in the glass should be weak so that the zero-phonon hole and the phonon sideband structure can be studied up to a temperature sufficiently high to allow for convincing theoretical interpretation of the data. Examples of such a system are Al-phthalocyanine tetrasulphonate in glassy water and ethanol. Other phthalocyanines as well as rhodamine and oxazine dyes should also be suitable. Cyanine dyes such as IR 144, which was used in ref. 20, should be avoided.

The non-linear response functions can, of course, accommodate finite pulses but at the expense of much longer computational times. For example, finite pulse calculations of the 2-pulse photon echo signal for the special pair were attempted with Mathematica (2.2 version) on a 200 MHz Pentium Pro computer. Stack overflow occurred after about two days. It was estimated that with that computer and the 2.2 version the calculation could take over a month.[47] But this problem will no doubt be overcome by use of much faster computers with adequate memory as well as improved algorithms for integral evaluation. Utilization of finite pulses is preferable to use of impulsive pulses because the echo signal can be determined as function of the pump frequency as it is tuned from the low to high energy sides of the absorption band. The equivalent of this in the frequency domain has been accomplished with hole burning of the special pair band of the bacterial reaction center.[44]

A temperature dependent 4-point correlation function without damping was derived for a system whose modes are both linearly and quadratically coupled and used to illustrate quantum beats due to the quadratic coupling which produces a mode frequency change upon electronic excitation. The intensities of such beats are strongly dependent on temperature and, therefore, can be distinguished from beats due to linearly coupled modes. Inclusion of damping for the phonons should be possible but would result in a 4-point correlation function of very considerable complexity. Currently, we are attempting to solve this problem for a system whose modes are either linearly or quadratically coupled. A solution for the linear response function is given in ref. 22.

ACKNOWLEDGMENTS

Research at Iowa State University was supported by NSF grant DMR-9630781 and at the University of Rochester by grants from NSF CHE9526125 and AFOSR F49620-96-1-0030.

REFERENCES

1. Y. J. Yan and S. Mukamel, J. Chem. Phys. **94**, 179 (1991).

2. W. B. Bosma, Y. J. Yan, and S. Mukamel, Phys. Rev. A. 42, 9620 (1990).

3. M. Cho and G. R. Fleming, J. Chem. Phys. **98**, 2848 (1993).

4. P. Vöhringer, D. C. Arnett, R. A. Westervelt, M. J. Feldstein, and N. F. Scherer, J. Chem. Phys. **102**, 4027, (1995).

5. M. S. Pshenichnikov, K. Duppen, and D. A. Wiersma, Phys. Rev. Lett. **74**, 674 (1995).

6. W. P. de Boeij, M. S. Pshenichnikov, K. Duppen, and D. A. Wiersma, Chem. Phys. Lett. **138**, 1 (1995).

7. T. Joo, Y. Jia, J-Y. Yu, M. J. Lang, and G. R. Fleming, J. Chem. Phys. **104**, 6089 (1996).

8. G. R. Fleming and M. Cho, Annu. Rev. Phys. Chem. **47**, 109 (1996).

9. C. H. B. Cruz, R. L. Frork, W. H. Knox, and C. V. Shank, Chem. Phys. Lett. 132, 341 (1986).

10. W. P. de Boeij, M. S. Pshenichnikov, and D. A. Wiersma, J. Phys. Chem. **100,** 11806 (1996).

11. P. Vöhringer, D. C. Arnett, T. -S. Yang, and N. F. Scherer, Chem. Phys. Lett. **237**, 387 (1995).

12. C. J. Bardeen and C. V. Shank, Chem. Phys. Lett. 226, **310** (1994).

13. T. Reinot, W.-H. Kim, J. M. Hayes, and G. J. Small, J. Chem. Phys. **104**, 793 (1996).

14. T. Reinot, W.-H. Kim, J. M. Hayes, and G. J. Small, J. Chem. Phys. **106**, 457 (1997).

15. J. M. Hayes, P. A. Lyle, and G. J. Small, J. Phys. Chem. **98**, 7337 (1994).

16. We are not aware of any chromophore/amorphous host system whose phonon structure cannot be interpreted in terms of a single phonon and its associated one-phonon profile, i.e. a single feature in the spectral density.

17. As discussed in ref. A, dephasing due to the exchange coupling mechanism for chromophores in amorphous solids has often been observed. For temperatures below about 10 K the homogeneous width of the ZPL is dictated by the two-level systems of the glass.

18. R. M. Shelby, C. B. Harris, and P. A. Cornelius, J. Chem. Phys. **70**, 34 (1979).

19. B. Jackson and R. Silbey, Chem. Phys. Lett. **99**, 331 (1983).

20. Y. Nagasawa, S. A. Passino, T. Joo, and G. R. Fleming. **106**, 4840 (1997).

21. C. J. Bardeen, G. Cerullo, C. V. Shank, Chem. Phys. Lett. 280, 127 (1997).

22. M. Toutounji, G. J. Small and S. Mukamel, J. Chem. Phys. (accompanying paper).

23. R. L. Beckman and G. J. Small, Chem. Phys. **30**, 19 (1978).

24. G. Fischer, Chem. Phys. Lett. **20**, 569 (1973).

25. S. Saikan, T. Nakabayashi, Y. Kanematsu, N. Tato, Phys. Rev. B. **38,** 7777 (1988).

26. S. Saikan, A. Imaoka, Y. Kanematsu, K. Sakoda, K. Kominami, M. Iwamoto, Phys. Rev. B. **41,** 3185 (1990).

27. S. Saikan, Y. Kanematsu, R. Shiraishi, T. Nakabayashi, T. Kushida, J. Luminescence. **38**, 15 (1987).

28. S. Saikan, J. W-I Lin, H. Nemoto, Phys. Rev. B. **46**, 11125 (1992).

29. S. Asaka, H. Nakatsuka, M. Fujiwara, M. Matsuka. Phys. Rev. A. **29**, 2286 (1984).

30. I. S. Osad'ko, *Spectroscopy and Excitation Dynamics of Condensed Molecular Systems*, edited by V. M. Agranovich and R. M. Hochstrasser (North-Holland, Amsterdam, 1983) p. 437.

31. I. S. Osad'ko, Adv. Poly. Sci. **114**, 125 (1994).

32. I. S. Osad'ko and M. V. Stashek, JETP **79**, 293 (1994).

33. I. S. Osad'ko, M. V. Stashek, and M. A. Mikhailov, Laser. Phys. **6**, 175 (1996).

34. S. Saikan, A. Imaoka, Y. Kanematsu, K. Sakoda and T. Kishida, Chem. Phys. Lett. **162**, 217 (1989).

35. P. Schellenberg, R. J. W. Louwe, S. Shochat, P. Gast, and T. J. Artsma, J. Phys. Chem. B. **101**, 6786 (1997).

36. S. Mukamel, *Principles of Nonlinear Optical Spectroscopy* (Oxford University, New York, 1995).

37. Our Eqs. (1) - (10) correspnd to Eqs. (5.27), (7.13), (7.14), (10.11), (10.16), (10.14), (10.15), (10.21), (10.22) of Ref. AF

38. We remind the reader that γ_{el} is the fwhm of the ZPL, thus the factor of 2 in the exponential rather than the more usual factor of 4.

39. Folding due to $n_j^{'}$ also occurs for hot $n_j^{''} \neq 0 \rightarrow n_j^{'}$ transitions. Widths are given by $\gamma_{el} + (n_j^{'} + n_j^{''})\gamma_j$.

40. Since $\gamma_{el} = 2.5\ cm^{-1}$ is small relative to $\gamma_j = 20\ cm^{-1}$, the uncertainty is quite large, $\pm 0.5\ cm^{-1}$. Thus, we increased γ_{el} to $10\ cm^{-1}$ in order to convincingly confirm that the width is $\gamma_{el} + \gamma_j$.

41. S. Völker. *Relaxation Processes in Molecular Excited States*, edited by J. Fünfschilling (Kluwer, Dordrecht, 1989), p. 113.

42. L. R. Narashiman, K. A. Littau, D. W. Pack, Y. S. Bai, A. Elschner, and M. D. Fayer, Chem. Rev. **90**, 439 (1990).

43. The optical reorganization energy is $\sum_j S_j \omega_j$ for a multimode system. The results of ref. Y and references therein show that for $S_j > 1$, the homogeneous contribution to the width of the absorption band is given approximately by the optical reorganization energy.

44. P. A. Lyle, S. V. Kolaczkoski, and G. J. Small, J. Phys. Chem. **97**, 6924 (1993).

45. V . Palanniappan, A. M. Adelma, A. H. frank, and F. D. Bocian, Biochmistry **31**, 11050 (1995).

46. P. A. Sherve, J. N. Cherepy, S. Franzen, G. S. Boxer, A. R. Mathies, Proc. Natl. Acad. Sci. U.S.A, **88**, 11207 (1991).

47. Technical support division at Wolfram Research.

APPENDIX A

Here we outline the derivation of $F(\tau_1,\tau_2,\tau_3,\tau_4)$ in the Condon approximation is outlined. The 4-point correlation function is given by

$$F(\tau_1,\tau_2,\tau_3,\tau_4)=\left\langle e^{iH_g\tau_1/\hbar}\ e^{iH_e(\tau_2-\tau_1/\hbar}\ e^{iH_g(\tau_3-\tau_2)/\hbar}\ e^{iH_e(\tau_4-\tau_3)/\hbar}\ e^{-iH_g\tau_4/\hbar}\ \rho_g\right\rangle \quad \text{(A1)}$$

Following ref. 22, where coherent states for the phonon field rather than number states were used to evaluate the 2-point correlation function, we use the following closure relation for coherent states to evaluate Eq. (A1):

$$\frac{1}{\pi}\int d^2z\,\frac{|z\rangle\langle z|}{\langle z|z\rangle}=1, \quad \text{(A2)}$$

where $d^2z = d(\text{Re } z)d\ \text{Im}(z)$. Applying Eq. (A2) to Eq. (A1) yields,

$$F(\tau_1,\tau_2,\tau_3,\tau_4)=\frac{1}{Q\pi}\int_{-\infty}^{\infty}\frac{d^2z}{\langle z|z\rangle}\langle z|e^{iH_g\tau_1/\hbar}\ e^{iH_e(\tau_2-\tau_1)/\hbar}$$

$$\times\ e^{iH_g(\tau_3-\tau_2)/\hbar}\ e^{iH_e(\tau_4-\tau_3)/\hbar}\ e^{-i'H_g\tau_4/\hbar}\ e^{-\beta H_g}|z\rangle, \quad \text{(A3)}$$

where $Q\equiv \text{Tr}(e^{-\beta H_g})$. Evaluation of the integral in Eq. (A3) leads to ($\Omega = 0$)

$$F(\tau_1\tau_2,\tau_3,\tau_4)=\frac{\exp(-\beta\hbar\omega''/2)}{Q}\exp\left[\frac{1}{2}i(\omega''-\omega')(\tau_{12}+\tau_{34})\times b_1^{-1}\exp\left(b_1^{-1}b_2+b_3\right)\right], \quad \text{(A4)}$$

where $\tau_{ij}=\tau_i-\tau_j$ and

$$b_1 \equiv 1 - e^{i\omega'(\tau_{21}-\tau_{34})-\beta\hbar\omega''+i\omega''\tau_1}\, e^{i\omega''(\tau_{34}-\tau_2)}, \tag{A5}$$

$$b_2 \equiv S_{eff}\, e^{-\beta\hbar\omega''}\Big[-e^{-i\omega''\tau_4} + e^{i\omega'\tau_{43}-i\omega''\tau_4} - e^{i\omega'\tau_{43}+i\omega''(\tau_{32}-\tau_4)}$$

$$+ e^{i\omega'(\tau_{21}+\tau_{43})+i\omega''(\tau_{32}-\tau_4)}\Big]\Big[-e^{i\omega''\tau_1} + e^{i\omega'\tau_{21}+i\omega''\tau_1}$$

$$- e^{i\omega'\tau_{21}+i\omega''(\tau_{12}-\tau_3)} + e^{i\omega'(\tau_{21}-\tau_{34})+i\omega''(\tau_{12}+\tau_3)}\Big], \tag{A6}$$

and

$$b_3 \equiv S_{eff}\Big[-2 + e^{i\omega'\tau_{21}} + e^{i\omega'\tau_{43}} + e^{i\omega''\tau_{32}} - e^{i\omega'\tau_{21}+i\omega''\tau_{32}} - e^{i\omega'\tau_{43}+i\omega''\tau_{32}}\Big]. \tag{A7}$$

where the effective Huang-Rhys factor S_{eff} is given by Eq. (18).

FIGURE CAPTIONS

Figure 1. Impulsive stimulated photon echo signal for a system with very large inhomogeneous broadening and a mode that exhibits both linear and quadratic coupling. It was calculated using Eqs. (A4), (8) and (10) with $\omega'' = 200\ cm^{-1}$, $\omega' = 150\ cm^{-1}$, $S = 2.0$, $\gamma = 0$ and $T = 300$ K.

Figure 2. Frequency domain slice obtained from Fig. 1 by taking the Fourier transform of Eq. (10) (Eq. (27)) with $\tau = 1$ fs and uniform damping corresponding to frequency domain widths of $3\ cm^{-1}$.

Figure 3. Impulsive photon echo (IPE) signals calculated with Eq. (25) for a model system ($\omega_j = 30\ cm^{-1}$, $\gamma_j = 20\ cm^{-1}$, $\gamma_{el} = 2.5\ cm^{-1}$, $w = 64\ cm^{-1}$ and $T = 0$ K) for $S = 0.01$ (top), 0.10 (middle) and 0.50 (bottom). PSB denotes phonon sideband (see text for discussion). For comparison, the corresponding single-site absorption spectra calculated according to Eq. (24) are shown in the right panel.

Figure 4. Continuation of Fig. 3 with $S = 1.7$. The 3-D graph is the IPE signal as a function of t and τ' calculated with Eq. (26), see text for discussion. The time-integrated signal calculated with Eq. (25) is shown in the lower frame. Inset B, with the PSB cutoff, shows the phonon quantum beats and the slow decay due to the ZPL. The single site absorption spectrum calculated with Eq. (24) is given in inset A.

Figure 5. Impulsive photon echo (IPE) signals as a function of temperature calculated with Eq. (26) for a model system ($\omega_j = 25\ cm^{-1}$, $S = 0.30$, $\gamma_j = 10\ cm^{-1}$, $w = 64\ cm^{-1}$ and $\gamma_{el}\ (cm^{-1}) = 8\,\bar{n}(\omega''_q)$ where $\omega''_q = 50\ cm^{-1}$. The top, middle and bottom graphs are for 15, 25 and 100 K, respectively.

Figure 6. Impulsive photon echo signals calculated as Fig. 4 at $T = 0$ K for the special pair absorption band of the bacterial reaction center characterized by two linearly coupled modes ($\omega_m = 30\ cm^{-1}$, $\gamma_m = 20\ cm^{-1}$, $S_m = 1.7$; $\omega_{sp} = 120\ cm^{-1}$, $\gamma_{sp} = 25\ cm^{-1}$, $S_{sp} = 1.5$; and $w = 64\ cm^{-1}$, $\gamma_{el} = 2.5\ cm^{-1}$). The 3-D graph shows the fast decay due to the PSB (a), phonon quantum beats b-e and the slow decay due to the ZPL. For comparison the time-integrated signals are shown in the lower frame.

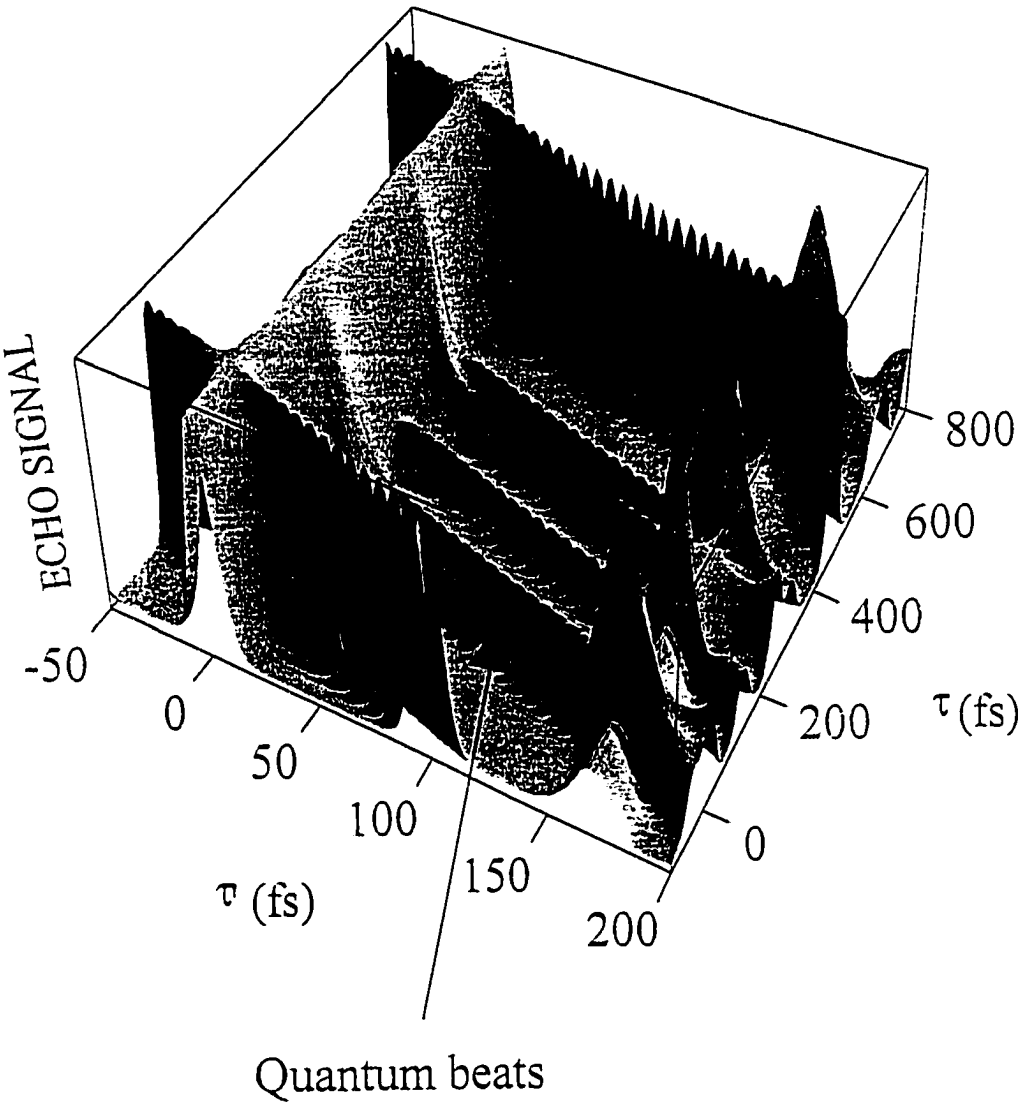
ECHO SIGNAL
-50
0
50
100
150
200
τ (fs)
0
200
400
600
800
τ (fs)
Quantum beats

Figure 1

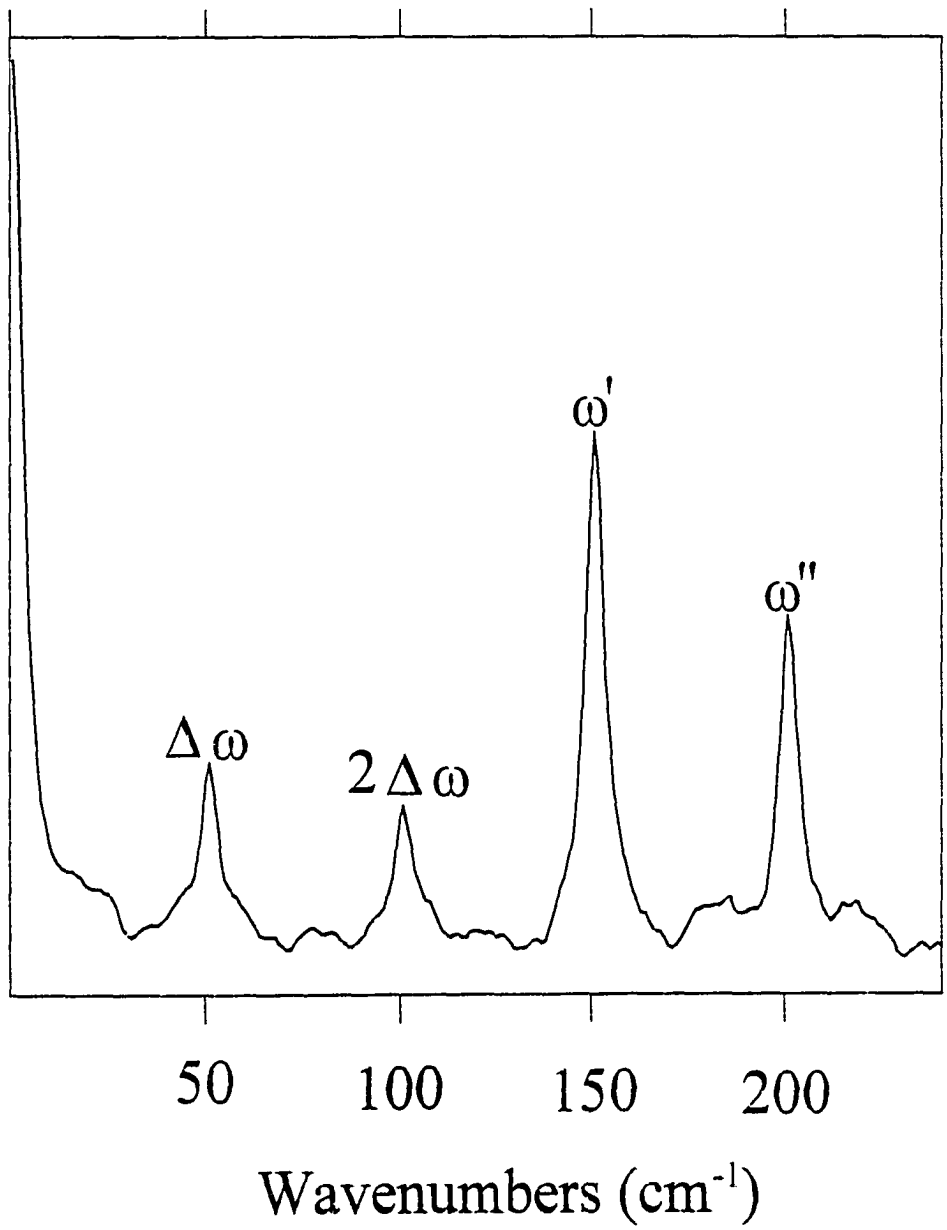

Figure 2

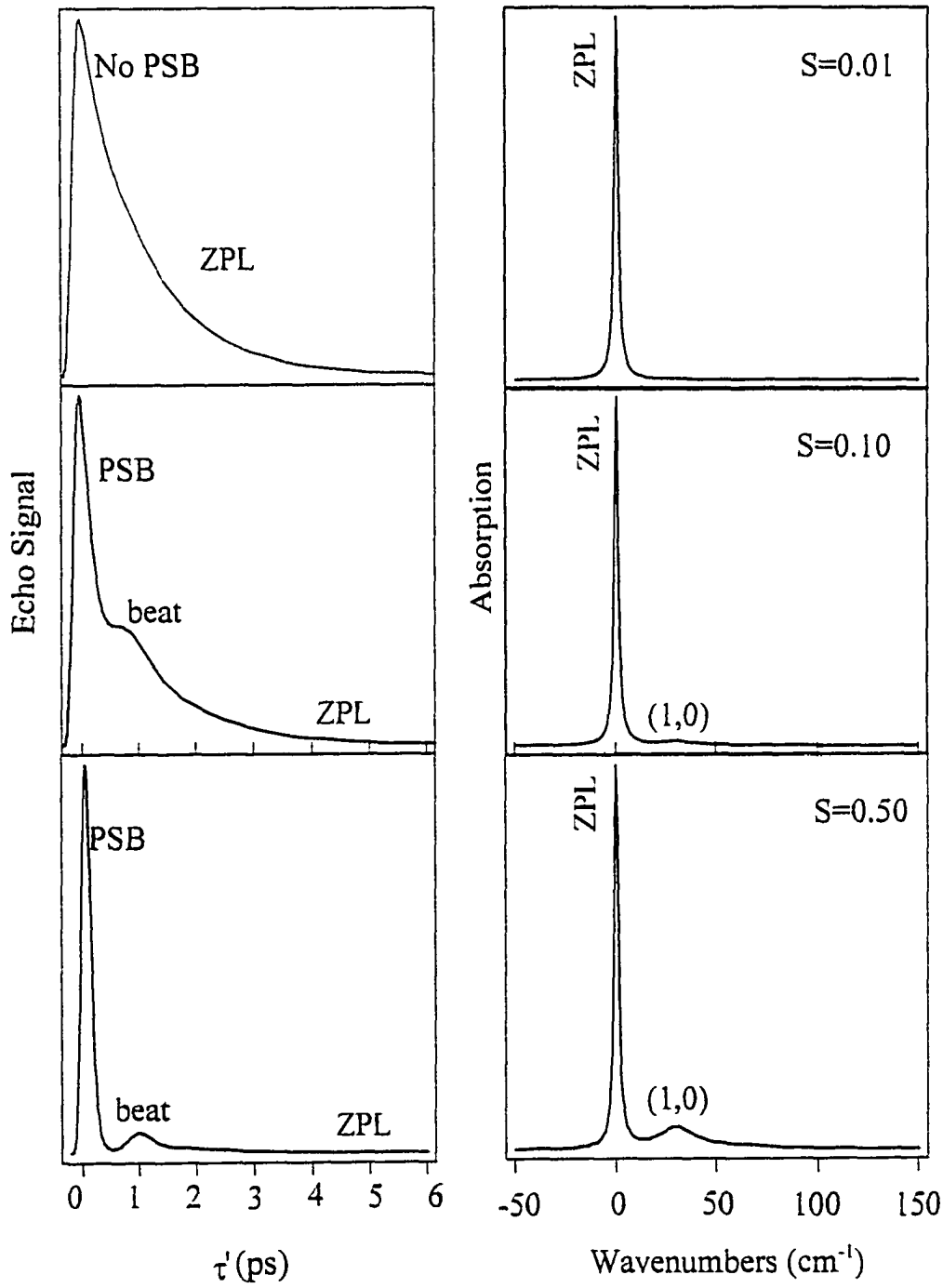
No PSB
ZPL
PSB
beat
ZPL
PSB
beat
ZPL
Echo Signal
0
1
2
3
4
5
6
τ' (ps)
ZPL
S=0.01
ZPL
S=0.10
(1,0)
ZPL
S=0.50
(1,0)
Absorption
-50
0
50
100
150
Wavenumbers (cm-1)

Figure 3

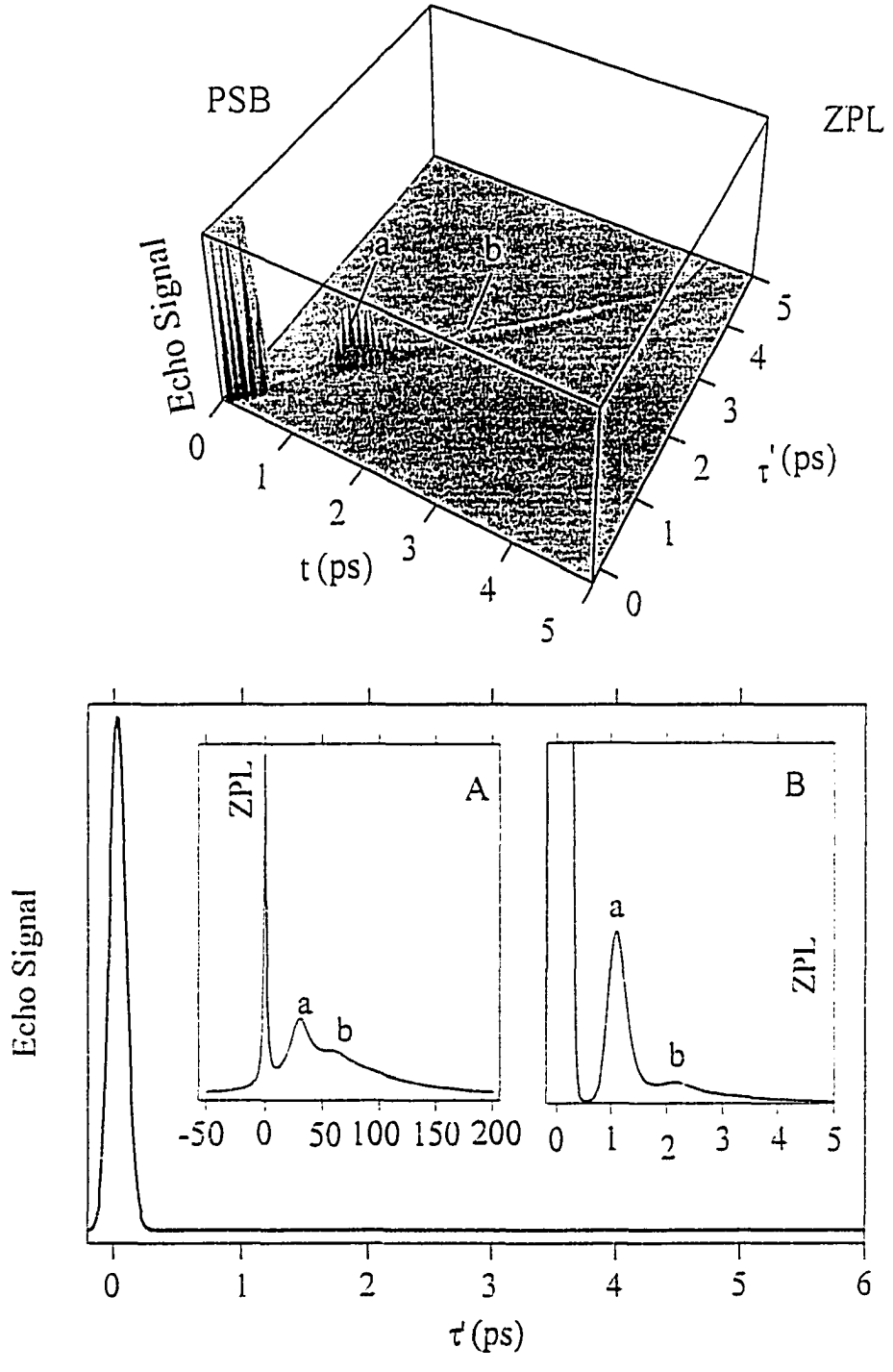
PSB
ZPL
Echo Signal
a
b
0
1
2
3
4
5
t (ps)
τ' (ps)
Echo Signal
ZPL
A
B
a
b
-50 0 50 100 150 200
0 1 2 3 4 5
0 1 2 3 4 5 6
τ' (ps)

Figure 4

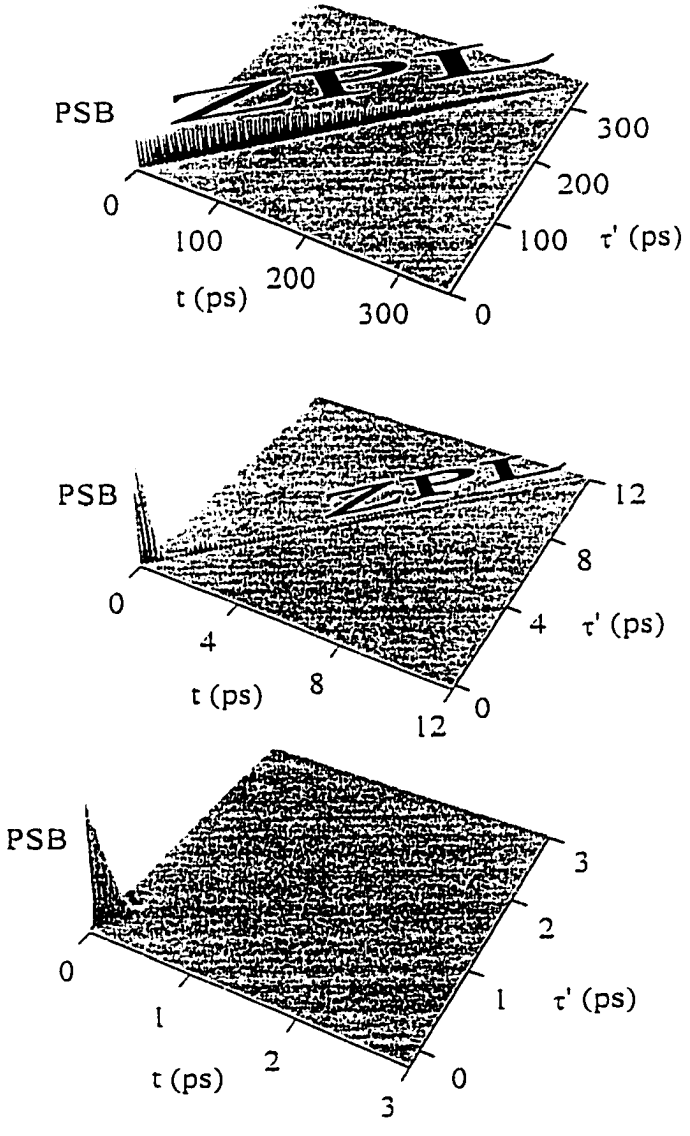
PSB
0
100
200
300
t (ps)
0
100
200
300
τ' (ps)
PSB
0
4
8
12
t (ps)
0
4
8
12
τ' (ps)
PSB
0
1
2
3
t (ps)
0
1
2
3
τ' (ps)

Figure 5

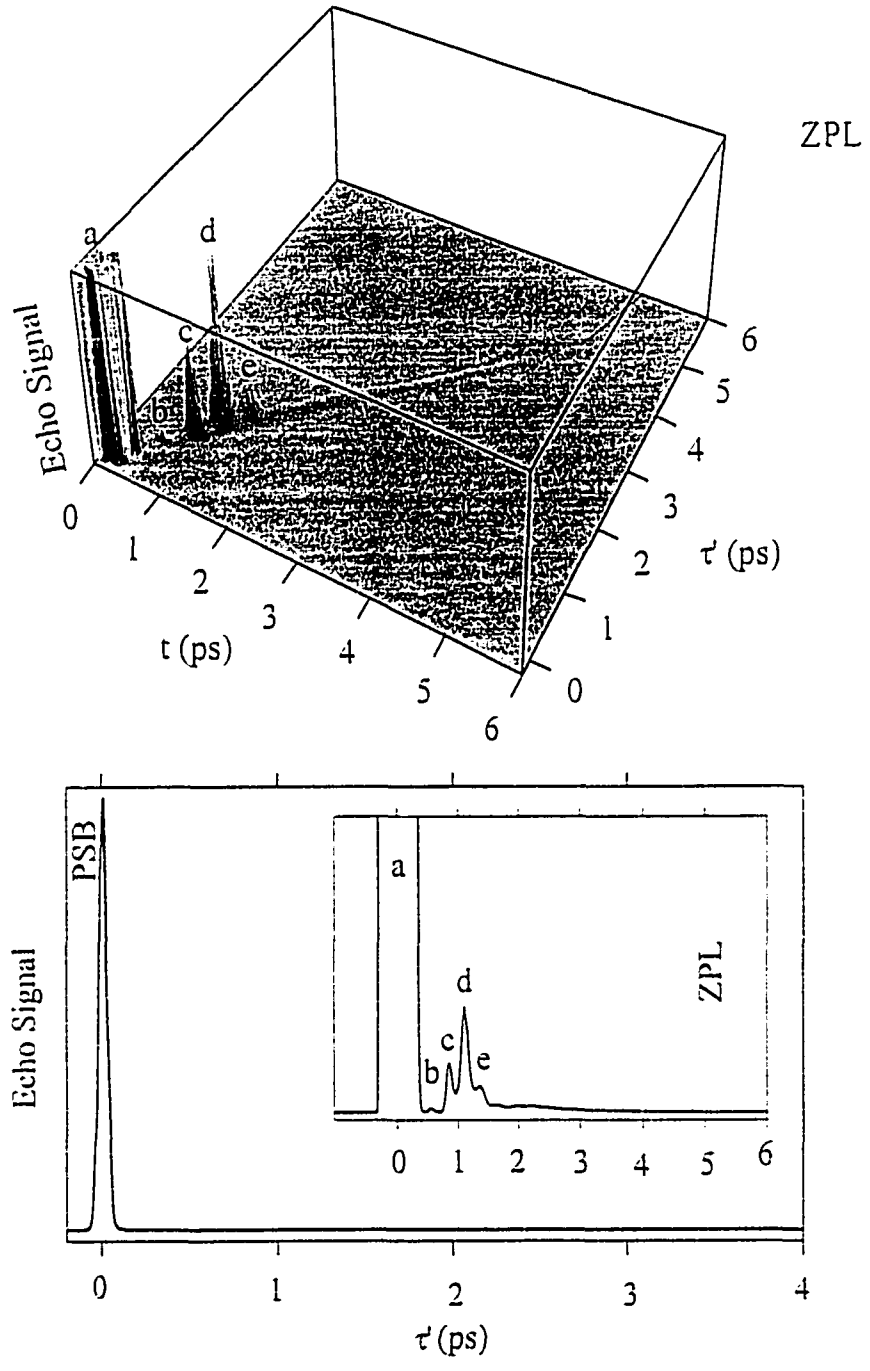
ZPL
a
d
c
e
b
Echo Signal
0
1
2
3
4
5
6
t (ps)
τ' (ps)
PSB
Echo Signal
a
d
c
b
e
ZPL
0
1
2
3
4
5
6
τ' (ps)

Figure 6

CHAPTER 5. CONCLUDING REMARKS

For only linear electon-phonon coupling, our proposed g(t;T) provides the most physical description of spectroscopic signals for chromophores in condensed phases compared with those developed by Osad'ko or Mukamel via the MBO model. Our g(t;T) correctly describes pure electronic dephasing and vibrational damping, and assigns each vibrational mode in a multi-mode system a different damping constant. Furthermore, it provides folding of the vibrational progression members of the absorption profile, which is often a desired result. On the other hand, g(t;T) obtained via the MBO model , although it assigns each vibrational mode a different damping constant and provides folding of the progression members, handles the pure electronic dephasing incorrectly. In addition, it provides unphysical description of the phononic transitions because they build on the electronic transiton. The g(t;T) developed by Osad'ko, although it does not have any damping constants (electronic or vibrational), is set up such that pure electronic dephasing and damping of the phonons can easily be taken into account. Thus, this g(t;T) handles homogeneous widths of the electronic and vibrational transitions correctly, but it does not take folding of the progression members into account. Furthermore, it is not apparent, in the time-domain, how this g(t;T) can assign different damping constants for a multi-mode system. This problem is taken care of in the frequency-domain expression. As pointed out in Chapter 2, g(t;T) is the essential component for calculating linear and non-linear temporal or spectral profiles, i.e, g(t;T) is the only mathematical quantity needed for calculating spectroscopic signals, in the linear coupling approximation. Therefore, combining our g(t;T) with Mukamel's formalism of optical linear and non-linear response functions yields spectroscopic signals that can account for structural and dynamical information (e.g., pure electronic dephasing, quantum beats and spectral diffusion) about the system.

The theory developed in this dissertation can easily be extended to take into account non-Condon (Hertzberg-Teller coupling), Duschinsky, and anharmonicity (e.g., using the Morse potential for the vibrational Hamiltonian in the excited state) effects, in addition to linear and quadratic coupling, to see how the associated spectroscopic features might change accordingly. The damping can be quantized, as was done in the linear and quadratic coupling cases, for the phonons in our J(t;T) in Eq. (12) of Chapter 3. This will break J(t;T) into a product of two response functions; one is phononic that handles the vibrational relaxation and the other is electronic that describes the pure electronic dephasing. As a result, the phonons can be assigned different damping constants in a multi-mode system. Spectral density (phonon density of states, $\rho(\omega)$) is a very important quantity in solvation dynamics and spectroscopy. One can obtain a physical $\rho(\omega)$ from g(t;T) using Mukamel's formalism.

Although an analytical expression was obtained for a two finite-pulse photon echo (PE) with finite inhomogeneous broadening (assuming static nuclei), it was not possible to numerically evaluate the triple-integral at T = 0 K using Mathematica 3.0 on a 200 MHz Pentium Pro computer due to the extreme complexity of the integrand. The presence of the double-integral (the polarization) modulus squared to be integrated over t complicates and slows down the integration process. Therefore, only a numerical evaluation of the double-integral (whose modulus squared generates a PE as a function of t and τ') over t_3 and t_1 was attempted. A stack overflow, caused by a build up of numerical uncertainties, occurred after one day. (If numerical uncertainties are not eliminated, they could lead to incorrect results.) A further simplification step was taken by only considering the zero-phonon line and one-phonon profile in the time-domain. This simplification certainly reduced the numerical uncertainties but did not completely resolve the problem. An alternative was to try a different numerical technique such as Monte Carlo. The Monte Carlo method was certainly able to eliminate the integration numerical uncertainties. However, it slowed the evaluation process considerably. It turned out that this evaluation was beyond the capacity of computer

resources. Mathematica 3.0 was able to symbolically evaluate the integral over t_3 and left the integration over t_1 unevaluated (remember that was only for the zero-phonon line and one phonon profile). The result was roughly 20 pages of Error, Hypergeometric, hyperbolic, and transcendental functions as a function of t_1. However, the computer could not handle this particular symbolic integration when Mathematica 2.2 was used.

APPENDIX A: SPECTRAL ANALYSIS OF THE MULTI-MODE BROWNIAN OSCILLATOR (MBO) MODEL

Here we spectrally analyze the MBO model. We will point out and demonstrate the MBO model deficiencies in handling the pure electronic dephasing associated with the phononless transition, the zero-phonon line (ZPL), by studying its resulting single-site absorption spectra, which can be obtained by Fourier transforming the MBO 2-point correlation function, $J_{MBO}(t)$. The MBO model has been used in different areas of optical spectroscopy [1-15], solvation dynamics [1, 8, 16-18], and energy transfer [1, 19, 20]. The optical dynamics are attributed entirely to the damping of Frank-Condon (FC) active modes which are often intermolecular. It has most often been used in photon echo techniques [1-18] to account for quantum beats, as well as homogeneous dephasing, inhomogeneous dephasing, and spectral diffusion. In this model the linearly coupled modes are the primary Brownian oscillators (BOs). The BOs and the bath oscillators are assumed to be harmonic with the coupling between the former and latter taken to be linear in the BO displacement which results from excitation of the BO via the electronic transition. The coupling gives rise to an effective damping, γ_j, for each BO j (frequency ω_j). A key quantity which enters into the MBO expressions for the linear and nonlinear response functions is the line broadening function, g(t;T), which depends on the linear couplings (Huang-Rhys factors), frequencies and damping constants of the BOs. The Fourier transform of the linear correlation function, exp(−g(t;T)), yields the linear absorption spectrum.

The concept of Brownian oscillators to describe the nuclear motion effects on solvation dynamics was originally developed by Adelman and co-workers [21-23] and Hynes and co-workers [24-26]. (The name "Brownian" stems from the fact that the nuclear coordinates coupled to a bath experience a Brownian motion which is governed by the

Langevin equation [27-35]). Mukamel and co-workers [1] generalized these treatments and developed the MBO model for linear and non-linear response functions.

The MBO model has most often been used in the interpretation of photon echo data in liquids at room temperature. However, only the overdamped ($\gamma_j >> \omega_j$) MBO in the high temperature limit has been employed in those experiments (photon echoes), which greatly simplifies the linear and non-linear calculations. We are not aware of any linear absorption homogeneous lineshapes (single-site absorption spectra) that have been generated before via the MBO model at finite temperature or in the low temperature limit.

Unfortunately, we found that g(t;T) (Eqs. (8.67) of Ref. [1]) for the MBO model at finite temperature is very complicated and does not easily lend itself to use. Therefore, we will only discuss the MBO model in the low temperature limit (T = 0 K).

A.1 The MBO Model at Zero Temperature

The linear 2-point correlation function is given by ($\Omega = 0$)

$$J_{MBO}(t) = \exp[-g(t)], \tag{A.1}$$

with g(t) given by [1]

$$g(t) = \sum_{j=1}^{N} g_j(t) \tag{A.2}$$

$$g_j(t) = u_j^2 \int_0^t d\tau_1 \int_0^{\tau_1} d\tau_2 \, C_j^{'}(\tau_2) + i\, u_j^2 \int_0^t d\tau_1 \int_0^{\tau_1} d\tau_2 \, C_j^{''}(\tau_2). \tag{A.3}$$

In the low temperature limit,

$$C_j^{'}(t) = \frac{\hbar}{2\zeta_j} \exp(-\gamma_j |t|/2) \cos(\zeta_j t), \tag{A.4}$$

$$C_j^{''}(t) = -\frac{\hbar}{2\zeta_j} \exp(-\gamma_j |t|/2) \sin(\zeta_j t), \tag{A.5}$$

and

$$u_j \equiv \frac{\omega_j^{3/2}}{\hbar^{1/2}} d_j, \tag{A.6}$$

$$\zeta_j = [\omega_j^2 - (\gamma_j/2)^2]^{1/2}. \tag{A.7}$$

Using Eqs. (A.3) — (A.6), g(t) reads

$$g_j(t) = \frac{\omega_j^3 d_j^2}{2\zeta_j} \int_0^t d\tau_1 \int_0^{\tau_1} d\tau_2 \exp[-\gamma_j \tau_2 / 2 - i\zeta_j \tau_2] \\ = S_j \omega_j t / 2\zeta_j + Y_j[1 - \exp(-\gamma_j t / 2 - i\zeta_j t)], \tag{A.8}$$

where

$$Y_j \equiv S_j(\omega_j^2 - \gamma_j^2 / 2 + i\gamma_j \zeta_j) / \zeta_j \omega_j, \tag{A.9}$$

where $S_j = d_j^2/2$ is the Huang-Rhys factor with d_j being the dimensionless linear displacement and γ_j is the damping constant (fwhm) of BO j. (Note that we have omitted the reorganizational term energy ($iS_j\omega_j t$) in Eq. (A.8) since $J_{MBO}(t)$ does not contain Ω_v because they both cancel in the end (see Eq. (1.51c)). With Eqs. (A.1) and (A.2) $J_{MBO}(t)$ reads

$$J_{MBO}(t) = \exp\{-S_j \omega_j t / 2\zeta_j - Y_j[1 - \exp(-\gamma_j t / 2 - i\zeta_j t)]\}. \tag{A.10}$$

Upon power series expansion of Eq. (A.10), one obtains

$$J_{MBO}(t) = \exp(-Y_j) \sum_{m=0}^{\infty} \frac{Y_j^m}{m!} \exp[-(S_j \omega_j / 2\zeta_j + m\gamma_j t / 2)t - im\zeta_j t]. \tag{A.11}$$

The linear absorption spectrum is given by

$$\sigma(\omega) = \mathrm{Re} \frac{1}{\pi} \int_0^{\infty} dt\, J_{MBO}(t) \exp(i\omega t). \tag{A.12}$$

Using Eqs. (A.11) and (A.12) for mode j yields

$$\sigma_j(\omega) = \frac{\mathrm{Re}}{\pi}\left\{\exp(-Y_j)\sum_{m=0}^{\infty}\frac{Y_j^m}{m!}\left[\frac{1}{(S_j\omega_j/2\zeta_j + m\gamma_j/2) - i(\omega - m\zeta_j)}\right]\right\}. \qquad (A.13)$$

It should be more informative to rewrite the lorentzian in Eq. (A.13) in this form

$$\sigma_j(\omega) = \frac{\mathrm{Re}}{\pi}\left\{\exp(-Y_j)\sum_{m=0}^{\infty}\frac{Y_j^m}{m!}\left[\frac{(S_j\omega_j/2\zeta_j + m\gamma_j/2) - i(\omega - m\zeta_j)}{(\omega - m\zeta_j)^2 + (S_j\omega_j/2\zeta_j + m\gamma_j/2)^2}\right]\right\}. \qquad (A.14)$$

Since we are in the low temperature limit, the quantum number of the initial state for the absorption transition is zero. m is the final state quantum number. Equation (A.14) shows, in part, that the MBO model yields a ZPL (m = 0) width of

$$\gamma_{el,j}^{MBO} = S_j\omega_j\gamma_j / \zeta_j \qquad (A.15)$$

which depends on the phonon damping γ_j and the Huang-Rhys factor S_j (for the underdamped case $\zeta_j \approx \omega_j$). Equation (A.15) is an unphysical result. In addition, the widths of the multi-phonon bands ($m \geq 1$)

$$(fwhm)_m = \gamma_{el,j}^{MBO} + m\gamma_j \qquad (A.16)$$

contain $\gamma_{el,j}^{MBO}$. Note, however, that the second term gives folding of the widths of the multi-phonon transitions which will often be the desired result. The resonances in Eq. (27) are determined by $\omega = m\,\zeta_j$.

In addition to the unphysical ZPL width that MBO (Eq. (A.15)) yields, there is a fundamental problem with the ZPL resulting FC factor. The MBO produces negative ZPL FC factor: That Y_j is a complex quantity presents a complication because there is another

complex quantity in the numerator of Eq. (A. 14), $i(\omega - m\zeta_j)$, which gives rise to an interference effect. This causes the ZPL to go negative. Figure A.1 is a single-site absorption spectrum calculated according to Eq. (A.13) with $\omega_j = 50$ cm^{-1}, $S_j = 1.7$, and $\gamma_j = 30$ cm^{-1}. The ZPL cannot be seen because according to Eq. (A. 14) its width is 53 cm^{-1} which is too broad to be seen. But if we plot the ZPL by itself, we can see its unphysical width and its negative intensity, as shown in Figure A.2. We can examine ZPL closer by taking the values of the absorption profile at couple of points; for example, $\sigma_j(\omega = 200) = 0.00073$ and $\sigma_j(\omega = -200) = -0.0014$. It might be argued that taking points is not an ultimatum in judging the ZPL behavior. It definitely form a problem if someone tries to do fitting, because fitting data is nothing but points.

We can fix the homogeneous ZPL width problem by removing the MBO width, $\gamma_{el,j}^{MBO}$, and replace it with the correct width γ_{el}, then Eq. (A.14) becomes

$$\sigma_j(\omega) = \frac{\mathrm{Re}}{\pi}\left\{\exp(-Y_j)\sum_{m=0}^{\infty}\frac{Y_j^m}{m!}\left[\frac{(\gamma_{el}/2 + m\gamma_j/2) - i(\omega - m\zeta_j)}{(\omega - m\zeta_j)^2 + (\gamma_{el}/2 + m\gamma_j/2)^2}\right]\right\}. \qquad \text{(A.17)}$$

Plotting Eq. (A.17) using the same parameters with $\gamma_{el} = 4$ cm^{-1} yields Figure A.3, in which the ZPL, clearly, has negative intensity. Furthermore, Figure A.3 shows that the absorption intensity goes slightly negative at ~ 300 cm^{-1}. This can be attributed to the interference effect, *vide supra*.

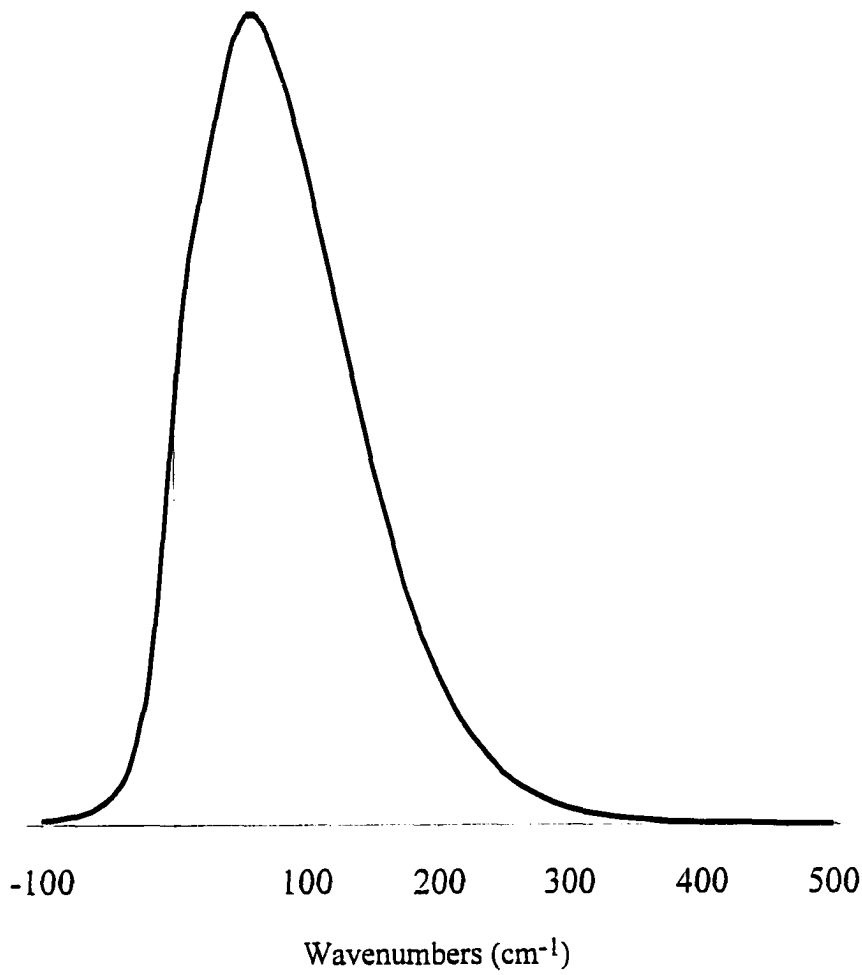

Figure A.1 Single-site absorption spectrum calculated according to Eq. (A.13) with ω_j = 50 cm^{-1}, S_j = 1.7, and γ_j = 30 cm^{-1} at T = 0 K. The homogeneous width of the ZPL is 53 cm^{-1} which is too broad to be seen.

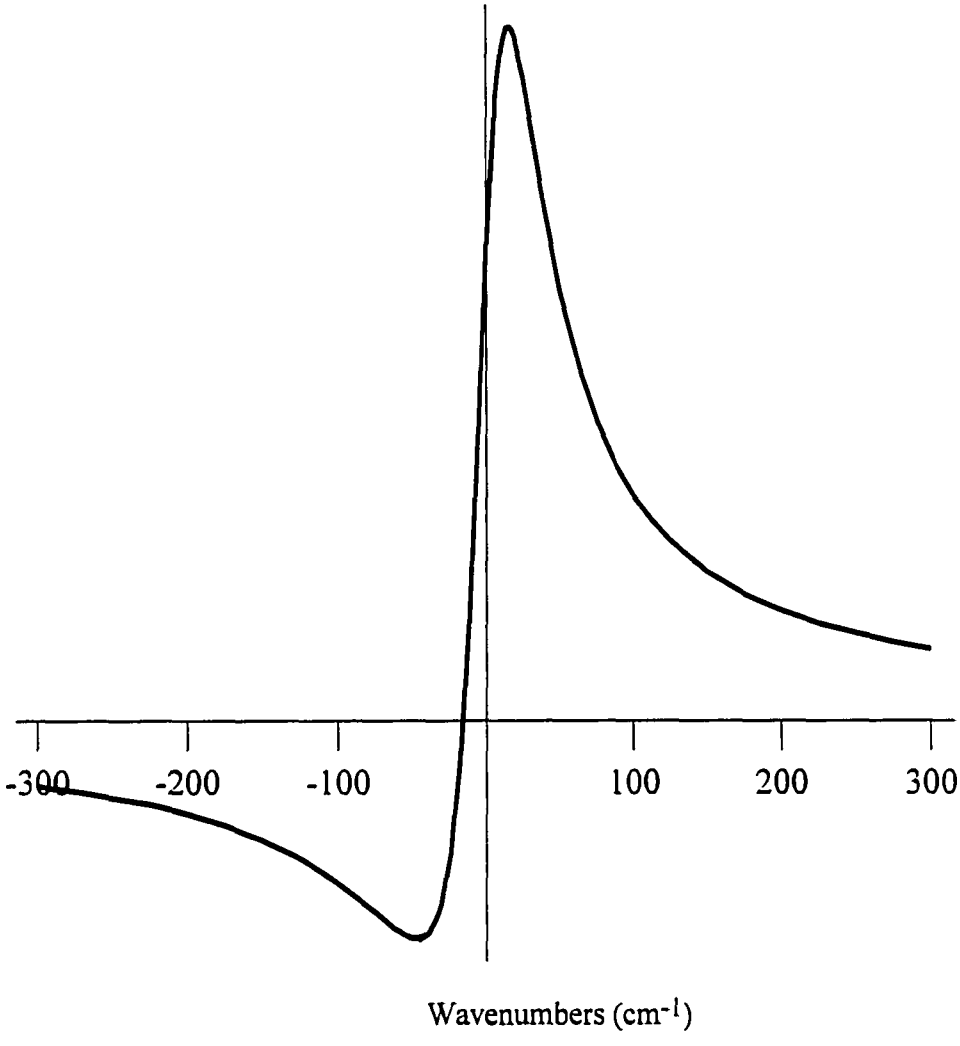

Figure A.2 The zero-phonon line calculated as in Figure A.1, the intensity goes negative due to the interference effect, see text.

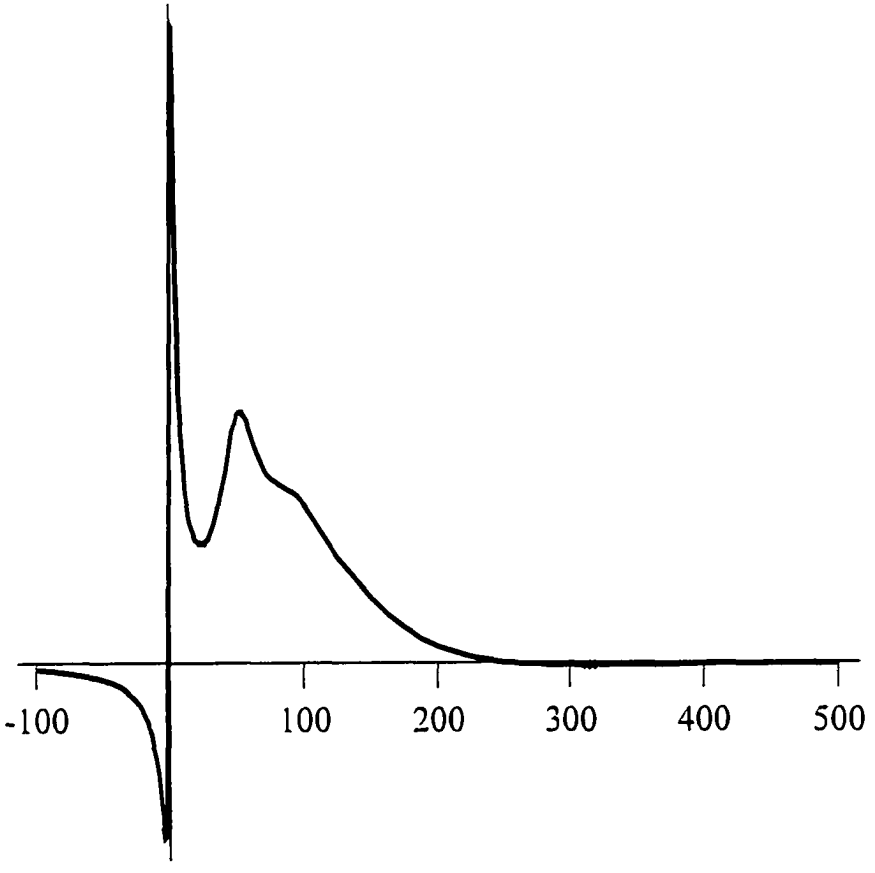

Figure A.3 Single-site absorption spectrum calculated according to Eq. (A.13) with ω_j = 50 cm^{-1}, S_j = 1.7, γ_j = 30 cm^{-1}, and γ_{el} = 4 cm^{-1} at T = 0 K. The ZPL intensity becomes very negative, and the PSB goes slightly negative at ~ 300 cm^{-1} due to the interference effect, see text for further details.

A. 2 References

1. S. Mukamel, *Principles of Nonlinear Optical Spectroscopy* (Oxford University, New York, 1995).
2. Y. J. Yan and S. Mukamel, J. Chem. Phys. **94**, 179 (1991).
3. R. F. Loring and S. Mukamel, Chem. Phys. Lett. **114**, 426 (1985); J. Chem. Phys. **83**, 2116 (1985).
4. Y. Nagasawa, S. A. Passino, T. Joo, and G. R. Fleming. **106**, 4840 (1997).
5. T. Joo, Y. Jia, J-Y. Yu, M. J. Lang, and G. R. Fleming, J. Chem. Phys. **104**, 6089 (1996)
6. N. F. Scherer, L. D. Ziegler, and G. R. Fleming, J. Chem. Phys. **96**, 5544 (1992).
7. R. F. Loring, Y. J. Yan, and S. Mukamel, J. Chem. Phys. **87**, 5840 (1987).
8. Y. J. Yan and S. Mukamel, Phys. Rev. A **41**, 6485 (1990).
9. S. Mukamel, Annu. Rev. Phys. Chem. **41**, 647 (1990); Adv. Chem. Phys. **70**, 165 (1988).
10. E. J. Nebbering, D. A. Wiersma, and K. Duppen, Chem. Phys. **183**, 167 (1994).
11. D. Thorn Leeson, O. Berg, and D. A. Wiersma, J. Phys. Chem. **98**, 3913 (1994).
12. R. W. Schoenlein, D. M. Mittleman, J. J. Shiang, A. P. Alivisatos, and C. V. Shank, Phys. Rev. Lett. **70**, 1014 (1993).
13. W. B. Bosma, Y. J. Yan, and S. Mukamel, Phys. Rev. A. 42, 9620 (1990).
14. M. Cho and G. R. Fleming, J. Chem. Phys. **98**, 2848 (1993).
15. P. Vöhringer, D. C. Arnett, R. A. Westervelt, M. J. Feldstein, and N. F. Scherer, J. Chem. Phys. **102**, 4027, (1995).
16. W. P. de Boeij, M. S. Pshenichnikov, K. Duppen, and D. A. Wiersma, Chem. Phys. Lett. **138**, 1 (1995).
17. G. R. Fleming and M. Cho, Annu. Rev. Phys. Chem. **47**, 109 (1996).
18. G. R. Fleming, T. Joo, and M. Cho, Adv. Chem. Phys. **101**, 141 (1997).

19. S. Mukamel and V. Rupasov, Chem. Phys. Lett. 242, 17, (1995).

20. V. Chernyak, N. Wang, and S. Mukamel, Phs. Stat. Sol. (b) **188**, 275 (1995).

21. S. A. Adelman, J. Chem. Phys. **64**, 124 (1976).

22. S. A. Adelman, Adv. Chem. Phys. **44**, 143 (1980).

23. S. A. Adelman, Adv. Chem. Phys. **53**, 61 (1983).

24. R. F. Grote, G. van der Zwan, and J. T. Hynes, J. Phys. Chem. **88**, 4676 (1984).

25. G. van der Zwan and J. T. Hynes, J. Phys. Chem. **89**, 4181 (1985).

26. J. T. Hynes, J. Phys. Chem. **90**, 3701 (1986).

27. R. Kubo, *Statistical Mechanics* (North-Holland, Amsterdam, 1971).

28. M. Weissbluth, *Photon-Atom Interactions* (Academic Press, New York, 1989).

29. D. A. McQuarrie, *Statistical Mechanics* (Harper & Row, New york, 1976).

30. D. Chandler, *Introduction to Modern Statistical Mechanics* (Oxford University Press, New York, 1987).

31. R. Reif, *Fundamentals of Statistical and Thermal Physics* (McGraw-Hill, 1965).

32. W. H. Louisell, *Quantum Statistical Properties of Radiation* (J. Wiley, New York, 1973).

33. R. Kubo, *In Lectures in Theoretical Physics*, Vol. 1, 120 (Wiley, Wiley, New York, 1958).

34. N. N. Bogolubov and N. N. Bogolubov Jnr, *Introduction to Quantum Statistical Mechanics* (Gordon and Breach Science, 1994).

35. C. C-Tannoudji, J. Dupont-Roc, and G. Grynberg, *Atom-Photon Interactions*(Wiley New York, 1989).

APPENDIX B: A MATHEMATICAL PROOF OF THE EQUIVALENCE OF EQ. (27) OF CHAPTER 3 TO EQ. (17) OF HAYES ET AL. [1]

Hays et al. [1] start with the thermally averaged Franck-Condon (FC) factors expressed in terms of modified Bessel function, I_m, as

$$FC = \exp[-S_j(2\bar{n}+1)]\sum_{m=-\infty}^{\infty}\left(\frac{\bar{n}+1}{\bar{n}}\right)^{m/2} I_m[2S_j\sqrt{\bar{n}(\bar{n}+1)}]\exp(-im\omega_j t), \tag{B.1}$$

where $\bar{n}$ is the phonon thermal occupation number and S_j is the Huang Rhys-factor. For convenience $x \equiv \beta\hbar\omega_j$ is defined, then one has

$$\begin{aligned}\left(\frac{\bar{n}+1}{\bar{n}}\right) &= \left[\frac{1}{e^x-1}+1\right](e^x-1)\\ &= \left[\frac{1}{e^x-1}+\frac{e^x-1}{e^x-1}\right](e^x-1)\\ &= \left(\frac{e^x}{e^x-1}\right)(e^x-1) = e^x\\ &= e^{\beta\hbar\omega_j}.\end{aligned} \tag{B.2}$$

It follows that

$$\left(\frac{\bar{n}+1}{\bar{n}}\right)^{m/2} = e^{m\beta\hbar\omega_j/2}. \tag{B.3}$$

Next, it is shown that the argument of modified Bessel function, I_m, can be written as

$$2S_j\sqrt{\bar{n}(\bar{n}+1)} = S_j\,\mathrm{csch}(x/2) \tag{B.4}$$

With the help of the following identity,

$$\text{csch}(x/2) = \sqrt{\coth^2(x/2) - 1}, \tag{B.5}$$

and that $2\bar{n} + 1 = \coth(x/2)$, it follows that

$$\begin{aligned} S_j \text{csch}(x/2) &= \sqrt{\coth^2(x/2) - 1} \\ &= S_j \sqrt{(2\bar{n}+1)^2 - 1} \\ &= S_j \sqrt{4\bar{n}^2 + 4\bar{n} + 1 - 1} \\ &= S_j \sqrt{4\bar{n}(\bar{n}+1)} \\ &= 2S_j \sqrt{\bar{n}(\bar{n}+1)}. \end{aligned} \tag{B.6}$$

Combining Eqs. (B.2) and (B.6), Eq. (B.1) reads

$$\begin{aligned} FC = \exp[-S_j(2\bar{n}+1)] \sum_{m=-\infty}^{\infty} \exp(m\beta\hbar\omega_j/2) I_m[S_j \text{csch}(\beta\hbar\omega_j/2)] \\ \times \exp(-i\omega_j t). \end{aligned} \tag{B.7}$$

Using the mathematical definition of $I_m[S_j \text{csch}(\beta\hbar\omega_j/2)]$,

$$I_m[S_j \text{csch}(\beta\hbar\omega_j/2)] = \sum_{\ell=0}^{\infty} \frac{[S_j \text{csch}(\beta\hbar\omega_j/2)]^{m+2\ell}}{\ell!\Gamma(m+\ell+1)2^{m+2\ell}}, \tag{B.8}$$

Eq. (B.7) can be written as

$$\begin{aligned} FC = \exp[-S_j(2\bar{n}+1)] \sum_{m=-\infty}^{\infty} \sum_{\ell=0}^{\infty} \exp(m\beta\hbar\omega_j/2) \\ \times \frac{[S_j \text{csch}(\beta\hbar\omega_j/2)]^{m+2\ell}}{\ell!\Gamma(m+\ell+1)2^{m+2\ell}} \exp(-i\omega_j t). \end{aligned} \tag{B.9}$$

The above shows that Eq. (B.1) is equivalent to Eq. (B.9), and the both have identical temperature dependencies. It is just a question of what lineshape form to replace the resulting δ-function when the Fourier transform is performed.

References

1. J. M. Hayes, P. A. Lyle, and G. J. Small, J. Phys. Chem. **98**, 7337 (1994).

APPENDIX C: DERIVATION OF EQ. (29) FROM EQ. (27) OF CHAPTER 3

Starting with Eq. (27),

$$\sigma(\omega;T) = \exp[-S_j(2\bar{n}+1)] \sum_{m=-\infty}^{\infty} \sum_{\ell=0}^{\infty} \exp(m\beta\hbar\omega_j/2) \times \frac{[S_j \operatorname{csch}(\beta\hbar\omega_j/2)]^{m+2\ell}}{\ell!\Gamma(m+\ell+1)2^{m+2\ell}} \frac{(\gamma_{el}+(m+2\ell)\gamma_j)/2\pi}{(\omega-m\omega_j)^2+((\gamma_{el}+(m+2\ell)\gamma_j)/2)^2} \tag{C.1}$$

Since ℓ is only significant when T > 0, the sum over ℓ is lost as T → 0 and, therefore, one can set $\ell = 0$. The negative values of the integer m can be dealt with if kept in mind that they give rise to the hot bands, which do not exist as T → 0 and therefore one must have m ≥ 0. Furthermore, the argument of Bessel functions imposes restriction that m ≥ 0 as T → 0. Consequently, Eq. (C.1) becomes

$$\sigma(\omega;T) = \exp[-S_j(2\bar{n}+1)] \sum_{m=0}^{\infty} \exp(my) \times \frac{[S_j \operatorname{csch}(y)]^m}{\Gamma(m+1)2^m} \frac{(\gamma_{el}+m\gamma_j)/2\pi}{(\omega-m\omega_j)^2+((\gamma_{el}+m\gamma_j)/2)^2} \tag{C.2}$$

Using $\Gamma(m+1) = m!$ and $\operatorname{csch}(y) = 2/(e^{y} - e^{-y})$, Eq. (C.2) can be rewritten as

$$\sigma(\omega;T) = \exp[-S_j(2\bar{n}+1)]\sum_{m=0}^{\infty}\exp(my)$$
$$\times\frac{[S_j 2/(e^{y}-e^{-y})]^m}{m!2^m}\frac{(\gamma_{el}+m\gamma_j)/2\pi}{(\omega-m\omega_j)^2+((\gamma_{el}+m\gamma_j)/2)^2}$$

$$=\exp[-S_j(2\bar{n}+1)]\sum_{m=0}^{\infty}\frac{S_j^m 2^m e^{my}/(e^{y}-e^{-y})^m}{m!2^m}$$
$$\times\frac{(\gamma_{el}+m\gamma_j)/2\pi}{(\omega-m\omega_j)^2+((\gamma_{el}+m\gamma_j)/2)^2}$$

$$=\exp[-S_j(2\bar{n}+1)]\sum_{m=0}^{\infty}\frac{S_j^m}{m!(1-e^{-2y})^m}$$
$$\times\frac{(\gamma_{el}+m\gamma_j)/2\pi}{(\omega-m\omega_j)^2+((\gamma_{el}+m\gamma_j)/2)^2}. \qquad \text{(C.3)}$$

As T $\rightarrow$ 0 (y $\rightarrow \infty$), $(1/(1-e^{-2y}))^m = 1$ and $\bar{n} = 0$, then Eq. (C.3) becomes

$$\sigma(\omega) = \exp(-S_j)\sum_{m=0}^{\infty}\frac{S_j^m}{m!}\frac{(\gamma_{el}+m\gamma_j)/2\pi}{(\omega-m\omega_j)^2+((\gamma_{el}+m\gamma_j)/2)^2}. \qquad \text{(C.4)}$$

IMAGE EVALUATION
TEST TARGET (QA-3)

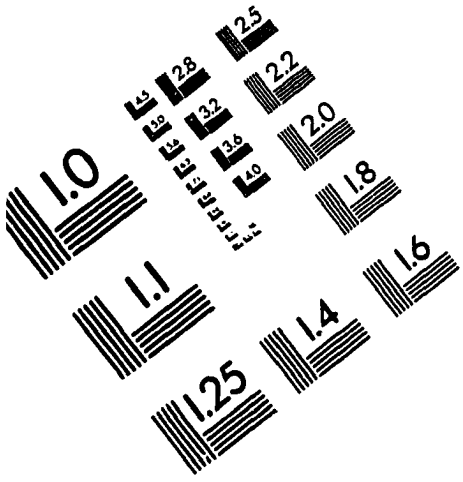

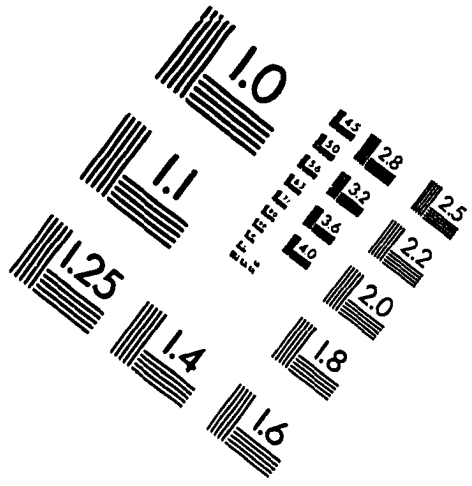

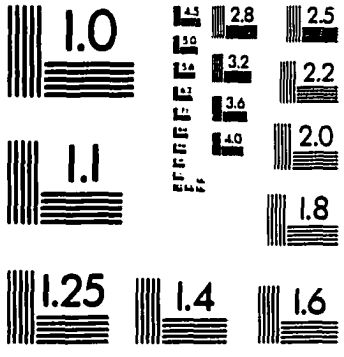

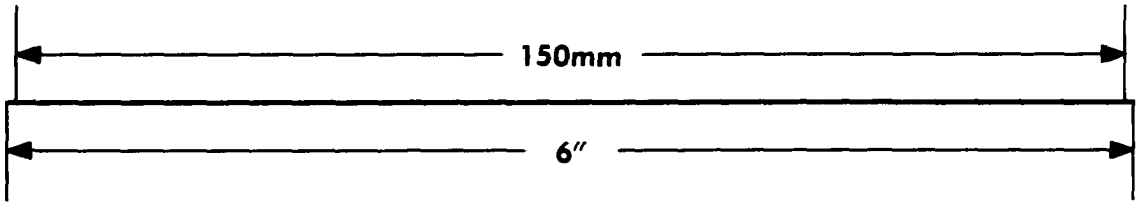

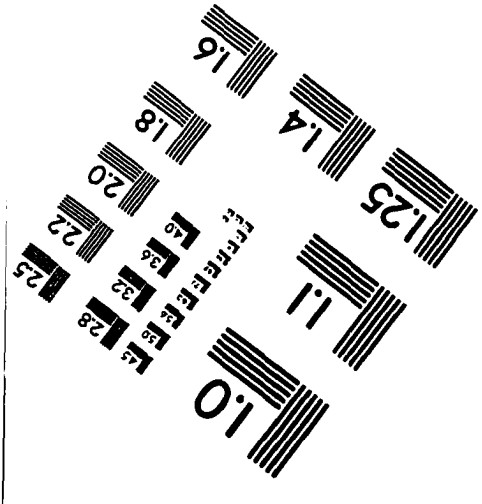

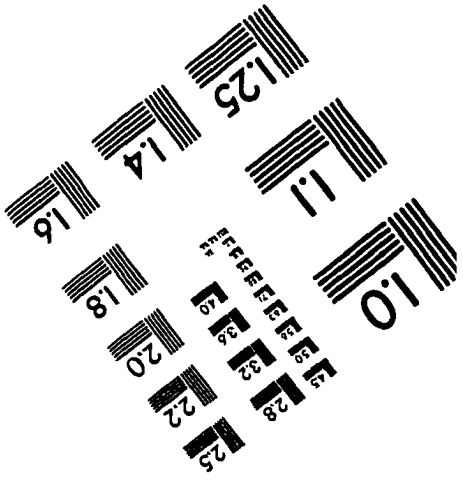

APPLIED IMAGE, Inc
1653 East Main Street
Rochester, NY 14609 USA
Phone: 716/482-0300
Fax: 716/288-5989